A COMPARATIVE STUDY OF DIFFERENT COOLING/DEHUMIDIFICATION SYSTEMS BASED ON COMPRESSOR, EJECTOR, AND MEMBRANE TECHNOLOGIES

A Thesis

by

YONGKI HENDRANATA

Submitted to the Office of Graduate and Professional Studies of
Texas A&M University
In partial fulfillment of the requirements for degree of

MASTER OF SCIENCE

Chair of Committee,	Michael Pate
Member of Committee,	Pavel V. Tsvetkov
	Shima Hajimirza
Head of Department,	Andreas Polycarpou

May 2018

Major Subject: Mechanical Engineering

ABSTRACT

Air conditioning and refrigeration systems for cooling and dehumidification are some of the largest consumers of energy with most of the systems using electricity or fossil fuels to operate. Additionally, refrigeration systems typically use refrigerants, which can deplete the ozone layer and contribute to global warming, as the working fluid during operations. Therefore, alternative cooling and dehumidification systems need to be developed and implemented as substitutes to conventional HVAC systems in order to reduce the destruction of the environment. In addition, it is important that these new non-refrigerant systems provide the same or better energy performance when compared to conventional system. The application of ejector and membrane technologies can provide an alternative approach to conventional systems; therefore, the performance characteristics of these systems are investigated herein by modelling and simulating.

Four systems were modelled, evaluated, and analyzed in this study with the simulations for each system being performed by using the Engineering Equation Solver (EES). The first major system investigated was a conventional cooling system, commonly referred to as a vapor-compression refrigeration system. The model inputs for this system are hot region temperatures of 27 to 33°C and cold region temperatures of 6 to18°C, with these regions forming the heat sinks and sources, respectively. Additionally, the working fluids to the vapor-compression system were assumed to be either refrigerant R-22, which is still widely used for HVAC applications, or an ozone-safe replacement, namely (R-410A). The second major system investigated was a steam-ejector refrigeration system, which has the same inputs as the vapor-compression refrigeration system. This system has been operated for some time but has seen only limited applications because of its lack of optimization. Therefore, a particular focus herein

for this system was the development of an ejector model capable of investigating optimum performance characteristics. The third major system was the membrane-ejector dehumidifier that uses a steam ejector for the purpose of creating a vacuum on the low-pressure side of a membrane, this low-pressure region promotes the removal of water vapor from the ambient air that is dehumidified as it flows on the other side of the membrane surface. A major difference between the compressor in the vapor-compression refrigeration system and the ejector in the membrane-ejector dehumidification system is that the compressor operates with high-cost mechanical and electrical energy while the ejector operates with low-cost thermal energy, which is used to produce driving steam in a 90-150°C boiler. The fourth system was also evaluated with this system being similar to the third system except that a condenser was installed between ejectors. As noted before, all four systems were simulated with idealized conditions in order to facilitate modelling. As such, the true value of the investigation reported herein is knowledge gained regarding the performance of each system as a function of various parameters, rather than a system to system performance comparison.

For the given conditions and assumptions, the coefficient of performance of the vapor-compression systems with either refrigerant R-22 or R410A was found to range from 8 to 30, which is higher than the COP found in real-world operating conditions because of the idealized model. The steam-ejector refrigeration system which operated at the same heat source and sink temperature conditions, had COP's ranging from 2.2 to 6.5. However, a direct comparison of COP's for the two technologies is not possible because the ejector system used low-cost thermal energy, and the idealized assumption. The membrane-ejector dehumidifier gave COP's of 0.12 to 0.19 but add in a condenser between the two ejectors doubled the COP to 0.44-0.5. Again, because the membrane-ejector system is the most innovative and complicated of the four systems, many opportunities exist for improvement and optimization. Of special note, the

COP's of the first two system is based on cooling while these last two system COP's are based on dehumidification, precluding COP comparison. Another consideration is that non-idealized assumptions in this study is the significant air leakage through the membrane, and as membrane improvement are made significant increase in COP's are expected. Furthermore, the small COP of the ejector system can be drastically increased if the thermal energy input comes from a renewable heat sources such as solar or geothermal.

DEDICATION

To

My Parent and my brother for love, pray, and full support during my time as a graduate student.

And not forget to Mbok Trubus

Who always believe in me that I will make it…

ACKNOWLEDGEMENTS

I would like to express my sincere gratitude to my advisor Dr. Michael Pate for all his encouraging, knowledgeable advice, patience, and support. This thesis would have been completed without his guidance. One simply could not wish for a better or friendlier advisor. Additionally, I would like to thank my committee members, Dr. Pavel V. Tsvetkov and Dr. Shima Hajimirza, for their guidance throughout the completion of this research.

I also thanks to Fulbright Scholarship Program and American Indonesian Exchange Foundation for giving me financial support and sponsor to pursue higher degree at Texas A&M University. I hope the program can be improved and widely open for all people in the world especially Indonesian people.

Finally, thank to my parent in Banyuwangi, Pak Istadi, Bu Kholifah, and Naufal Ghaninajib who sacrificed so much to make me have better future. Their love and support have inspired me to do my best in every aspect of life.

CONTRIBUTORS AND FUNDING SOURCES

Contributors

This work was supported by a thesis committee consisting of Professor Michael Pate and Dr. Shima Hajimirza of Department of Mechanical Engineering, and Dr. Pavel V. Tsvetkov of Department of Nuclear Engineering.

The analysis for Chapter V is provided by the student with guidance from Professor Michael Pate, especially for discussion section.

All other work conducted for the thesis was completed by student independently.

Funding Sources

Graduate study was supported by a fellowship from Texas A&M University and Fulbright Program.

TABLE OF CONTENTS

Page

ABSTRACT ii

DEDICATION v

ACKNOWLEDGEMENTS vi

CONTRIBUTORS AND FUNDING SOURCES vii

TABLE OF CONTENTS viii

LIST OF FIGURES x

LIST OF TABLES xiii

NOMENCLATURE xiv

CHAPTER I 1

Background 1
Literature Review 3
Research Description 11
Research Objective 12

CHAPTER II 13

Nozzle and Diffuser 13
One-Dimensional Steady Flow in Ejector 22
Vapor-Compression Refrigeration System 28
Steam-Ejector Refrigeration Systems 32
Psychrometric Principles 37

CHAPTER III 43

Vapor-Compression Refrigeration Systems 43
Ejector Refrigeration Systems 45
Membrane-Ejector Dehumidifier 48

CHAPTER IV 55

CHAPTER V 64

Vapor-Compression Refrigeration Systems 64
Steam-Ejector Refrigeration System 67
Membrane-Ejector Dehumidifier 71
Improved Membrane-Ejector Dehumidifier 78

CHAPTER VI 84

CHAPTER VII 86

REFERENCES 88

APPENDIX A 92

Membrane-Ejector Dehumidifier 92

APPENDIX B 115

Vapor-Compression Refrigeration System 115
Ejector Calculation 116
Steam-Ejector Refrigeration System 120
Membrane-Ejector Dehumidifier 121

LIST OF FIGURES

Page

Figure 1. The capacity ratio of R-410A relative to R-22 (Payne and Domanski 2002) 4

Figure 2. The system performance ratio of R-410A relative to R-22 (Payne and Domanski 2002) 4

Figure 3. Operational modes of ejector (Huang et al. 1999) 7

Figure 4. Entrainment ratio for various boiler operating temperature and evaporator temperature (Sun 1997) 9

Figure 5. System performance for various boiler operating temperature and evaporator temperature (Sun 1997) 9

Figure 6. A hollow fiber spacesuit water membrane (Bue and Makinen 2011) 10

Figure 7. The control volume of flow through changing cross-section area 14

Figure 8. Effects of area change in subsonic and supersonic flows. (a) Nozzles: V increase; h, p, and ρ decrease. (b) Diffuser: V decrease h, p, and ρ increase. (Moran & Shapiro, 2006) 17

Figure 9. Variation of $A/A*$ with Mach number in isentropic flow for $\kappa = 1.4$ (Liao 2008) 19

Figure 10. Effects of back pressure on the operation of a converging-diverging nozzle (Liao 2008) 21

Figure 11. Schematic diagram of ejector layout and the fluid flow (Huang 1998) 23

Figure 12. Schematic of a compression refrigeration system 28

Figure 13. T-s diagram of idealized vapor-compression refrigeration system 30

Figure 14. Schematic view and the variation in stream pressure and velocity as functions of location along a steam ejector (Huang 1998) 33

Figure 15. Schematic of steam-ejector refrigeration system 34

Figure 16. Performance of a steam jet refrigerator based on experimental data provided by Eames and Aphornratana 35

Figure 17. Effect of operating temperatures on performance of a steam jet refrigerator based on data provided by Eames 36

Figure 18. Dehumidification. (a) Equipment schematic. (b) Psychrometric chart representation. 40

Figure 19. Adiabatic mixing of two moist air streams 41

Figure 20. Schematic of vapor-compression refrigeration system. 44

Figure 21. Schematic of steam-ejector refrigeration system 46

Figure 22. Schematic of membrane-ejector dehumidifier 49

Figure 23. Flowchart of membrane-ejector dehumidifier calculation 53

Figure 24. Flowchart of ejector calculations for critical and subcritical conditions 57

Figure 25. Comparison between experimental result (Huang et al. 1999) and theoretical prediction from Chen, Huang, and present model 58

Figure 26. Performance plot for steam ejector using present model in critical condition 60

Figure 27. Performance curve of vapor-compression refrigeration system for R22 and R410A. 64

Figure 28. Evaporation capacity in vapor-compression refrigeration system for R22 and R410A 66

Figure 29. Work of compressor in vapor-compression refrigeration system for R22 and R410 66

Figure 30. Performance of steam-ejector refrigeration system in different area ratio of the ejector. 68

Figure 31. Entrainment ratio of the ejector in steam-ejector refrigeration system in different area ratio. 68

Figure 32. Performance of steam-ejector refrigeration system with different hot and cold region temperature ($Ar = 210.3$) 69

Figure 33. Required boiler temperature in optimum operation for steam-ejector refrigeration system. 71

Figure 34. Overall entrainment ratio at humidity ratio $\omega = 13$ and $Tamb = 27°C$ 73

Figure 35. Overall entrainment ratio at humidity ratio $\omega = 13$ and $Tamb = 30°C$ 73

Figure 36. Overall entrainment ratio at humidity ratio $\omega = 10$ and $Tamb = 30°C$ 74

Figure 37. Performance curve of membrane-ejector dehumidifier..... 75

Figure 38. Overall entrainment ratio of membrane-ejector dehumidifier 76

Figure 39. Energy consumption for membrane-ejector dehumidifier 77

Figure 40. Schematic of improved membrane-ejector dehumidifier..... 78

Figure 41. Overall entrainment ratio at humidity ratio $\omega = 13$ and $Tamb = 27°C$ 79

Figure 42. Overall entrainment ratio at humidity ratio $\omega = 13$ and $Tamb = 30°C$ 80

Figure 43. Overall entrainment ratio at humidity ratio $\omega = 10$ and $Tamb = 30°C$ 80

Figure 44. Performance curve of improved membrane-ejector dehumidifier 81

Figure 45. Energy consumption of improved membrane-ejector dehumidifier 82

Figure 46. Overall entrainment ratio of improved membrane-ejector refrigeration..... 83

LIST OF TABLES

Page

Table 1. Operating condition for R22 and R410A 45

Table 2. Input parameter for vapor-compression refrigeration system 45

Table 3. Input parameters for the membrane-ejector dehumidifier. 50

Table 4. Regression result using Least-Square approximation 62

Table 5. Performance comparison of vapor-compression refrigeration for R22 and R410A 65

Table 6. Optimum geometry and condition for given condition. 75

Table 7. Comparison of all systems 85

NOMENCLATURE

A	area (m^2)
c	speed of sound at medium (m/s)
cp	heat capacity at constant pressure ($kJ/kg.K$)
cv	heat capacity at constant volume ($kJ/kg.K$)
COP	coefficient of performance
d	diameter (mm)
ER	entrainment ratio
η	efficiency
H	static enthalpy (kJ/kg)
h	enthalpy (kJ/kg)
κ	heat capacity ratio
m	mass flow rate (kg/s)
M	Mach number
p	pressure (kPa, bar)
P	static pressure (kPa, bar)
ρ	density (kg/m^3)
q	heat per mass flow rate (kJ/kg)
$Q, \dot{Q}$	heat rejected/absorbed (kW)
R	gas constant ($kJ/kg.K$)
T	temperature (C, K)
ϕ	relative humidity or loss coefficient (%)
V	velocity (m/s)
w	work per mass flow rate (kJ/kg)
$W, \dot{W}$	Work rate (kW)
ω	humidity ratio

y	mole fraction

Subscripts

1	state condition, outlet of nozzle, number of equipment
2, 3	state condition, constant area section, number of equipment
4, 5, 6	state condition
a	state condition a or air
b	state condition b
c	downstream of ejector or compressor
f	saturated fluid condition
g	saturated gas condition
in	system inlet
m	mixture flow
out	the system exit
p	primary flow
p1	primary flow at outlet of nozzle
py	primary flow at section y-y
p2, p3	primary flow at constant area section
r	ratio
s	secondary flow
sy	secondary flow at section y-y
t1	throat of nozzle 1
t2	throat of nozzle 2
v	vapor
*	critical condition

CHAPTER I

INTRODUCTION

Background

Refrigeration and air-conditioning systems are necessary for cooling and dehumidification in many important applications, such as food storages, petrochemicals, health sectors, and building air conditioning. Most approaches to achieve low temperature and humidity still use conventional vapor-compression, which uses a compressor as the main driver, thus consuming a large amount of electricity and hence fossil fuel. Additionally, conventional vapor-compression refrigeration systems use refrigerants as the thermal fluid agent during operations, and many of these common refrigerants have been shown to be harmful to the environment, causing either ozone layer destruction or global warming. Fortunately, there are alternative cooling and dehumidification methods that can alleviate these harmful issues, with two of these methods being the Ejector Refrigeration System and the Membrane Dehumidification system.

Ejector Refrigeration Systems have the advantage over conventional vapor-compression refrigeration systems in that they do not use refrigerants; rather, these systems can be operated by using water as the working fluid. Other advantages are the simplicity of the construction does not require mechanical rotating components and motors for moving refrigerants, but rather steam ejectors that are easier for installation and maintenance (Chen et al. 2013). Furthermore, possibilities exist to utilize low-grade energy, such as thermal power from solar energy, small-scale geothermal, and industrial waste heat to create low-pressure steam that can help to address the issues related to harming the environment, particularly by reducing greenhouse gases and fossil fuel utilization.

A number of past studies have investigated the performance of ejectors, with the

performance of ejectors represented by an entrainment ratio, which closely relates to the performance of the overall refrigeration system (Sun 1993). Of special importance, several models have been developed to obtain optimum operations and designs for ejectors. Regarding ejector design, ejectors can be classified into two categories according to the position of the nozzle. The first design has the nozzle exit located within a constant-area section of the ejector, and this is known as "constant-area mixing ejector". The second design has the nozzle located within the suction chamber, which is in front of the constant area, or and this is known as a "constant-pressure mixing ejector". Previous studies have shown that the constant-pressure ejector has a better performance compared to the constant-area ejector (Huang et al. 1999).

By analyzing the relationship between gas dynamics and constant-pressure mixing in ejectors, by Keenan et al. (1950), developed a model to predict ejector performance, and Huang et al. (1999) performed experiments to evaluate ejector operations with different geometries. Of special notes, the previous model predicted the performance of ejectors in critical modes, while a new model developed by Chen et al. (2013) predicted the performance of ejectors at both critical and sub-critical operations.

With regards using ejectors in refrigeration systems, Sun (1997) published the relationship between ejector performance and system performance, stating that the ejector should be operated at critical conditions in order to achieve an optimum system performance. However, it was also stated that operations should not go beyond the critical condition too far because the consumption of energy can increase, even though the entrainment ratio remains constant because of a choked condition in the nozzle throat. It was also observed that high evaporator temperatures make the ejector perform better.

In research reported herein, vapor-compression refrigeration technology and ejector refrigeration technology will be simulated to better understand how both technologies perform

when applied to cooling and dehumidification. In addition to the previous two technologies, with membrane-based technology for dehumidification will be simulated to better understand those parameters affecting both system performance and economic feasibility, which can lead to performance enhancing design improvement for future application.

Literature Review

Vapor-Compression Refrigeration System

The most common system presently used for refrigeration systems is the vapor-compression refrigeration system which uses refrigerant as the working fluid. The basic system consists of four components, namely a compressor, condenser, expansion device and evaporator. Jensen and Skogestad (2007) showed that the cycle has five steady-state degrees of freedom that contribute to the performance of the system. Example of these degrees of freedoms are compressor power, heat transfer in the condenser, heat transfer in the evaporator, and expansion valve opening. Furthermore, they found that there are three constraints for optimization, which are maximum heat transfer in the condenser, maximum heat transfer in the evaporator and minimum super-heating. With the load specified, they found one unconstrained steady-state degree of freedom, which is the outlet temperature of the condenser.

Presently, the most common refrigerant for vapor-compression refrigeration systems used for residential cooling are R-22 and R-410A. However, a phase out of R-22 is underway due to environmental concerns. Payne and Domanski (2002) compared these two refrigerants as outdoor temperatures ranged from 27.8°C (82°F) to 54.4°C (130°F) as shown in Figure 1 and 2. They stated that the outdoor temperature increased, the R-410A system performance degraded more than the R-22 system performance for the same refrigeration capacity. For example, at an outdoor

temperature of 54.4°C (130°F), the R-410A capacity was 9% below R-22, while, the R-410A COP was only 4% lower than the R-22 COP.

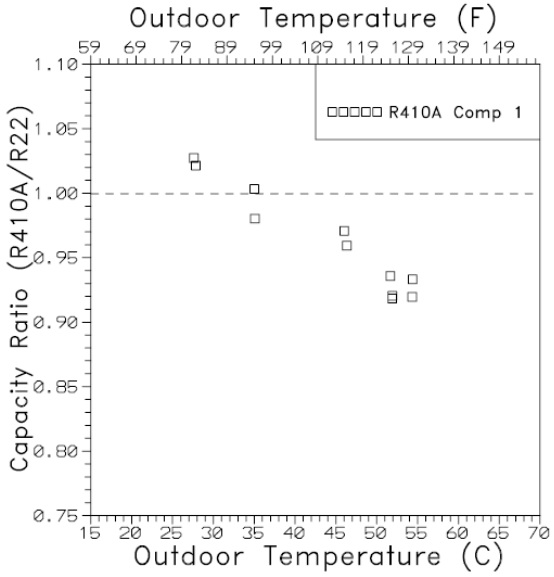

Figure 1. The capacity ratio of R-410A relative to R-22 reprinted from Payne and Domanski, 2002

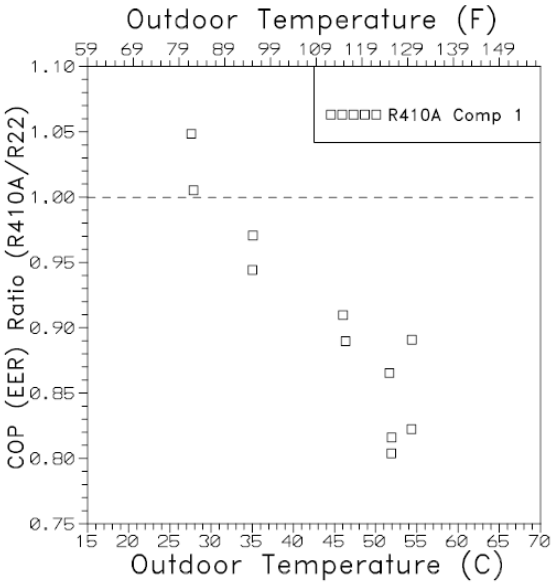

Figure 2. The system performance ratio of R-410A relative to R-22 reprinted from Payne and Domanski, 2002

It can also be seen in Figures 1 and 2 that R-410A has a lower capacity and COP when the outdoor temperature is above 30°C (86°F) and, then there is a degradation of COP for R-410 relative to R-22 as the outdoor temperature increases. In addition to typical measurement uncertainties part of the scatter shown in Figures 1 and 2. At a given outdoor temperature was reported to be due to day-to-day variations of the voltage at the testing facility.

Steam-Ejector Refrigeration System

An advantage of the steam-ejector refrigeration system is that it can replace a compressor driven system which can in turn reduce the amount of electricity purchased from utility companies based on utilizing waste heat from the industrial processes. Even though the steam-ejector refrigeration system has these advantages, it is less dominant compared to vapor-compression refrigeration system because of its lower coefficient of performance. However, a number of studies reported in the literature have focused on improving system performance and ejector operations. For example, a one-dimensional analysis was performed by Huang et al. (1998) to predict and verify the performance of 11 ejectors that had previously been evaluated. The test result than used to determine efficiencies of primary flows (η_p), secondary flows (η_s), loss coefficients due to geometry (ϕ_p), and loss coefficients due to mixing flow (ϕ_m). These coefficients together with gas dynamic relations predicted the performance of ejectors along with identifying the area ratios that gave the higher performance.

Several parameters can be used to describe the performance of a steam-ejector system for refrigeration applications, with Chunnanond and Aphornranata (2003) introducing important parameters, such as entrainment ratios and pressure lift ratios that can be described as follows.

$$entrainment\ ratio, ER = \frac{mass\ of\ secondary\ flow, m_s}{mass\ of\ primary\ flow, m_p} \quad (1)$$

$$pressure\ lift\ ratio = \frac{static\ pressure\ at\ diffuser\ exit}{static\ pressure\ at\ secondary\ flow} \quad (2)$$

The entrainment ratio is related to the energy efficiency of the refrigeration cycle, while the pressure ratio limits the temperature at which the heat can be rejected. Furthermore, the most desired ejector is the one that achieves the highest entrainment ratio while maintaining the highest possible discharge pressure at the given operating conditions.

McGovern et al. (2012) stated that certain regimes are more conducive to achieving a high ejector performance which corresponds to high entrainment ratio. In this regard, the entrainment ratio is seen to be the highest when the entrained fluid reaches a choked condition in the mixing region. By understanding the flow regimes of an ejector, entrainment ratio can be described as a function of inlet fluid conditions, discharge pressure, primary fluid, nozzle throat area, and mixing chamber area. Huang et al. (1998) experimental data used to provide an insight into critical pressure and ejector entrainment ratio based on in three distinct regimes shown in Figure 3 and described as follows:

1. Double-choking or critical mode as $p_c \leq p_c^*$, while primary and entrained flows are both choking, and the entrainment ratio is constant. ER = constant
2. Single-choking or subcritical mode as $p_c^* < p_c < p_{c0}$, while only the primary flow is choked and omega changes with the back-pressure p_c
3. Back-flow or malfunction mode as $p_c \leq p_{c0}$, while both the primary and secondary flow are not choked, and the entrained flow is reversed (malfunction). $ER \leq 0$

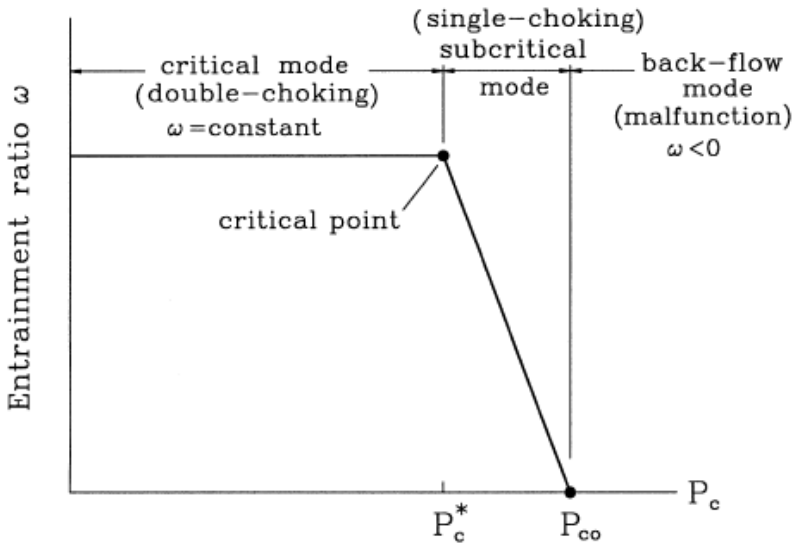

Figure 3. Operational modes of ejector reprinted from Huang et al. 1999

To predict ejector performance for all modes, Chen et al. (2013) developed a new model for both critical and sub-critical regimes based on the development of gas dynamic models by Huang et al. (1998). The result is a one-dimensional model that can predict the entire range of operations with an error of less than 20%. Another model also developed by Zhu et al. (2007) predicted the performance for real-time control and optimization using 2 to 3 empirical parameters that can be determined from either catalog data or real-time operation.

The working performance of a steam-ejector refrigeration system is measured by the coefficient of performance that is defined as the ratio between the cooling capacity of the evaporator and the energy input at the boiler and pump as follows.

$$COP = \frac{Cooling\ effect\ at\ the\ evaporator}{Energy\ input\ at\ the\ boiler\ and\ pump} = \frac{Q_e}{Q_b + W_p} \tag{3}$$

It should be noted that, the energy input to the pump is usually negligible being less than 1 % of the generator heat input and therefore it can be neglected.

As noted previously, the ejector is the most important component in the steam-ejector refrigeration system. In this study, ejector performance contributes greatly to the overall refrigeration system performance. In practice, the ejector uses water as the working fluid, because it is cheap, abundant, and environmentally friendly compared to refrigerants. Chunnanond and Aphornratana (2004) performed experiments on an ejector refrigeration system with a cooling capacity of 3 kW and evaporator and condenser temperatures of 5°C and 22°C, respectively. The overall COP of the system ranged from 0.28 to 0.48, and they found that a decrease in boiler pressure causes the cooling capacity and COP to rise while the critical condenser pressure was reduced. In addition, an increase in the evaporator pressure increased the critical condenser pressure, cooling capacity and COP, but in turn sacrificed the desired cooling temperature. Similar experiments were performed by Ma et al. (2010) for a system capacity around 5 kW and a COP ratio around 0.17-0.32. Their experimental results confirmed an observation from Chunnanond and Aphornratana (2004) about boiler temperature not always being accompanied by the increase in system efficiency. A simulation study was also performed by Eames et al. (1995). for a small-scale ejector refrigeration system that used water as the working fluid. Their model was based on a constant-pressure mixing process, but without considering the choking of the secondary flow, and it had evaporator and condenser temperatures around 5°C and 26°C respectively.

Sun (1997) carried out an extensive experimental study of an ejector refrigeration system, confirming that the entrainment ratio increases with boiler temperature until it reaches a maximum value and then decreases with boiler temperature. This result, which is shown in Figures 4 and 5, means that the ejector has an optimum operation for a certain optimum boiler temperature, with this optimum boiler temperature being the one at which the condenser pressure is critical pressure. Therefore, the system can achieve maximum performance only when the system operates under critical condenser conditions, which means that for a given condenser pressure the boiler

temperature should be adjusted to allow the ejector to operate at a critical back pressure.

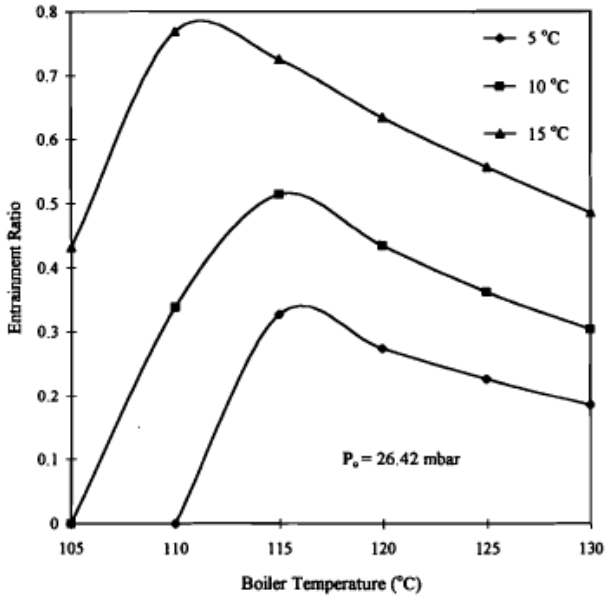

Figure 4. Entrainment ratio for various boiler operating temperature and evaporator temperature reprinted from Sun 1997

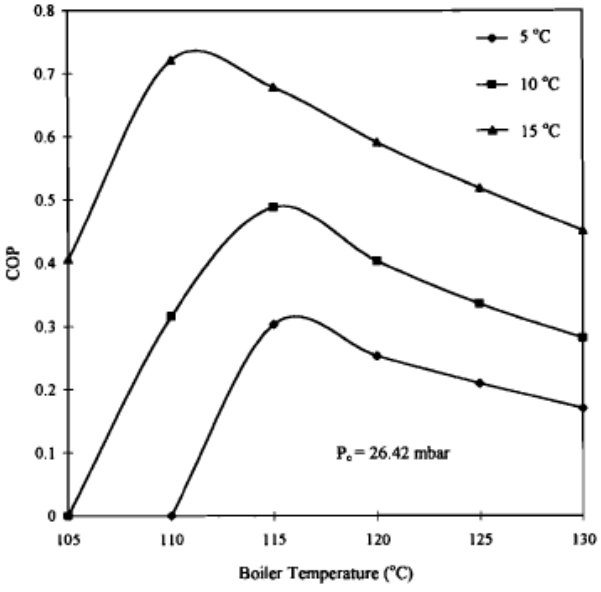

Figure 5. System performance for various boiler operating temperature and evaporator temperature reprinted from Sun 1997

The results from Sun (1997) in Figures 4 and 5 also show that as the evaporator temperature increases then the optimum operating boiler temperature move to a lower temperature, thus increasing the entrainment ratio and system performance in terms of COP.

Membrane Dehumidification

Air dehumidification has an important role in energy savings because of its effect on human comfort and the fact that cooling systems can be created by integrating dehumidification and evaporative cooling. The ASHRAE Standard 62-2001 recommends a relative humidity of 30-60% for comfort in the indoor environment, while in some special circumstances, such as machine rooms, museums, and libraries, high humidity should be avoided altogether. Membrane-based dehumidification technologies have advantages over other HVAC technologies because of their simple structure, lack of rotary parts, reliability, and high dehumidification performance.

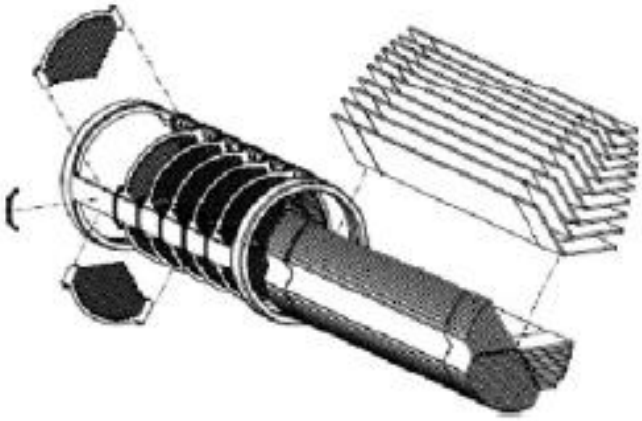

Figure 6. A hollow fiber spacesuit water membrane reprinted from Bue and Makinen, 2011

Yang and Yuan (2013) stated that membrane modules can treat both sensible heat and latent heat simultaneously, while having a small foot-print, being light weight, with a simple structure, and being highly compact, with the ability to work continuously without moving parts.,

Membrane-based dehumidification technology with all of its advantages is finding applications in HVAC and research is taking place to make this happen.

Research Description

The research performed herein focuses on understanding the performance of ejector refrigeration technology and membrane-dehumidification technology along with study of a reference point of consulting of a conventional vapor-compression refrigeration for cooling applications. Membrane-based technology for dehumidification applications can also be used for cooling by use of an evaporative cooler located downstream of the dehumidification points. For this research, each of 4 technologies was simulated for idealized conditions to remove component performance factors that may not be readily available, especially for the newer membrane-dehumidifier systems that are just now being studied and designed for applications. The one area where a non-ideal assumption was made is for the membrane where air was assumed to leaking through with the water vapor. The modeling was performed in Engineering Equation Solver (EES) software for a range of operating conditions.

With simulation being performed in four scenarios as follows:

1. Simple vapor-compression refrigeration system
2. Steam-ejector refrigeration system
3. Membrane-ejector dehumidification system
4. Improved Membrane-ejector dehumidification system

The models developed and then simulated are used to obtain system performances, with primary focus on providing insight and understanding as to the effect that various parameters have on system performances. These simulations utilize different operating conditions with and these conditions being described in detail in Chapter 3. Furthermore, these simulations are used to obtain

the coefficient of performances for each scenario by using either refrigerants for a simple vapor-compression refrigeration system or steam for others.

Research Objective

The goal of this study is to develop models for 4 air conditioning and dehumidification scenarios and then to perform simulations at different operating conditions and ambient temperatures. By studying system performances for these variations, the resulting information can be used to better understand the operating characteristics of the various ejector systems.

Of special note, the use of ejectors for the proposed dehumidifier system with membranes is new, meaning no previous studies have been undertaken. Therefore, a particular focus of the research performed and reported herein will be the modeling and simulation of ejectors, especially using a new approach to obtain a simple model, and ejector-membrane, system for the purpose of predicting performances at optimum operating conditions and geometries to include multi-stage ejectors. Then results can then be used make design improvements for real-world applications.

CHAPTER II

THEORY

In this chapter, the theoretical background needed for modelling major and system components are presented for vapor-compression and steam-ejector refrigeration systems and the membrane-ejector system, especially the general theory about one-dimensional ejector flow with nozzles and diffusers, vapor-compression refrigeration systems, and steam-ejector. The equations and concepts from these theories are presented as used in the modelling simulations, which in turn form the foundation for the research performed herein.

Nozzle and Diffuser

In this chapter, the theoretical background needed to perform a one-dimensional analysis of nozzles and diffusers will be presented. This compressible gas analysis for the ejector is based on applying the conservation of mass, the conservation of momentum, and the conservation of energy through to a changing cross-section area with the ideal gas law as well as property relationships also being used. The process of an ejector involves supersonic flow where the compressible flow velocity exceeds the speed of sound represented by the Mach Number. The isentropic expansion is an important assumption for the nozzle and diffuser model.

The idea of the ejector is to accelerate the velocity of the primary flow through a converging-diverging cross-section so that critical condition can be reached. Most modern ejectors usually operate in critical condition in order to obtain a high entrainment ratio, which again is defined as critical condition. The high velocity from the primary flow sucks vapor by creating a secondary flow from a vacuum chamber and then joins together with the primary flow.

Generally, the one-dimensional flow in the ejector can be described with the conservation equations and the ideal gas law applied to the control volume that is shown in Figure 7.

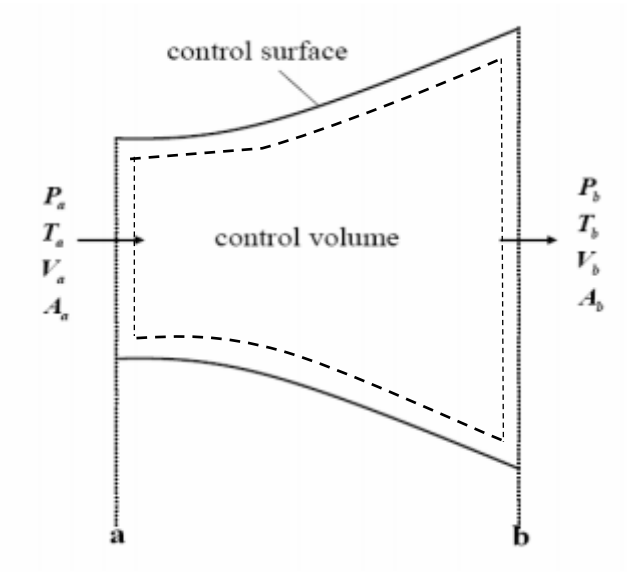

Figure 7. The control volume of flow through changing cross-section area

Referring to Figure 7, the conservation of mass is

$$\dot{m} = \rho_a V_a A_a = \rho_b V_b A_b \tag{4}$$

while the conservation of momentum is

$$P_a A_a + m_a V_a + \int_{A_b}^{A_a} P dA = P_b A_b + m_b V_b \tag{5}$$

and the conservation of energy is

$$h_a + \frac{V_a^2}{2} = h_b + \frac{V_b^2}{2} \tag{6}$$

and finally, the ideal gas law is

$$\frac{P}{\rho} = RT \tag{7}$$

where R is the gas constant with units of *J/(kg.K)*, with R being related to its molecular weight by the following equation

$$R = \frac{\bar{R}}{M} \tag{8}$$

where $\bar{R}$ is the universal gas constant with unit of *J/(kmol.K)* and M being the molecular weight with units of *kg/(kmol)*.

The property relationship for compressible flow is

$$dp = \left(\frac{\partial p}{\partial \rho}\right)_s d\rho + \left(\frac{\partial p}{\partial s}\right)_\rho ds \tag{9}$$

Mach Number

Mach number is a dimensionless parameter, which has an important role in compressible flow, and it is defined as the ratio of the fluid velocity relative to local sonic speed as follows.

$$M = \frac{local\ fluid\ velocity}{local\ sonic\ speed} = \frac{V}{c} \tag{10}$$

For the special case of an ideal gas, the relationship between pressure and specific volume of the ideal gas is as follows

$$pv^\kappa = constant \tag{11}$$

with the speed of sound for an ideal gas being

$$c = \sqrt{\kappa RT} \tag{12}$$

where κ is the specific heat ratio for an ideal gas. Furthermore, when $M > 1$, the flow is said to be supersonic; when $M < 1$, the flow is subsonic; and when $M = 1$, the flow is sonic.

The effect of area change in subsonic and supersonic flows can be derived from the continuity, momentum, energy equations, as well as property relationships for an ideal gas, which results in the following equation.

$$\frac{dA}{A} = -\frac{dV}{V}\left[1 - \left(\frac{V}{c}\right)^2\right] = -\frac{dV}{V}(1 - M^2) \tag{13}$$

The above relationship shows how area varies with velocity. Based on this equation, the following cases can be identified:

- Subsonic nozzle, $dV > 0, M < 1 \Rightarrow dA < 0$: the duct converges in the direction of flow
- Supersonic nozzle, $dV > 0, M > 1 \Rightarrow dA > 0$: The duct diverges in the direction of flow
- Supersonic diffuser, $dV < 0, M > 1 \Rightarrow dA < 0$: The duct converges in the direction of flow
- Subsonic diffuser, $dV < 0, M < 1 \Rightarrow dA > 0$: The duct diverges in the direction of flow

with all of these cases being described in Figure 8.

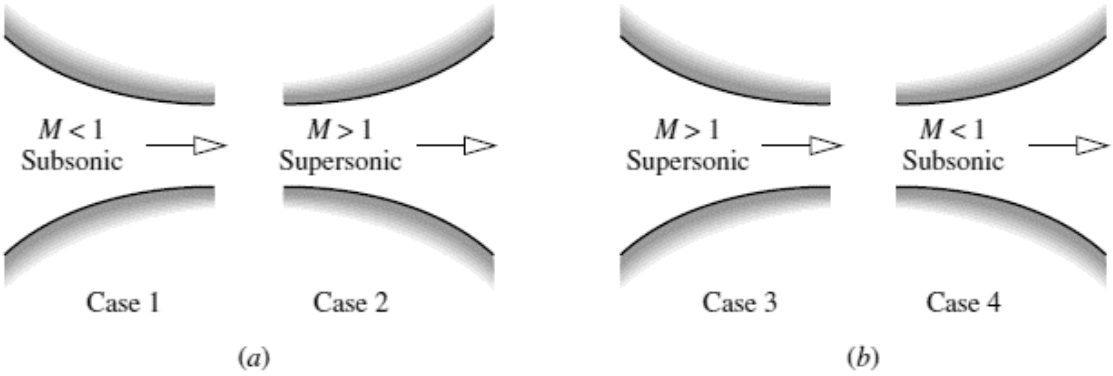

Figure 8. Effects of area change in subsonic and supersonic flows. (a) Nozzles: V increase; h, p, and ρ decrease. (b) Diffuser: V decrease h, p, and ρ increase, reprinted from Moran & Shapiro, 2006

Isentropic Expansion of Ideal Gas

The equation for isentropic flow of an ideal gas is

$$\frac{P}{\rho^{\kappa}} = constant \tag{14}$$

This isentropic equation, along with the basic equations namely continuity, momentum, energy, second law, equation of state, can be used to determine the properties of local pressure, temperature, and density at stagnation conditions in an isentropic flow as follows.

$$Pressure: \frac{P_0}{P} = \left(1 + \frac{\kappa - 1}{2} M^2\right)^{\frac{\kappa}{\kappa - 1}} \tag{15}$$

$$Temperature: \frac{T_0}{T} = 1 + \frac{\kappa - 1}{2} M^2 \tag{16}$$

$$Density: \frac{\rho_0}{\rho} = \left(1 + \frac{\kappa - 1}{2} M^2\right)^{\frac{\kappa}{\kappa - 1}} \tag{17}$$

The parameters with subscript 0 refer to stagnation properties. which are constant throughout a steady, isentropic flow field. The relationship for area A at a given section to area A^* that would be required for sonic flow (M= 1) at the same mass flow rate and stagnation state can be described as follows

$$\frac{A}{A^*} = \frac{1}{M}\left[\left(\frac{2}{\kappa+1}\right)\left(1+\frac{\kappa-1}{2}M^2\right)\right]^{(\kappa+1)/2(\kappa-1)} \tag{18}$$

Using this equation, the variation of A/A^* with Mach number is shown in Figure 9, where it can be observed that a converging-diverging passage with a minimum area section is required to accelerate a flow from a subsonic to a supersonic velocity.

Choking Phenomena

In order to explain the choking phenomena, a convergent-divergent nozzle with its static pressure distribution along the flow direction is shown in Figure 10. Flow through the converging-diverging nozzle is induced by an adjustable downstream pressure at the discharge section; the upstream supply is constant and stagnation conditions with $V_0 \cong 0$, P_e and P_b represent the static pressure at the nozzle exit and back pressure respectively. The effect on static pressure along the nozzle of changing the back pressure P_b is shown in Figure 10. Specifically, Figure 10 shows that the back-pressure changes not only the static pressure, but also the flow velocity in term of Mach number. The flow rate is low when the back pressure P_b is slightly lower than the pressure at the entrance plane P_0, with curve (*i*) showing the distribution of pressure for this subsonic case. Since the flowrate is low enough (M < 0.3), the behavior of the flow is incompressible, and the minimum pressure is reached at the throat. If the back pressure is reduced, which corresponds to case (*ii*), the flow condition is still subsonic along the nozzle, although now the flow with its higher velocity leads to a higher mass flow rate. Since the velocity is higher (0.3 < M < 1), the compressibility of

the flow must be taken into account. When the back pressure is reduced further which corresponds to case (*iii*), the flow at the minimum cross-section area reaches a sonic condition (M = 1). In addition, the mass flow rate at this condition is a maximum and does not increase by lowering the back pressure, which is called a *choked condition*.

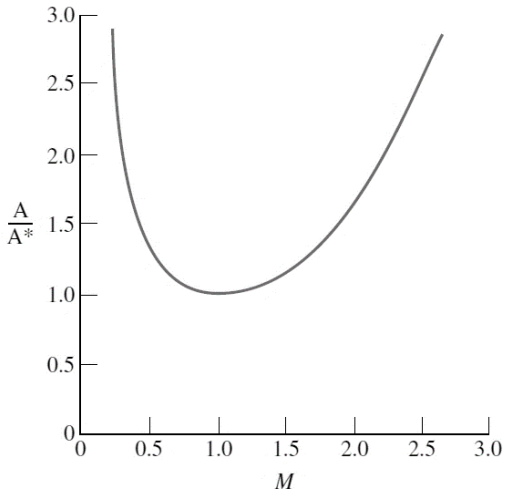

Figure 9. Variation of A/A^* with Mach number in isentropic flow for κ = 1.4, reprinted from Liao, 2008

The relationships between stagnation conditions and critical conditions can be expressed for each parameter in the following equations.

Pressure:

$$\frac{P^*}{P_0} = \left(\frac{2}{\kappa + 1}\right)^{\frac{\kappa}{\kappa-1}} \tag{19}$$

Temperature:

$$\frac{T^*}{T_0} = \frac{2}{\kappa + 1} \tag{20}$$

Density:

$$\frac{\rho^*}{\rho_0} = \left(\frac{2}{\kappa+1}\right)^{\frac{1}{\kappa-1}} \tag{21}$$

while velocity at the throat can be expressed as follows

$$V^* = c^* = \sqrt{\left(\frac{2\kappa}{\kappa+1}\right) RT_0} \tag{22}$$

Using Equations 19 to 22, air with $\kappa = 1.4$, the maximum static pressure drop, temperature, and density at critical condition are $P^* = 0.528P_0$, $T^* = 0.833T_0$, and $\rho^* = 0.634P_0$, respectively. Furthermore, the maximum mass flowrate at critical condition can be derived from equation above as follows

$$m = \frac{A_t P_0}{T_0} \sqrt{\frac{\kappa}{R}\left(\frac{2}{\kappa+1}\right)^{(\kappa+1)/(\kappa-1)}} \tag{23}$$

Thus, the maximum flow through the given nozzle is a function of the $P_0/\sqrt{T_0}$ ratio.

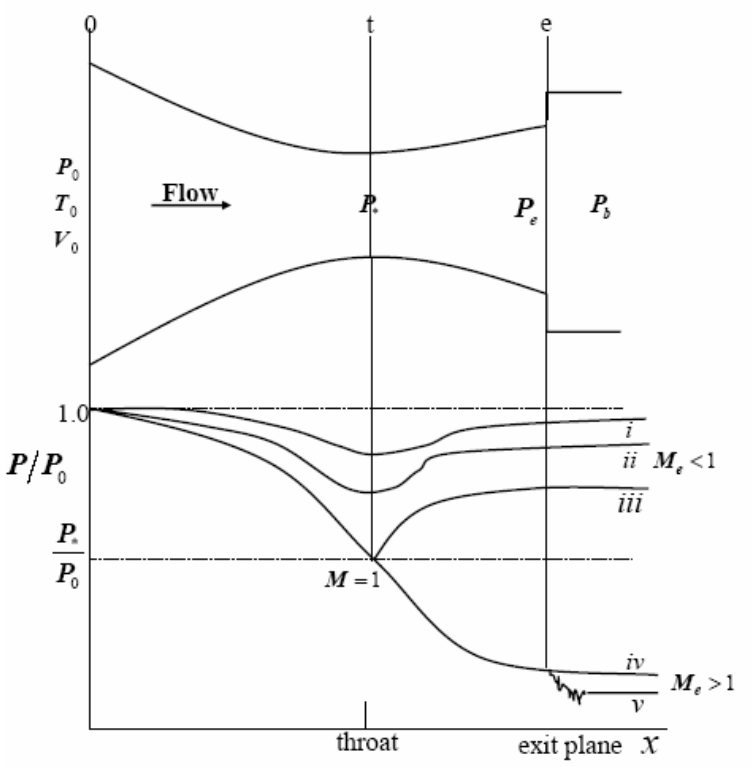

Figure 10. Effects of back pressure on the operation of a converging-diverging nozzle, reprinted from Liao, 2008

When the back pressure is reduced further, below P_*, such as conditions (*iv*) and (*v*) in Figure 10, Where P_b is below P_*, the condition at the nozzle throat section does not change; thus, neither the pressure nor mass flow is affected by this reduction because the velocity at its throat is fixed at a Mach number of unity. However, the reduction of back pressure causes adjustments of flow downstream of the nozzle throat. For example, in case (*iv*) and (*v*), the pressure is decreased as the fluid expands isentropically through the nozzle and then increases to the back pressure outside the nozzle.

One-Dimensional Steady Flow in Ejector

The previous section presented the theoretical background for a nozzle, which, for the primary and secondary flows, forms the foundation for the ejector and its simulation. In this section, nozzle theory is combined with other theoretical elements to create the ejector theoretical model.

Keenan et al. (1950) assumed that the mixing of the two streams takes place inside the suction chamber with a constant or uniform pressure from the exit of the nozzle to the inlet of the constant-area section, which is essentially a nozzle. Munday and Bagster (1977) postulated that the primary flow spreads out without mixing with the entrained flow, and then induces a converging duct that entrains the secondary flow. This converging duct causes the induced flow to accelerate to a sonic velocity in some cases. The location where the induced flow reaches a sonic velocity is called the hypothetical, and it becomes an important part of the ejector. In this study, this hypothetical area is assumed to occur in the constant area section with uniform pressure.

As noted above, in this present study, we assume that the hypothetical throat occurs inside the constant-area section of the ejector, and as a result, the mixing of primary and secondary streams occurs inside the constant area section with uniform pressure as shown in Figure 11. This Figure 11 schematic diagram shows the mixing process of the two streams in the ejector and it provides significant insight into how the ejector operates.

The ejector model and analysis based on the following assumptions are made in support of the analysis:

1. The working fluid is an ideal gas with constant properties C_p and κ.
2. The flow inside the ejector is steady and one-dimension.
3. The kinetic energy at the inlets of the primary and suction ports, and along with the exit of the diffuser, are negligible.

4. For simplicity in deriving the one-dimension model, the isentropic relations are assumed to be applicable.
5. After exiting the nozzle, the primary flow spreads out, without mixing with the secondary flow until reaching the cross-section y-y (hypothetical throat), which is inside the constant area section, as shown in Figure 11.
6. The two streams mix at cross-section y-y (hypothetical throat) with uniform pressure, i.e. $P_{py} = P_{sy}$, which is upstream of the shock is at the cross-section s-s
7. The secondary flow isassumed to be choked at the cross-section y-y (hypothetical throat)
8. The inner wall of the ejector is assumed to be adiabatic

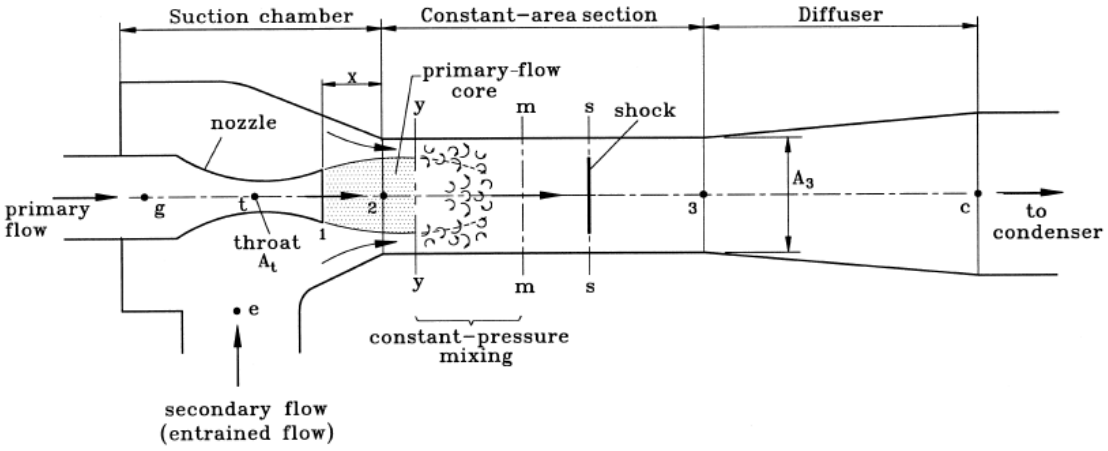

Figure 11. Schematic diagram of ejector layout and the fluid flow, reprinted from Huang 1998

Primary Flow at Nozzle

In the choking condition, for a given inlet stagnation pressure P_p and temperature T_p, the mass flow through the nozzle is governed by the gas dynamic equation that follows:

$$\dot{m}_p = \frac{P_p A_t}{\sqrt{T_p}} \sqrt{\frac{\kappa}{R}\left(\frac{2}{\kappa+1}\right)^{(\kappa+1)/(\kappa-1)}} \sqrt{\eta_p} \tag{24}$$

where η_p is the coefficient of isentropic efficiency for primary flow stream assuming compressible flow. Using the isentropic flow relations presented earlier as an approximation, the gas dynamic relationship between the Mach number at the exit of nozzle M_{p1} and the exit cross section area A_{p1} and pressure P_{p1} are as follows

$$\left(\frac{A_{p1}}{A_t}\right)^2 \approx \frac{1}{M_{p1}^2}\left[\frac{2}{\kappa+1}\left(1+\frac{(\kappa-1)}{2}M_{p1}^2\right)\right]^{\kappa+1/(\kappa-1)} \tag{25}$$

$$\frac{P_p}{P_{p1}} \approx \left(1+\frac{(\kappa-1)}{2}M_{p1}^2\right)^{\frac{\kappa}{\kappa-1}} \tag{26}$$

Primary Flow from Section 1-1 to Section y-y

For flow at section y-y, the isentropic approximation can be used to determine M_{py} as follows.

$$\frac{P_{py}}{P_{p1}} \approx \frac{\left(1+\left(\frac{\kappa-1}{2}\right)M_{p1}^2\right)^{\frac{\kappa}{\kappa-1}}}{\left(1+\left(\frac{\kappa-1}{2}\right)M_{py}^2\right)^{\frac{\kappa}{\kappa-1}}} \tag{27}$$

For the calculation of the of primary flow area at y-y section, Huang et al. introduces a coefficient ϕ_p, which accounts for loss in the primary flow from section 1-1 to section y-y

$$\frac{A_{py}}{A_{p1}} = \frac{\left(\frac{\phi_p}{M_{py}}\right)\left[\left(\frac{2}{\kappa+1}\right)\left(1+\left(\frac{\kappa-1}{2}\right)M_{py}^2\right)\right]^{(\kappa+1)/(2(\kappa-1))}}{\left(\frac{1}{M_{p1}}\right)\left[\left(\frac{2}{\kappa+1}\right)\left(1+\left(\frac{\kappa-1}{2}\right)M_{p1}^2\right)\right]^{(\kappa+1)/(2(\kappa-1))}} \tag{28}$$

This loss may result from the slipping or viscous effects at the boundary of both the primary and the entrained flows. It can be seen through that with the introduction of coefficient ϕ_p in Equation 28 above, the loss actually reflects the reduction of throat area A_{py} at the y-y section.

Secondary Flow from Inlet Through Section y-y

The secondary flow reaches a choking condition at the y-y section, i.e. M_{sy} = 1, and the pressure at section y-y for a given inlet stagnant pressure of the secondary flow can be expressed as follow

$$\frac{P_s}{P_{sy}^*} \approx \left(1+\frac{\kappa-1}{2}M_{sy}^2\right)^{\frac{\kappa}{\kappa-1}} \tag{29}$$

For sub-critical mode operations, it is assumed that there is an effective area where the velocity of the secondary flow is highest (but lower than the speed of sound in this case), and as such, the following equation is valid:

$M_{sy} < 1$

$P_{sy} > P_{sy}^*$

with the secondary flow rate at choking conditions being

$$\dot{m}_s = \frac{P_s A_{sy}}{\sqrt{T_s}}\sqrt{\frac{\kappa}{R}\left(\frac{2}{\kappa+1}\right)^{\frac{\kappa+1}{\kappa-1}}}\sqrt{\eta_s} \tag{30}$$

where η_s is the coefficient related to the isentropic efficiency of the secondary flow.

Cross-Sectional Area at Section y-y

The geometrical cross-sectional area at section y-y is A_3 which is the sum of the areas for the primary flow A_{py} and for the secondary flow A_{sy}, as follows

$$A_{py} + A_{sy} = A_3 \tag{31}$$

with the temperature and Mach number at section y-y being

$$\frac{T_p}{T_{py}} = 1 + \frac{\kappa - 1}{2} M_{PY}^2 \tag{32}$$

$$\frac{T_s}{T_{sy}} = 1 + \frac{\kappa - 1}{2} M_{sy}^2 \tag{33}$$

Mixed Flow at Section m-m Before The Shock

The primary and secondary flows start to mix at section, and then y-y. A shock then takes place resulting in a sharp pressure rise at section s-s. A momentum balance relationship can be derived as follows

$$\phi_m \left[\dot{m}_p V_{py} + \dot{m} V_{sy}\right] = \left(\dot{m}_p + \dot{m}_s\right) V_m \tag{34}$$

where V_m is the velocity of the mixed flow and ϕ_m is the coefficient accounting for the frictional loss. Similarly, an energy balance relationship can be derived as follows

$$\dot{m}_p \left(C_p T_{py} + \frac{V_{py}^2}{2} \right) + \dot{m}_s \left(C_P T_{sy} + \frac{V_{sy}^2}{2} \right) = \left(\dot{m}_p + \dot{m}_s\right) \left(C_p T_m + \frac{V_m^2}{2} \right) \tag{35}$$

where V_{py} and V_{sy} are the steam velocities of the primary flow and secondary flow respectively at section y-y

$$V_{py} = M_{py}a_{py}; \qquad a_{py} = \sqrt{\kappa R T_{py}} \tag{36}$$

$$V_{sy} = M_{sy}a_{sy}; \qquad a_{sy} = \sqrt{\kappa R T_{sy}} \tag{37}$$

Mixed Flow Across The Shock from Section m-m to Section 3-3

A supersonic shock takes place at section s-s, resulting in a sharp pressure rise. Assuming that the mixed flow after the shock undergoes an isentropic process, the mixed flow between section m-m and section 3-3 inside the constant-area section has a uniform pressure P_3. Therefore, the following gas dynamic relationships are applicable:

$$\frac{P_3}{P_m} = 1 + \frac{2\kappa}{\kappa + 1}(M_M^2 - 1) \tag{38}$$

$$M_3^2 = \frac{1 + \left(\frac{\kappa - 1}{2}\right) M_m^2}{\kappa M_m^2 - \left(\frac{\kappa - 1}{2}\right)} \tag{39}$$

Mixed Flow through The Diffuser

Assuming an isentropic process, the pressure at the exit of the diffuser is as follows

$$\frac{P_c}{P_3} = \left(1 + \frac{\kappa - 1}{2} M_3^2\right)^{\frac{\kappa}{\kappa - 1}} \tag{40}$$

For a given nozzle throat area A_t and nozzle exit area A_{pl}, the performance of an ejector is characterized by the stagnation temperature and pressure at the nozzle inlet (T_p,P_p) and the suction inlet port (T_s,P_s), and the critical back pressure P_c^*. Therefore, 5 independent variables

(T_p,P_p, T_s,P_s, P_c^*) are used in the ejector performance analysis. The analysis output includes the primary flow $\dot{m}_p$, the secondary flow $\dot{m}_s$, the entrainment ratio ER, along with the cross-sectional area A_3 and the area ratio A_3/A_t.

Vapor-Compression Refrigeration System

In addition to the background and theoretical model for the nozzle and ejector that is used in two of the four systems in this study, another important theoretical model that needs describing in preparation for a system simulation, is the vapor-compression refrigeration system. To summarize, the modeling theory and simulation is based on applying the general conservation of energy to each of four major components that make up a vapor-compression cycle and then utilizing available refrigerant properties to solve for state point conditions.

As noted earlier, vapor-compression refrigeration systems are the most common cooling and dehumidification systems in use today, and a typical system consists of an evaporator, compressor, condenser and expansion valve, as shown in Figure 12.

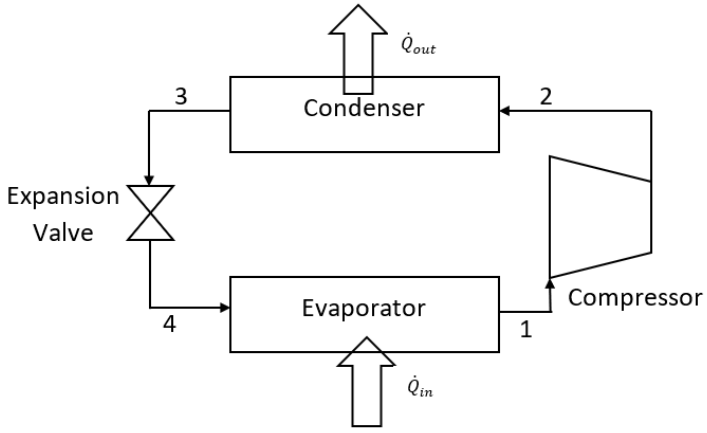

Figure 12. Schematic of a compression refrigeration system

In terms of simulations, it is important to note that kinetic and potential energy changes are neglected in the modelling and analysis of all four components. Because the simulations performed in this study are for ideal cycles, the following additional assumptions can be made based on ignoring irreversibilities.

1. There are no frictional pressure drops in the two heat exchangers, meaning the refrigerant flows is at constant pressure.
2. The heat transfer from and to the refrigerant occurs with a zero driving temperature, meaning the space and the surroundings are at the same temperature as the adjoining refrigerant.
3. The compressor follows an isentropic process.

The refrigeration cycle based on the above reversible assumptions, except for the throttling process, is commonly referred to as the *ideal vapor-compression refrigeration cycle*. The T-s diagram for the ideal refrigeration cycle and all of the component processores can be seen in Figure 13.

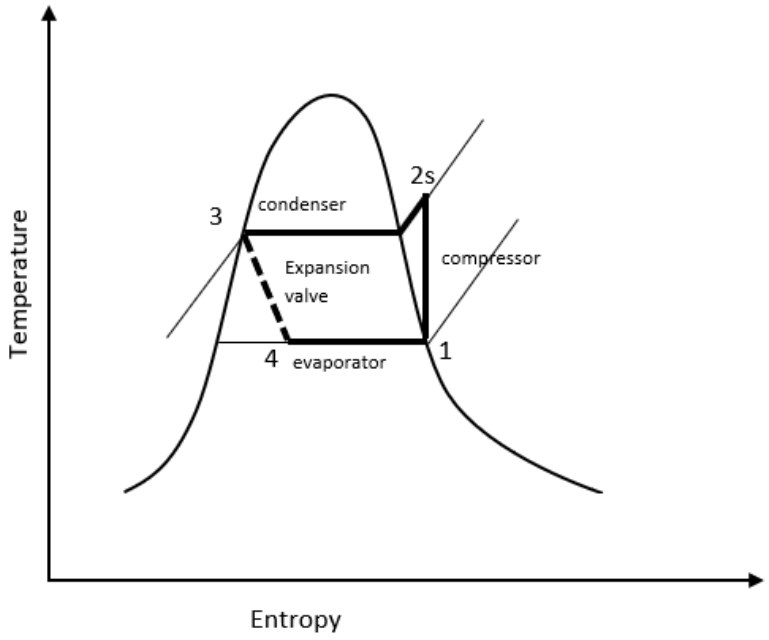

Figure 13. T-s diagram of idealized vapor-compression refrigeration system

As a first step in the simulation, models of all four components are derived by applying the conservation of energy to each component. Referring to Figures 12 and 13, the refrigerant passing through the evaporator from state 4 to 1, is evaporated as heat is transferred from the refrigerated space, via either an air or a water flow system, to the refrigerant. Using appropriate assumptions given earlier, the general energy rate equation can be reduced to a working equation as follows

$$\dot{Q}_{in} = \dot{m}(h_1 - h_4) \tag{41}$$

where $\dot{m}$ is the flow rate of the refrigerant. Of special importance, the heat transfer rate $\dot{Q}_{in}$ is referred to as the "refrigeration capacity".

The refrigerant exiting the evaporator as a superheated vapor at state 1, it is then compressed by the compressor to a state 2 superheated vapor at a higher pressure and temperature.

An energy rate balance on the compressor, assuming negligible heat transfer to or from the compressor, results in

$$\dot{W}_c = \dot{m}(h_2 - h_1) \tag{42}$$

Entering the condenser as a superheated vapor and exiting as a subcooled liquid, the rate of heat transfers from the refrigerant to the cooler ambient air, based on an energy balance is

$$\dot{Q}_{out} = \dot{m}(h_2 - h_3) \tag{43}$$

In the expansion valve, subcooled liquid enters the valve at state 3 and exits as a two-phase liquid-vapor mixture at state 4. The decrease in pressure caused by irreversible adiabatic expansion, is accompanied by increase in entropy. The expansion valve can be modeled as a throttling or constant enthalpy process, which results in

$$h_4 = h_3 \tag{44}$$

The coefficient of performance (COP), represents a cycle, thermodynamic efficiency is defined as the useful energy divided by the energy that must be input to all components, which is also the cost of operation. In the case of refrigeration cooling, the coefficient of performance (COP) of the vapor-compression refrigeration system is the refrigerating capacity, being the "useful" energy, divided by the "input", which is compressor work. Substituting useful energy and input work from the above equations, result in a working equation for the Coefficient of Performance (COP) as follows

$$COP = \frac{\dot{Q}_{in}}{\dot{W}} = \frac{h_1 - h_4}{h_2 - h_1} \tag{45}$$

The above COP equation is a general relationship that depends on refrigerant state conditions only. Therefore, it is in fact applicable to a cycle with irreversibilities, In the case of an

ideal or reversible cycle, except for the expansion valve, this COP value represents an upper limit, which still allows for an investigation of performance as a function of system parameters.

Steam-Ejector Refrigeration Systems

The steam-ejector refrigeration system is a heat-operated refrigeration cycle, unlike the vapor-compression refrigeration cycle presented in the previous section, which utilized electricity to drive a compressor. This cycle can be driven by low-temperature thermal energy, 100°C-200°C, which can be either waste heat from many industrial processes or else thermal energy relatively cheap to produce. Although it is classified as a heat-operated cycle, the system still requires some amount of mechanical power to circulate the working fluid, which is in a liquid phase, by means of a mechanical pump, with the power consumption of the pump being almost negligible compared to the thermal energy required.

System model, equations, and theory were presented earlier for the steam ejector; however, the actual hardware for a complete system and its operation can be described in the context steam ejector schematic shown in Figure 14. As the high-pressure steam P, known as the "primary fluid", expands and accelerates through the primary nozzle (*i*), it fans out with supersonic speed to create a low-pressure region at the nozzle exit plane (*ii*) and subsequently in the mixing chamber. This primary fluid's expanded wave is thought to flow and form a converging duct without mixing with the secondary fluid. At the same cross-section along this duct, the speed of the secondary flow chokes. This mixing then causes the primary flow to be retarded while the secondary flow is accelerated. By the end of the mixing chamber, the two streams are completely mixed, and the static pressure is assumed to remain constant until the flow reaches the throat section (*iv*). Due to a high-pressure region downstream of the mixing chamber's throat, a normal shock with essentially zero thickness, is induced (*v*). This shock causes a major compression effect

and a sudden drop in the flow speed from supersonic to subsonic. Further compression of the flow is achieved (*vi*) as it is bought to a stagnation condition through a subsonic diffuser.

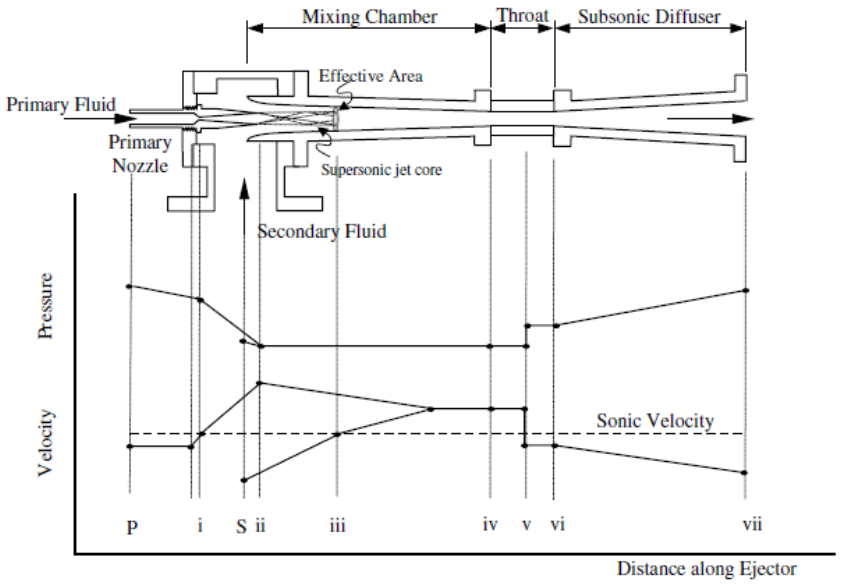

Figure 14. Schematic view and the variation in stream pressure and velocity as functions of location along a steam ejector, reprinted from Huang 1998

Figure 15 shows the schematic diagram of a complete steam-ejector refrigeration cycle, which also contains the steam ejector component described previously. Of special importance, a boiler, an ejector, and a pump can be used to replace the mechanical compressor of a conventional vapor-compression refrigeration system. As heat is added to the boiler, the ejector draws a low-pressure water vapor, which is the secondary fluid, from an evaporator. The liquid water evaporating at the low pressure gets its energy from the remaining liquid water, thus lowering its temperature and producing the cooling effect of useful refrigeration. The ejector discharges its exhaust, which includes the secondary fluid, to the condenser where it is liquefied again by rejecting heat to the ambient temperature. Part of the liquid is then pumped back to the boiler (primary fluid) while the remainder is returned to the evaporator (secondary fluid) via the throttling

device. The input required for the pump is typically less than 1 % of the heat supplied to the boiler. So that, the actual COP is follow

$$COP = \frac{refrigeration\ effect\ at\ evaporator}{heat\ input\ at\ the\ boiler} \tag{46}$$

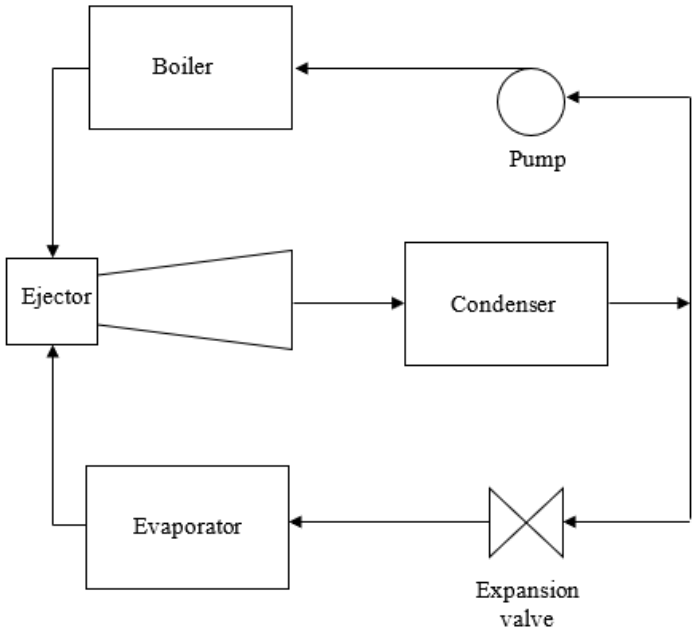

Figure 15. Schematic of steam-ejector refrigeration system

Figures 16 and 17 show typical performance curves, meaning COP as a function of condenser pressure and boiler temperature for a steam-ejector refrigeration cycle. At condenser pressures below the "critical value", the ejector entrains the same amount of secondary fluid, meaning changing the condenser pressure has no effect. This in turn causes the cooling capacity and COP to remain constant, a phenomenon caused by the flow choking within the mixing chamber. When the ejector is operated in this pressure range, then a transverse shock, which creates a compression effect, is found to appear in either the throat or diffuser section. The location of the shock process varies with the condenser back pressure. In that, if the condenser pressure is

further reduced, the shock will move toward the subsonic diffuser. When the condenser pressure is increased higher than the critical value, then the transverse shock tends to move backward into the mixing chamber, and then it interferes with the mixing of the primary and secondary fluid. As a result, at the higher condenser pressure, the secondary flow is no longer choked, causing the secondary flow to vary, and the entrainment ratio begins to fall off rapidly. If the condenser pressure is increased further, then the flow will reverse back into the evaporator, and the ejector loses its function completely.

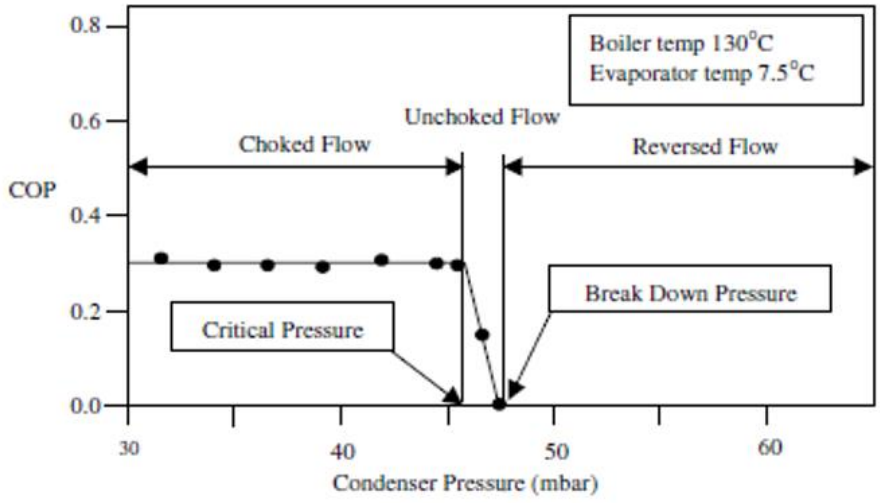

Figure 16. Performance of a steam jet refrigerator based on experimental data, reprinted from Eames and Aphornratana, 1997

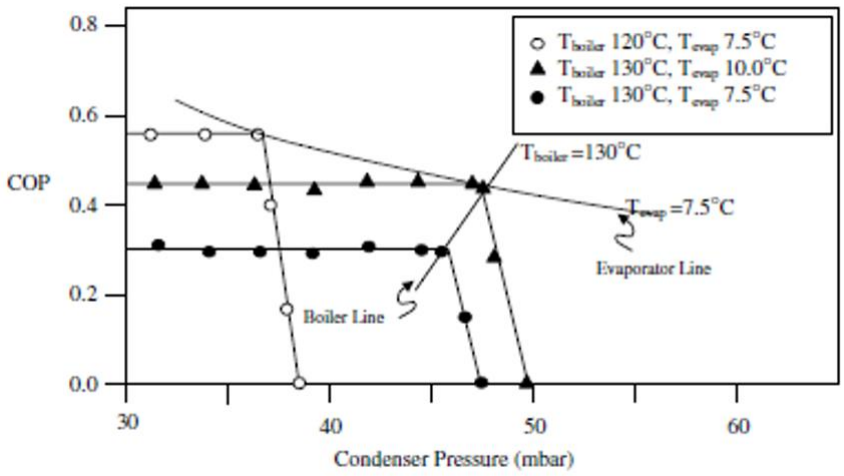

Figure 17. Effect of operating temperatures on performance of a steam jet refrigerator based on data reprinted from Eames and Aphornratana, 1997

As mentioned earlier, if the condenser pressure is below the critical value, then the mixing chamber is always choked, so that, the flow rate of the secondary flow, is independent from the downstream (condenser) pressure. In these cases, the water vapor is evaporated from the liquid causing the cooling on refrigeration effect. The flow rate can only be raised by an increase of the upstream (evaporator) pressure. since the critical condenser pressure is dependent on the momentum and pressure of the mixed flow.

A decrease in the boiler temperature and pressure causes the primary fluid mass flow to be reduced. Because the flow area in the mixing chamber is constant, an increase in the secondary flow results, which in turn causes the cooling capacity and COP to rise as shown in Figure 17. However, this causes the momentum of the mixed flow to drop, and the critical condenser pressure is reduced. On the other hand, an increase in the evaporator pressure, or the ejector's upstream pressure, will increase the critical condenser pressure, which in turn increases the mass flow through the mixing chamber as well as cooling the capacity and COP. Even though raising the

evaporator pressure helps to increase the entrainment ratio, the net result is a sacrifice of the desired cooling capability.

Psychrometric Principles

Psychrometrics is the study of dry air and water vapor mixtures, otherwise known as moist air, with ambient air being the most common example. In fact, it is fair to say that dry air does not exist except in carefully controlled laboratory conditions. In this section, important parameters that characterize moist air, along with equations that relate to these parameters, are introduced. There are two processes that are important for membrane-ejector dehumidification cycles, namely dehumidification and adiabatic mixing, which are modelled by using energy and mass balances. The most important parameter for characterizing the composition of moist air is humidity ratio ω, which is often referred to as the specific humidity, and it is defined as the mass ratio of water vapor and dry air, as follows

$$\omega = \frac{m_v}{m_a} \tag{47}$$

Humidity ratio can be related to other parameters by using the ideal gas equation for water vapor and dry air. Resulting in,

$$m_v = \frac{p_v V M_v}{\bar{R} T} \tag{48}$$

$$m_a = \frac{p_a V M_a}{\bar{R} T} \tag{49}$$

Combining the above equations, while cancelling out gas constants, temperature, and volume, the humidity ratio can then be expressed in term of water vapor partial pressure. After plugging in the molecular weight ratio of water to dry air, which is 0.622, and substituting $p_a = p - p_v$ where p is the total pressure (e.g. atmospheric pressure), the resulting equation is

$$\omega = 0.622\frac{p_v}{p - p_v} \tag{50}$$

The humidity ratio can also be written in terms of relative humidity ϕ, defined as the ratio of the actual water-vapor partial pressure, p_v, to the maximum possible partial pressure, which is the saturation pressure, p_{sat}, corresponding to the dry bulb temperature of the moist air, with the result being

$$\phi = \frac{p_v}{p_{max}} = \frac{p_v}{p_{sat}(T)} \tag{51}$$

One of the useful function of the above relative humidity relationship is that it can be used to calculate water vapor partial pressure as follows.

$$p_v = \phi p_{sat}(T) \tag{52}$$

The humidity ratio can then be written in terms of relative humidity as follows

$$\omega = 0.622\frac{\phi p_{sat}(T)}{p - \phi p_{sat}(T)} \tag{53}$$

Another important parameter in psychrometrics is the dew point temperature, which is defined as the saturation temperature corresponding to the actual water vapor partial pressure. The importance of the dew point is that if a moist air sample is cooled, then the temperature where liquid droplets first appear is the dew point. In addition, if one knows the dew point temperature then the actual water vapor partial pressure is the corresponding saturation pressure.

The enthalpy of the moist air is an important parameter that is used in the conservation of energy as applied to psychrometrics. For example, in dehumidification or adiabatic mixing process, the total enthalpy for a moist air sample is found by summing the component enthalpies of dry air and water vapor as follows

$$H = H_a + H_v = m_a h_a + m_v h_v \tag{54}$$

For ease of use, it is better to define moist air enthalpy in terms of humidity ratio and units of dry air mass by dividing by mass of dry air to obtain h_m, kJ/kgair, as follows

$$h_m = \frac{H}{m_a} = h_a + \frac{m_v}{m_a} h_v = h_a + \omega h_v \tag{55}$$

The individual dry air and water vapor enthalpy are evaluated at the mixture temperature, otherwise called the dry bulb temperature. In the case of the water vapor enthalpy, h_v the saturated vapor enthalpy at the dry bulb temperature is used, as a word of caution, when selecting the individual component enthalpies, the same reference point temperature must be used for dry and water vapor or else corrections for the reference point values must be applied, which are relatively straight forward in the case of dry air, especially when specific heats are being used for determining enthalpies.

For moist air being cooled by a cold surface or a cooling coil, a constant humidity ratio process is followed, which also corresponds to a constant water-vapor partial pressure. Eventually, if cooling continues until the dew point is reached then water droplets form, from the water vapor. As additional condensation occurs, it continuously reduces the humidity ratio and vapor partial pressure, with moist air remaining saturated or at a 100% relative humidity condition. The above process where air is cooled to the saturation point or 100% relative humidity, so that the water vapor is condensed and removed from the moist air is called dehumidification, and the device that accomplishes this is called a dehumidifier. Both the dehumidification process and the dehumidification device are shown in Figure 18. In actual HVAC practices, discharging dehumidified air at 100% relative humidity to a space can cause material and comfort problems, therefore, reheating at constant humidity ratio is often employed.

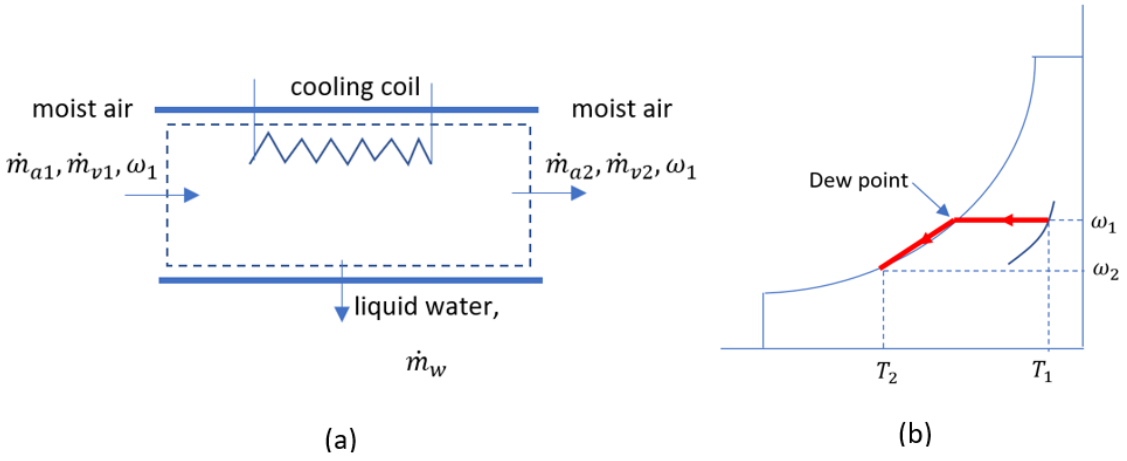

Figure 18. Dehumidification. (a) Equipment schematic. (b) Psychrometric chart representation.

Of special importance for the study performed herein, reducing the humidity ratio or dehumidifying air can also be accomplished directly without cooling to 100% relative humidity or to the dew point. An important example in terms of this study is using the membrane in the membrane-ejector dehumidification system to remove water vapor from the adjoining flow stream, which is typically in ambient air. For this case, the humidity ratio of the flowing air is reduced in a constant temperature process without the need for cooling. Water removal from the air, including for the case of the membrane-ejector system can be found from a mass balance on the water. so that, the resulting water removed, liquid in the case of cooling and vapor in the case of the membrane-ejector system, as follows

$$\dot{m}_w = \dot{m}_{v1} - \dot{m}_{v2} \tag{56}$$

If $\dot{m_{v1}} = \omega_1 \dot{m}_{a1}$ and $\dot{m}_{v2} = \omega_2 \dot{m}_{a2}$, are substituted into the above equation then the amount of water removal either in a liquid or vapor phase from air passing through the dehumidifier is

$$\dot{m}_w = \dot{m}_a(\omega_1 - \omega_2) \tag{57}$$

Adiabatic Mixing of Two Moist Air Streams

For the membrane-ejector dehumidifier system, it is possible that two adiabatic flow streams undergo mixing as shown in Figure 19. For modelling purpose, the state points of the two flow streams, namely 1 and 2, that join are used to find the exiting stream at state point 3, which is on a line connecting 1 and 2. An example of the schematic flow diagram and the process with state points on a psychrometrics chart are shown in Figure 19.

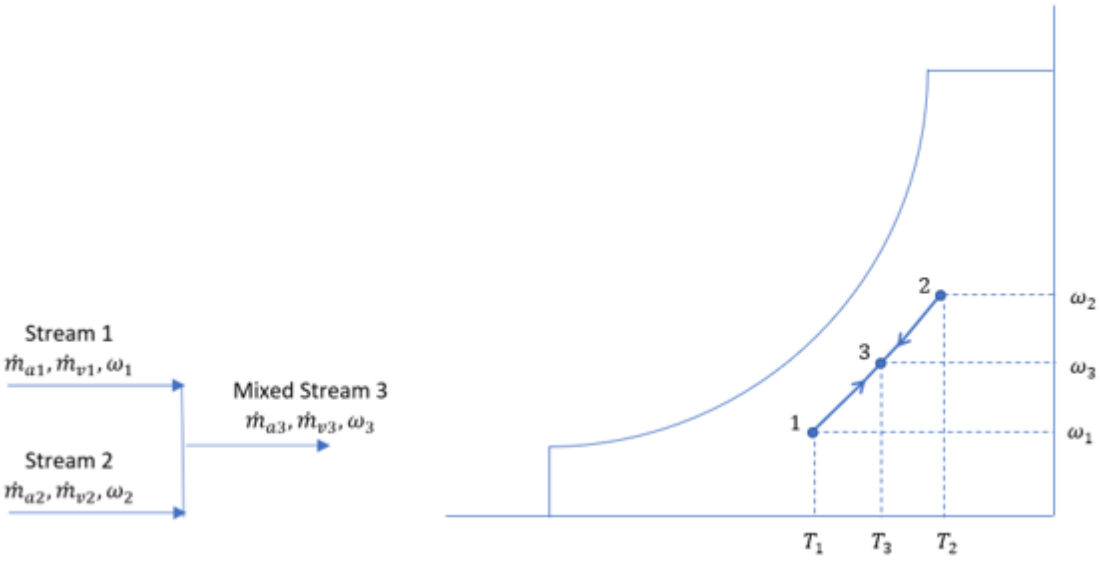

Figure 19. Adiabatic mixing of two moist air streams

The governing equations for this mixing process are based on separate mass balances for dry air and water vapor as follows

dry air:

$$\dot{m}_{a1} + \dot{m}_{a2} = \dot{m}_{a3} \tag{58}$$

water vapor:

$$\dot{m}_{v1} + \dot{m}_{v2} = \dot{m}_{v3} \tag{59}$$

and plugging into the humidity ratio, ω_3 the result is

$$\omega_3 = \frac{m_{v3}}{m_{a3}} = \frac{\dot{m}_{v1} + \dot{m}_{v2}}{\dot{m}_{a1} + \dot{m}_{a2}} \tag{60}$$

As we can see in Figure 19, the exiting flow is defined by two properties and so a second property is needed to go with the fluid property ω_3. This second property needed to define the state is T_3, and it can be found from an energy rate balance, assuming zero heat transfer and work, while neglecting kinetic and potential energy change. So that, the resulting equation is

$$\dot{m}_{a1}\left(h_{a1} + \omega_1 h_{g1}\right) + \dot{m}_{a2}\left(h_{a2} + \omega_2 h_{g2}\right) = \dot{m}_{a3}\left(h_{a3} + \omega_3 h_{g3}\right) \tag{61}$$

where the enthalpies of the entering and exiting water vapor are taken as saturated vapor values at their respective dry bulb temperatures.

CHAPTER III

RESEARCH METHODOLOGY

In this research, modeling simulations are carried out to obtain and analyze the performance characteristic of each of four different types of refrigeration systems. Of special importance, the simulation processes use assumptions, especially ideal assumption except in the case of the membrane, to simplify the models and analysis. Each simulation case is run individually, separately from the others, with an emphasize on evaluating system performances as a function of parameters and variables to the point of providing insight into how each system performs and how they can be improved. These simulations were performed, by using the Engineering Equation Solver (EES), along with thermodynamic properties in the software. This chapter will explain the process of simulation and describe the parameters that as input and output in the simulation. Each of the four scenarios will be evaluated for the same input parameters and conditions and in the case of ejectors extra optimization steps are necessary for identifying the best values of the design parameters.

Vapor-Compression Refrigeration Systems

The vapor-compression refrigeration cycle uses refrigerants while the ejector systems use water as the working fluid, which is both cheap and abundant. The refrigerant candidates for this study are “R-22” and “R-410A”. Although R-22 is discontinued for use in new air conditioning systems, many systems today still operate with it, making it the reference fluids.

A simple idealized vapor-compression refrigeration system is assumed for the simulation with a system schematic for simulation being shown in Figure 20.

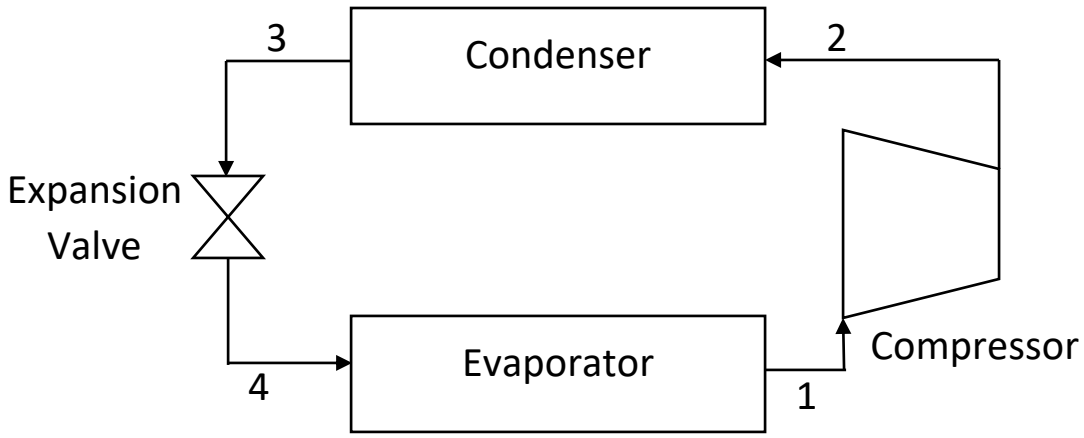

Figure 20. Schematic of vapor-compression refrigeration system.

The following assumptions are used in the simulations

- The system uses reversible processes in the evaporator, compressor, and condenser.
- Processes are adiabatic for all components.
- The friction loss of the refrigerant is neglected.
- The temperature difference between the refrigerant in the condenser and hot region along with the refrigerant in the evaporator and cold region is neglected.
- The output flow from the evaporator is saturated vapor and output of condenser is saturated liquid.

Limitations on refrigerant operating pressures have been established, and they are presented in Table 1.

Table 1. Operating condition for R22 and R410A

Refrigerant	R-22	R-410A
Allowable low-pressure	68 psi (470 kPa)	118 psi (815 kPa)
Allowable high-pressure	250 psi (1724 kPa)	400 psi (2760 kPa)

The input of the system.

The range of inputs representing typical indoor and outdoor conditions, otherwise referred to low and high region temperatures is presented in Table 2.

Table 2. Input parameter for vapor-compression refrigeration system

Input	low-temperature	high-temperature
Temperature (C)	6-18°C, step = 3°C	27-33°C, step = 3°C
Pressure (kPa)	100 kPa	100 kPa
Humidity Ratio	0.0214 kgv/kga	0.0101 kgv/kga
Relative Humidity	Assumed to be 100 %	70%

The number of simulations based on the inputs that were performed are 3 × 5 times with the high-temperature steps being 3°C for 3 setpoints and the low-temperature steps being 3°C for 5 setpoints. The cold region has a 100% relative humidity as the assumption, so that, the setpoint temperature at the low temperature is the dew point condition for the cold region.

Ejector Refrigeration Systems

The system uses the ejector to pressurize steam and to induce vapor from a vacuum condition as shown in the system scenario presented in Figure 21. Huang et al. (1999) conducted

experiments to analyze the performance characteristics of ejectors. This performance is used to predict the theoretical area in the ejector that results in higher performances for the boiler and the best vacuum condition. The mathematical model based on gas dynamic relations developed by Keenan et al. (1950) was used in the Huang's experiment to predict the characteristics of the ejector. Additionally, from the experimental results, Huang determined coefficients for the primary flow efficiency (η_p), the secondary flow efficiency (η_s), including the loss coefficient due to geometry (ϕ_p), and the loss coefficient due to mixing (ϕ_m). These coefficients can all be used by engineers to predict the characteristic of ejectors for particular working fluids, such as water, for range of operating conditions.

-

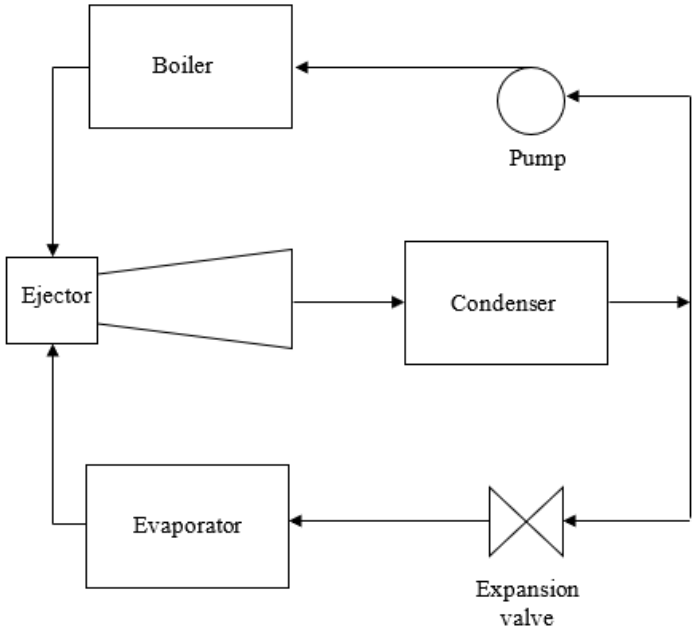

Figure 21. Schematic of steam-ejector refrigeration system

An additional investigation was conducted by Chen et al. (2013) to find the predicted ejector performances in both the critical and subcritical regions, with model results also being validated with past experiments for a range of refrigerants. Furthermore, they claimed that the

model can predict performances accurately, with error margins being less than 20%. Therefore, this model is used in this study to predict the ejector performance, with some modifications being made to the Mach number estimation at the hypothetical area (A_{sy})

As explained in Chapter 4, a simple ejector model was obtained and then combined with a refrigeration cycle model to obtain a combined model capable of being used to evaluate the effect of ejector performance on the refrigeration system. The simulations were performed by changing input temperature variables in the hot and the cold regions. Because the ejector works in a critical condition, the boiler pressure was adjusted to meet this condition, which in turn affected the COP results. As a final note, the input parameters used in the ejector refrigeration system are the same as those in Table 2. for vapor-compression refrigeration system.

In this simulation, certain assumptions are applied to the steam-ejector refrigeration system in order to simplify and remove individualized component performance factors, such as condenser and evaporator heat transfer coefficient, which are in most cases difficult to determine and beyond the scope of this study. Therefore, similar to the vapor-compression refrigeration system, the steam-ejector refrigeration cycle is treated as an idealized system based on the following assumptions:

- reversible heat transfer for condenser and evaporator, meaning the temperature difference between working fluid (water/steam) and ambient air is neglected.
- processes are adiabatic and reversible in all components, except the throttling process.
- The friction effects in piping and fitting are neglected.
- The ejector process operates in critical condition.
- The boiler output is saturated vapor, the condenser output is a saturated liquid.

The simulation of steam-ejector refrigeration system is carried out in Engineering Equation Solver (EES) by utilizing the property of water in its library. The outputs of the

simulation are Coefficient of Performance (COP), the thermal energy required by the system (Q_{in}), and the entrainment ratio (ER). As noted, a schematic of the ejector refrigeration system that was modeled in EES is shown Figure 21.

Membrane-Ejector Dehumidifier

The membrane-ejector dehumidifier system that is presented and described in this study is a new technology has not been studied, or even been mentioned for that matter, in the open literature. This membrane-ejector dehumidifier system operates by essentially creating vacuum on one side of a membrane by using a steam ejector, and then using this vacuum to draw water vapor from ambient air that is flowing at atmospheric pressure on the other side of the membrane, thus creating a dehumidification process.

A schematic of membrane-ejector dehumidifier is shown in Figure 22 on the vacuum side, two ejectors are arranged in series in order to create an even lower vacuum pressure, than would be possible with only one ejector. The operation of the ejector requires that additional steam, known as the primary flow, be added to the fluid that passes through the membrane, which is known as the secondary flow. Consequently, heat is rejected to the environment by condensing the mixing flows steam in the condenser.

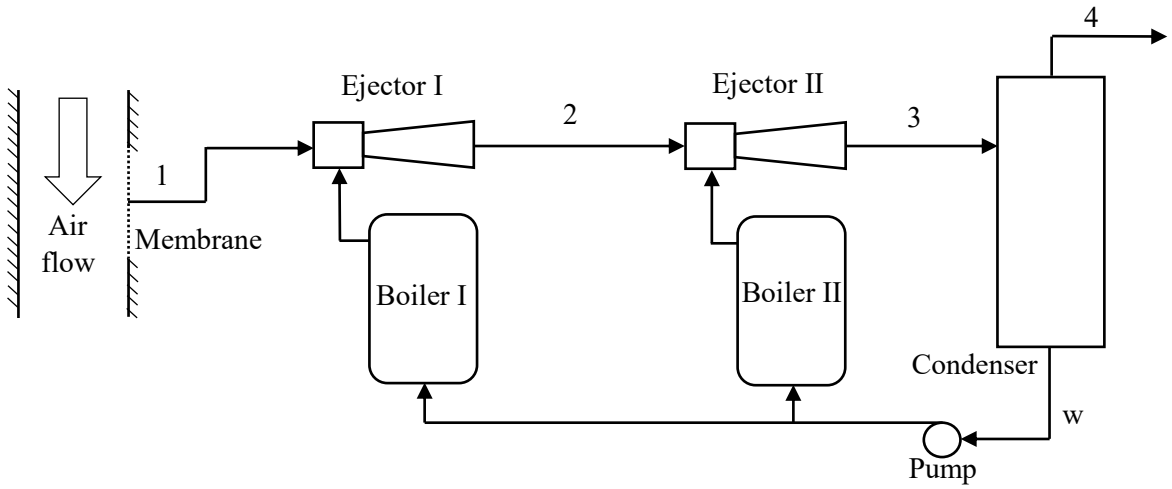

Figure 22. Schematic of membrane-ejector dehumidifier

As can be seen in the Figure 22 schematic, the system operates with the boiler being supplied by condensate water from the water vapor that is condensed in the condenser. In the simulation, the membrane is not ideal in that it allows both water vapor and air to pass through to the vacuum side. If the membrane worked ideally, then it would preclude any air from passing to the vacuum side of the membrane, and the COP would undoubtedly be much larger. The transfer of fluids, whether it is water vapor or air, through the membrane occurs due to the vacuum condition at point 1, which is caused by the ejector system. Furthermore, the ejector forms the vacuum as the high-pressure stream from the boiler mixes with the membrane stream in the ejector, in which, is where the pressure increases to the state 2 condition. However, the partial pressure at the state 2 condition is not high enough to condense the water vapor in the mixture and therefore, it is necessary to install the second ejector to further increase the temperature and pressure to state 3. At this state, the pressure is high enough to condense the water vapor, meaning the saturation temperature of the water vapor is higher than the ambient temperature air used to cool the condenser. The net result is to decrease the humidity ratio of the fluid flow rejected to environment, which required the use of an energy-consuming vacuum pump.

The performance of the ejector is determined by the geometry of the ejector, and therefore, optimization is performed in this simulation by changing the geometry of both ejectors in order to find the best performance for a given mass flow rate. Therefore, to find the minimum energy consumption by the boilers, the system was simulated for many cases. Using a range of input variables and geometries for specific operating conditions. Example of inputs that are important for the system are listed in Table 3.

Table 3. Input parameters for the membrane-ejector dehumidifier.

Parameter	Value
Mass flow of air from membrane (m_{sa})	0.4 kg/hr
Mass flow of water vapor from membrane (m_{sv})	5.2 kg/hr
Vacuum Temperature (T_{s1})	27-33°C
Vacuum pressure (p_{s1})	1.6 kPa
Ambient temperature (T_{amb})	27-33°C
Ambient pressure (p_{amb})	100 kPa
Outlet pressure of dehumidifier (p_{s5})	11.3 kPa
Boiler Temperature (T_p)	90-150°C
Nozzle diameter of ejector I (d_{t1})	2.5 mm

As can be seen in Table 3, the membrane used in this study is assumed to transport a specific amount of water vapor and air to the vacuum chamber on low-pressure side of membrane. The above amounts, namely 0.4 kg/hr for air and 5.2 kg/hr for water vapor, are based on the ambient air losing water vapor as it passes over the membrane until its water vapor partial pressure is assumed to have the same partial pressure as on the vacuum side of the ejector. It is also

important to note that these flow rate value are for one specific non-ideal membrane used in recent experiments. In that regard, the results of this simulations are presented only as an example of how the models developed and presented in this can be in future analysis and design. For these parameters, the size of the first ejector can be optimized, which matches the supply of steam from the boiler for a critical condition. The output of ejector 1 then enters ejector 2 where optimization is again performed to find the correct geometry and boiler pressure that enables the ejector to induce the water vapor at the critical condition.

The optimization of the ejector is carried out by running simulations with different boiler temperatures, because boiler temperature controls the ability of the ejector to entrain the water vapor and air that passes through the membrane, also, different optimum geometries for the ejector correspond to different boiler temperatures. Minimum boiler energy consumption is the objective for optimization, in addition to entrainment ratio (ER). The flowchart of the simulation process and optimization is presented in Figure 23.

Similar to the other two systems, the membrane-ejector dehumidifier model is assumed to be idealized except for the membrane and the mixing process where the mixing coefficient (ϕ_m) is assumed to be 0.88 taken from Huang et al. (1999). Furthermore, the assumptions applied to the system are

- The process is adiabatically reversible in all components.
- No temperature difference between water vapor inside condenser and the ambient temperature (perfect heat transfer).
- No friction loss in the system.
- The boiler produces saturated steam.
- The outlet of the ejector is in saturated steam.
- The pump operates with isentropic compression.

- Membrane is non-ideal, allowing air to pass through with the water vapor.

The simulation focuses on the entrainment ratios and coefficient of performance as a function of other parameters along with the characteristics of the ejector. Since the system simulated has two boilers, the coefficient of performance, useful divided by cost, is defined as follows:

$$COP = \frac{\dot{H}}{Q_{in1} + Q_{in2}} \tag{62}$$

Where $\dot{H}$ is the total mixture energy passing through the membrane, while Q_{in1} and Q_{in2} are the heat inputs to the boiler. Because the work of the pump is less than 1% of total energy input, it can be neglected

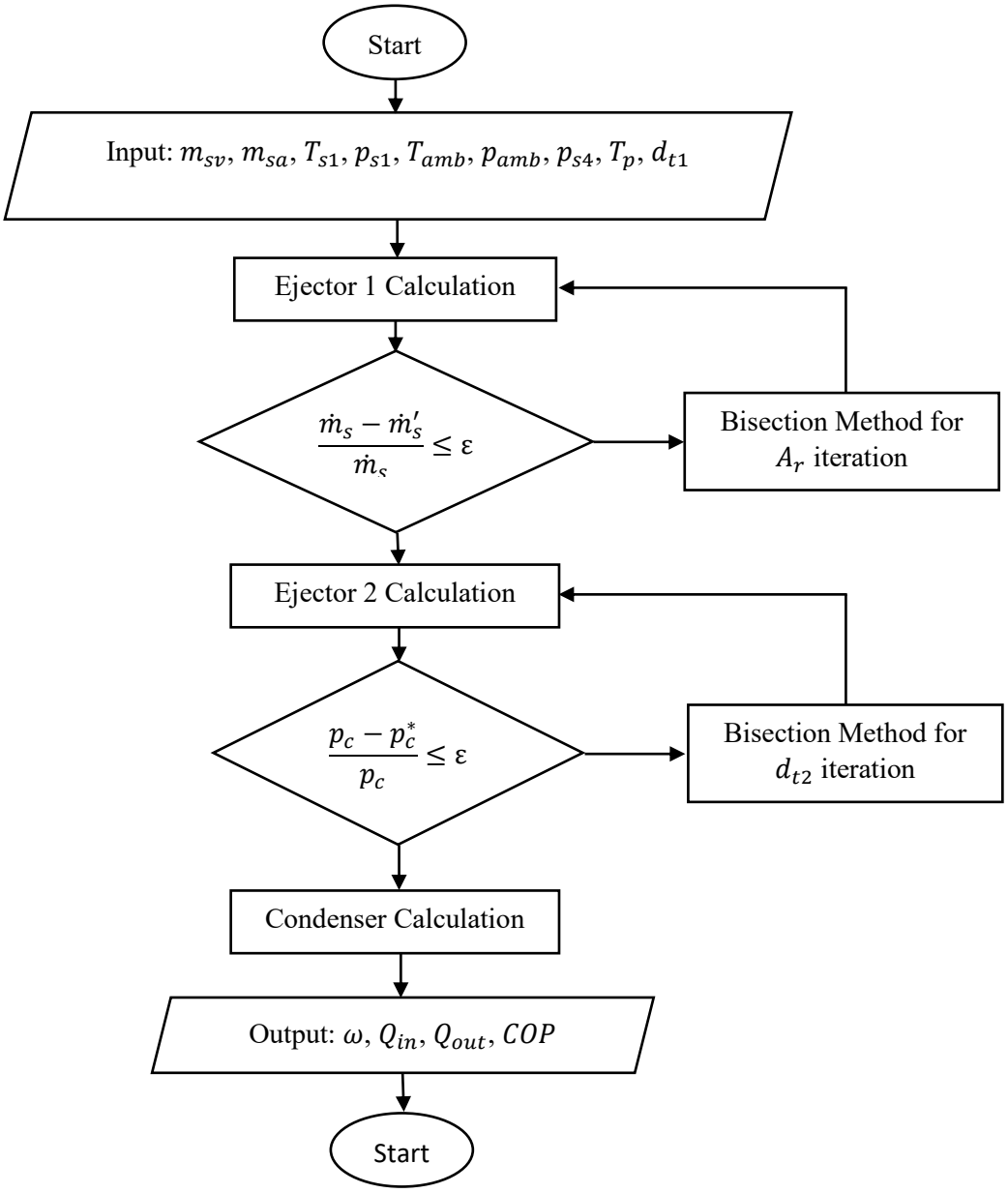

Figure 23. Flowchart of membrane-ejector dehumidifier calculation

As can be seen in the Figure 23 system simulation flowchart. the iteration is carried out in first and second ejector calculations. The parameter that can affect and adjust mass flow rate the most is area ratio (A_r), because this parameter determines the size of the hypothetical area of the

secondary flow (A_{sy}) required to reach critical conditions. The iteration uses the bisection method since this method gives a less expensive calculation process, and in addition, it can reduce the calculation time by only 10% for a step increase in iterations. In the second ejector, the optimization is carried out by checking the downstream pressure (p_c) as input, which should match (p_c^*) the calculation at the critical condition. The downstream pressure can be adjusted by finding the nozzle diameter geometry for the primary flow in ejector 2 (d_{t2}). The condenser liquifies the water vapor by rejecting heat to the ambient. Finally, the output parameters of this dehumidifier system predict the coefficient of performance (COP) for the ejector system, again as shown in Figure 23 flowchart.

CHAPTER IV

EJECTOR MODEL SIMPLIFICATION

The procedure used herein for ejector modeling is similar to that used in Chen's study to obtain the characteristic of ejector performance. However, in the study reported herein, the modeling effect focus on simplification by fixing some constraints and by using given assumption. The entrainment ratio, which is an important performance parameter is a function of numerous parameters, $ER = f(p_p, p_s, p_c, T_p, T_s, A_t, A_r)$. Based on following assumptions, the model can be simplified:

- Ejector operates in critical conditions for both primary and secondary flows, so that $(M_p = M_{sy} = 1)$.
- Ejectors work with idealized conditions such as ($\eta_p = \eta_s = \phi_p = \phi_m = 1$).
- The water vapor exiting the boilers, and condenser is in a saturated condition.
- The ejector is adiabatic, reversible.
- The shocks occur within the constant area section of the ejector.

The process of ejector simplification using these assumptions is explained in this chapter with the background that this is the most important component in the steam-ejector refrigeration system and the membrane-ejector dehumidification system. The procedure to obtain the simplification form is described in the Figure 24 flowchart.

In this procedure, the output is either a critical condition or subcritical condition. The geometries of the ejector in this study are taken from experimental studies, especially experimental studies performed by Eames and Aphornratana (1997). These geometries are sizes of the ejector that one would expect for air conditioning applications. Based on the above discussion, the input parameters for the ejector are described as follows:

- Saturated temperature of boiler T_p : 90 - 100°C
- Saturated temperature of vacuum T_s : 6 - 18°C
- Saturated temperature of downstream T_c : 27 - 33°C
- Nozzle throat diameter d_t : 2 mm
- Constant area section d_3 : 19 mm, 24 mm, 29 mm
- Error tolerance ε : 0.2%
- Working fluid : Steam

These parameters are input to the simulation, and the iteration step parameter is the Mach number at a hypothetical area (M_{sy}), which is used to determine whether the condition is either in the critical mode or subcritical mode. For this study, the iteration step parameter (ΔM_{sy}) is set to be 0.01. The pressure of the boiler, vacuum, and downstream are obtained from the steam thermodynamic tables for a saturated vapor condition, which Huang used to predict the ejector performance in their study.

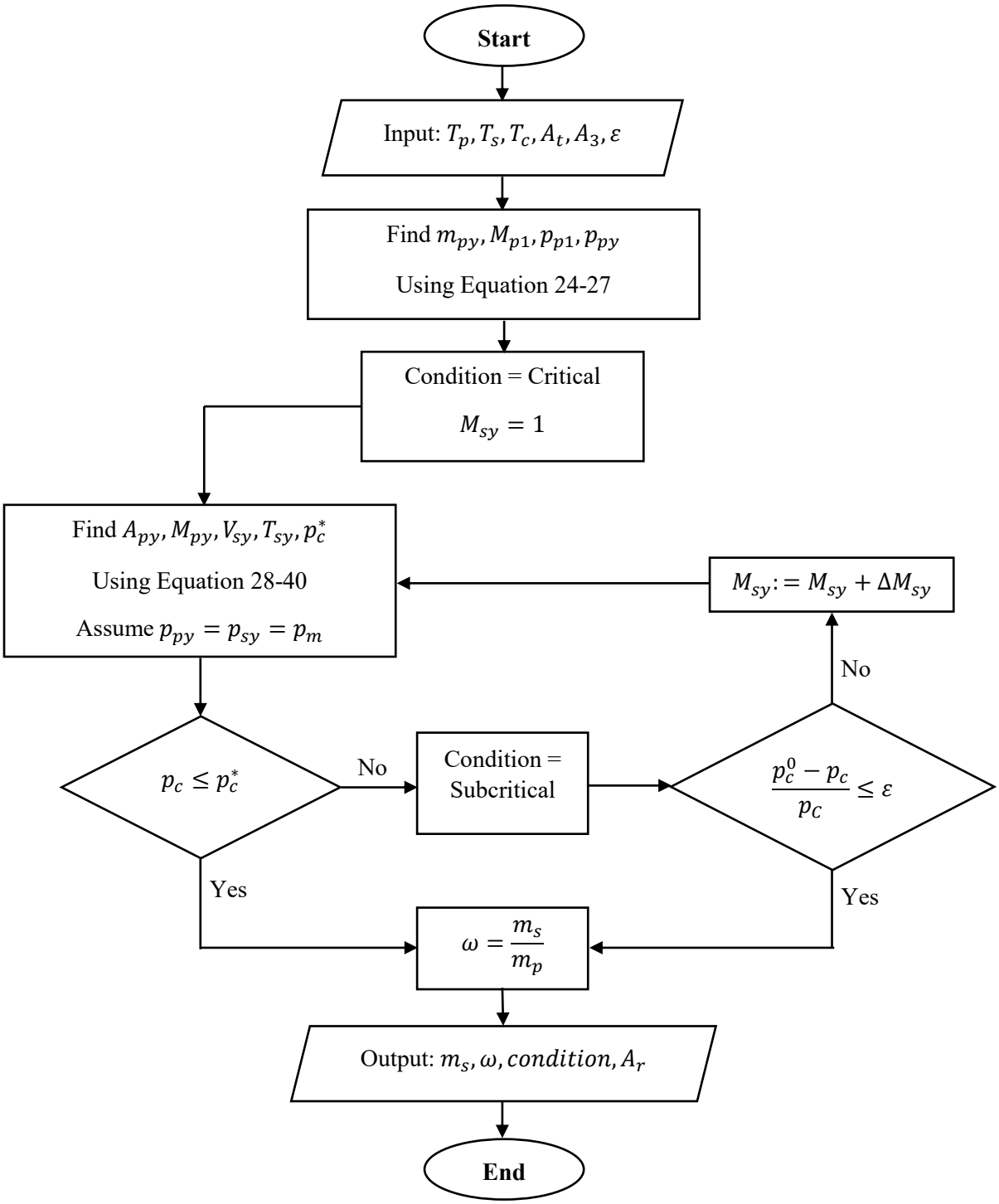

Figure 24. Flowchart of ejector calculations for critical and subcritical conditions

The inputs ranges used in the simulation were set to the needed conditions driving the operation of the steam-ejector refrigeration system by using incremented step change. For example, with the saturated temperature of the boiler (T_p) was varied from low to high temperatures by increasing in 10°C increments for every simulation. This variation also applies to other parameters, such as the saturated temperature of the vacuum (T_s), and the saturated temperature of discharge (T_c) both increasing by 3°C for both inputs.

The Figures 25 comparison between the model in this study and the experimental data of Huang validate the simplified model. This validation uses parameters from the study conducted by Huang including the coefficient of loss such η_p, η_s, ϕ_p, and ϕ_m as inputs. Huang's study used refrigerant R141b as the working fluid. The result of validation can be seen as follows.

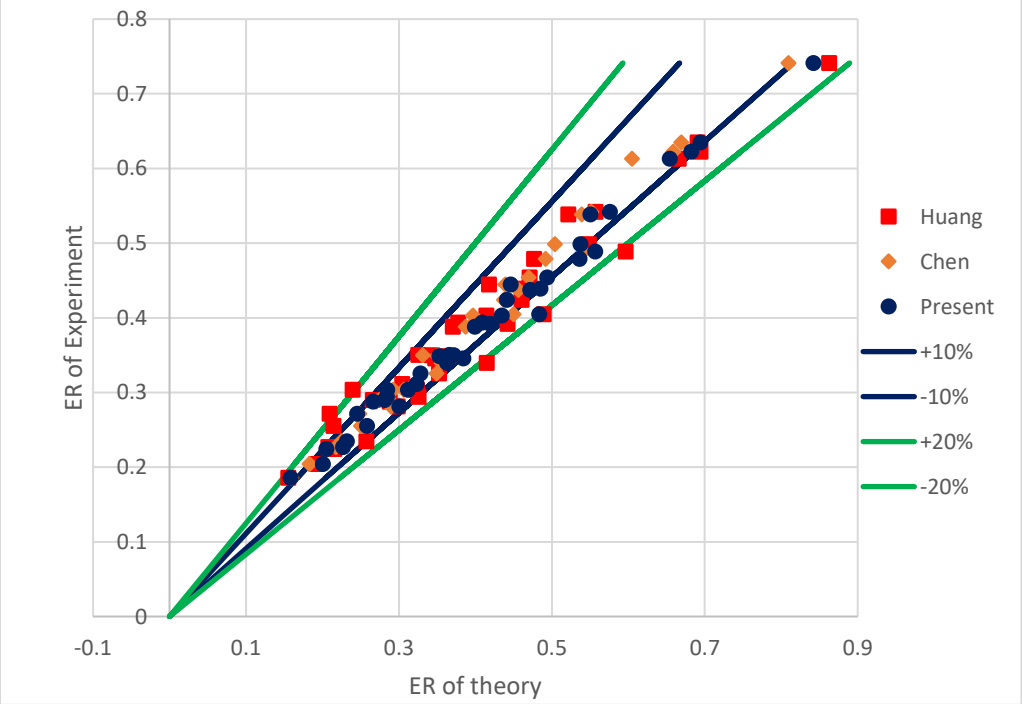

Figure 25. Comparison between experimental result (Huang et al. 1999) and theoretical prediction from Chen, Huang, and present model

As can be seen in Figure 25, there are three models that are compared in this validation plot. Huang's model is developed from the Keenan (1950) model of the ejector, and which changes the cross-section area of the constant area section in the ejector so as to obtain the experiment results, which is represented by the red square markers in the Figure 25 validation plot. Chen's model is based on further development of Huang's model, which predicts the characteristics of the ejector in a critical and subcritical region by changing the pressure at the hypothetical area of the secondary flow. The orange diamond marker represents Chen's model, while the simplified model in this study modifies the Chen's model by changing the iteration step parameter to the Mach number of the secondary flow in the hypothetical region. The round blue cap represents the current model study.

From the Figure 25, Chen's model shows the highest accuracy compared to the experiment results of Huang and the current model study. Huang's model has an accuracy with less than 20% error while Chen model's prediction accuracies have almost all points located under a 10% error tolerance. The current simplified model, which use the same parameters as Huang's model, has predictions that are only slightly less accurate than the Chen's model, which is a trade-off with major simplification being made. The current model can predict the entrainment ratio with less 20% error, which means the simplified model is validated.

An important step in the simplification method is to curve fit the ejector model output so that it can be integrated with the system models. Specifically, a non-Linear Least-Square Regression (nLLSR) is used to curve fit performance data which can then be used to predict the performance of ejector. This simplification was also carried out by Zhu et al. (2007), which obtained performance equations for control and optimization by using two or three empirical parameters to predict ejector performance. In the current study, two non-dimensional parameters are used to obtain the entrainment ratio (ER). These parameters are the area ratio (A_r), namely the

nozzle throat area (A_t) divided by the constant area section of the ejector (A_3), and the pressure ratio (p_r), namely the boiler pressure (p_p) divided the vacuum pressure (p_s). A plot of the simulation results is presented in Figure 26 for the above parameters.

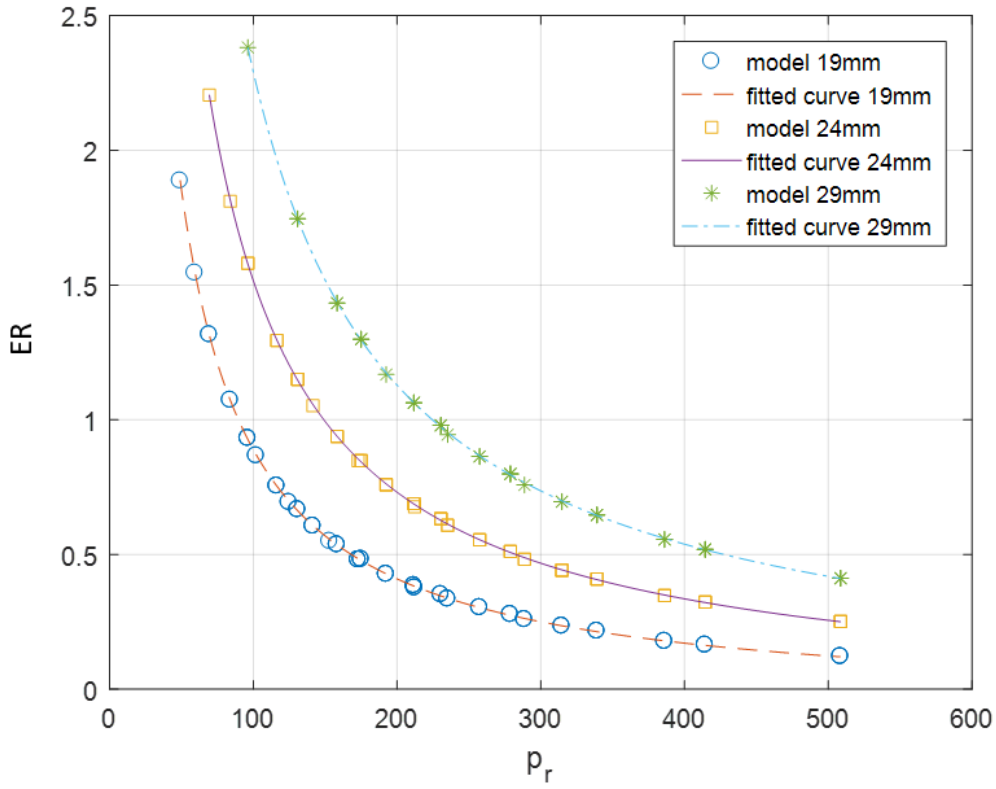

Figure 26. Performance plot for steam ejector using present model in critical condition

The characteristics and behavior of the three parameters plotted in Figure 26 provides insight into ejector operations. For example, the entrainment ratio (ER) decreases with increases in the pressure ratio (p_r). This behavior confirms the statement from McGovern et al. (2012) who stated that the increase of primary pressure (p_p) which in turn increases the pressure ratio (p_r) since $p_r = p_p/p_s$, it decreases the amount of entrained vapor from the vacuum chamber. In

Summary, the primary pressure and the pressure ratio have an inverse relation to entrainment ratio (ER).

Another observation from Figure 26 is that the area ratio (A_r) will increase the amount of entrained vapor (m_s) which leads to an increase in the entrainment ratio (ER) since $ER = \dot{m}_s/\dot{m}_p$. This area ratio also indicates the ejector size, in that a bigger ejector has a larger cross-sectional area, which has the added effect of creating larger hypothetical areas for the secondary flow to pass through the ejector.

The power equation shown below can be used to approximate the ejector performance data in Figure 26.

$$power\ equation: \quad y = ax^b + c \tag{63}$$

From this equation, non-Linear Least Square Regressions are used to find the coefficients of a, b, and c that best approximates the power performance. Specifically, a MATLAB curve fitting tool was used to find the coefficients that produced the best optimizing curve with the highest R^2 and the smallest Root Mean Square Error (RMSE).

Each of the three plots shown in Figure 26, which represents different areas, was curve fit as described above and the results for the coefficient values are as follows

- Curve fitting for $d_3 = 19\ mm \Rightarrow a = 98.72,\ b = -1.007$, and $c = -0.06534$.
- Curve fitting for $d_3 = 24\ mm \Rightarrow a = 150.2,\ b = -0.9887$, and , $b = -0.0666$.
- Curve fitting for $d_3 = 29\ mm \Rightarrow a = 212.9,\ b = -0.9775$, and , $b = -0.07082$.

Of special note, the curve fit coefficients result in $R^2 \simeq 1$ and $RMSE \leq 0.004$, which indicates an extremely accurately fitting for the performance curve.

It is also possible to do combination of the three curves in Figure 26, so as to obtain a single equation that satisfies the conditions in this study. The regression of the coefficients with

respect to area ratios (A_r) which make the final equation both a function of area ratio and pressure ratio, was performed, and the coefficient results are presented in Table 4.

Table 4. Regression result using Least-Square approximation

Coefficient	Regression equation
a	$0.9509A_r + 13.033$
b	$-10^{-6}A_r^2 + 0.0007A_r - 1.0563$
c	$-3 \times 10^{-7}A_r^2 + 5 \times 10^{-5}A_r - 0.0673$

The regression equation, that uses the above coefficients take on a different form and as a result the entrainment ratio (ER) can be described as a function of pressure ratio and area ratio as follows:

$$ER = a\left(\frac{p_p}{p_s}\right)^b + c \tag{64}$$

where the coefficient $a, b,$ and c are tabulated in Table 4.

It should be noted that Equation 64 explains the relationship of entrainment ratio to its parameters for the critical condition case. Furthermore, it is also possible to predict the condition at the downstream of the ejector such as pressure (p_c) and temperature (T_c), by using an energy balance relation, so that, the downstream condition can be described as follows

$$h_c = \frac{\omega h_s + h_p}{\omega + 1} \tag{65}$$

As stated before, because the downstream condition is saturated vapor, the pressure and temperature can be determined from the value of the downstream enthalpy.

The final form of the ejector simplification models as described by Equation 64, can be used to predict the characteristics of the ejector performance. Consequently, this simplified model is useful for control and optimization, along with making ejector performance predictions by using only limited data such as geometry and operating conditions, which can be found in product catalogs. Additionally, by using the simplified ejector model, the calculation of parameters is easier in that if information is available for two parameters, either in the boiler, vacuum, or downstream, then third parameter can be determined for a critical condition.

CHAPTER V

RESULT AND DISCUSSION

Vapor-Compression Refrigeration Systems

The model described and derived earlier was used to simulate the vapor-compression refrigeration cycle, for R22 and R410A as working fluids. These simulations were performed for a range of low and high temperature reservoirs representative of residential HVAC applications and systems, as discussed earlier.

The parameter of focus for discussions in this section is the coefficient of performance (COP), which are plotted in Figure 27 as a function of high and low side temperature and refrigerant type.

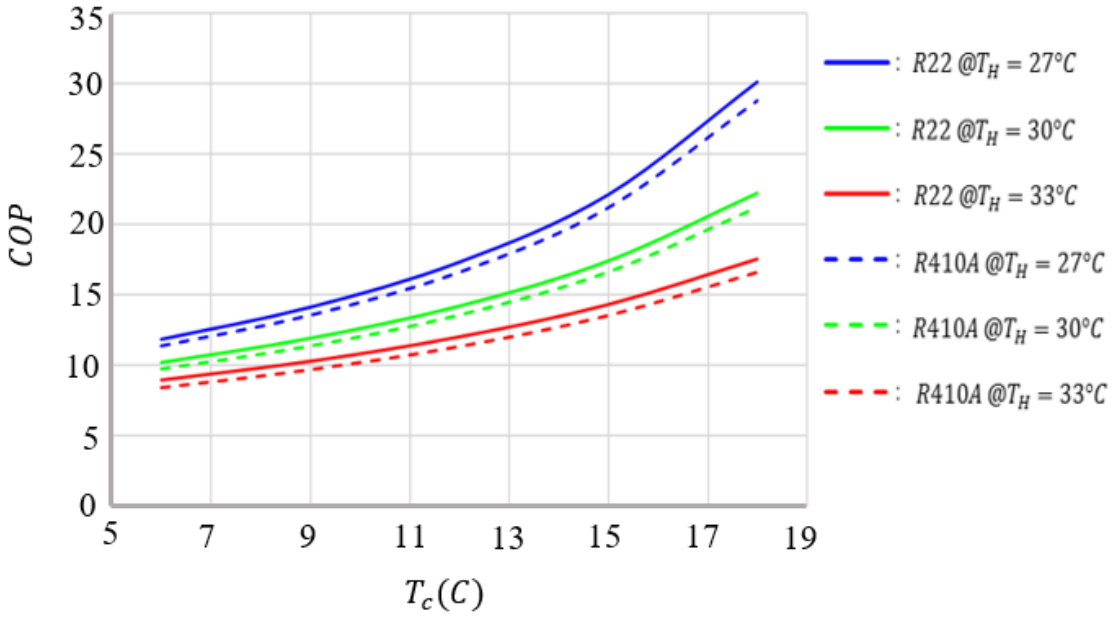

Figure 27. Performance curve of vapor-compression refrigeration system for R22 and R410A.

The results plotted in Figure 27 show that the performance (COP) increases as the temperature in the cold region (T_C) increases, while the performance decreases when the temperature in the hot region (T_H) increases. In other words, HVAC systems are less efficient on hot days as the outdoor temperature increases. They are also less efficient the more they lower the temperature of the indoor space, so it is best not to set the thermostat too low. This performance trend with temperature can also be observed in the COP equation, for a Carnot Cycle, as follows

$$COP = \frac{T_C}{T_H - T_C} \tag{66}$$

Also shown in Figure 28 is the fact that the R22 lines are always above the R410A lines for every cold region temperature, which means that R22 has a better performance compared to R410A. These results confirm the experimental of results from Payne and Domanski (2002), who stated that for hot region temperatures above 30°C, the performance of R22 is slightly better than R410A. The above COP performances are summarized in Table 5.

Table 5. Performance comparison of vapor-compression refrigeration for R22 and R410A

	R-22 COP	R-410A COP
MIN	9.0	8.5
MAX	30.1	28.8

Further performance analysis can be done by focusing on cooling capacity (Q_{eva}) shown in Figure 28 and compressor work (kJ/kg) shown in Figure 30. As can be seen in Figure 28, the cooling capacity increases with cold region temperatures for both refrigerants. In contrast, the cooling capacity decreases with increases in hot region temperatures. The cooling capacity lines appear to linearly increase with hot region temperature. Furthermore, refrigerant R410A has a

higher cooling capacity compared to R22 at the same temperature. Also, the cooling capacity rate increases as the low temperature increases, and it is slightly higher for R22 compared to R410A.

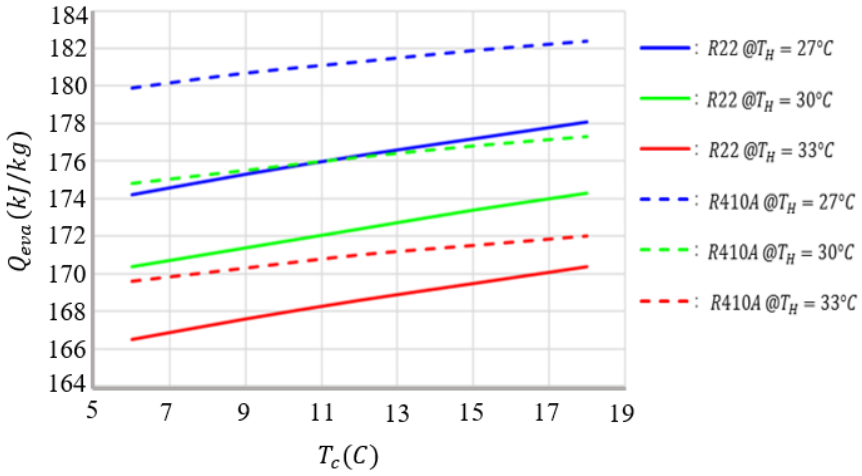

Figure 28. Evaporation capacity in vapor-compression refrigeration system for R22 and R410A

The refrigeration cycle performance also depends on the compressor work (kJ/kg) which can be analyzed from the Figure 30 plot, where work is shown as a function of the two temperatures.

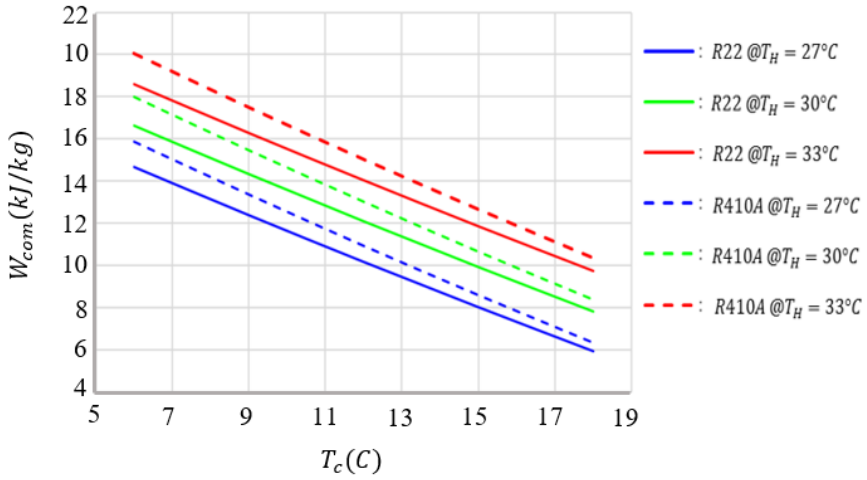

Figure 29. Work of compressor in vapor-compression refrigeration system for R22 and R410

As can be seen in Figure 29, the compressor work decreases linearly with increases in cold region temperatures. Additionally, as the temperature of the hot region increases, the work of the compressor also increases. With R410A generally needing more compressor work compared to R22.

Steam-Ejector Refrigeration System

Previously the model for the steam-ejector refrigeration system was derived, along with a new approach for simplifying the ejector to be integrated with the refrigeration cycle. The combined models formed the simulation developed, which was then carried out for varying hot and cold temperature conditions similar to those used in the vapor-compression refrigeration system that was analyzed previously. The results of the simulation are plotted in order to understand the performance characteristic of the steam-ejector refrigeration system. As a first step, the performance of the ejector model is investigated to see how it contributes to the refrigeration cycle model. Next, the ejector performance of the combination simulation results, which forms the complete cycle are analyzed. The detail calculation process with the EES code can be found in Appendix B.

Since the ejector operating condition depends on the geometry especially area ratio (A_r), the simulation for performance (COP) was carried out with different area ratios with the results being plotted in Figure 30.

As can be seen in Figure 30, the performance (COP) of the steam-ejector refrigeration system increases linearly with increases in the area ratio of the ejector. Essentially, to obtain higher performances for the steam-ejector refrigeration system, then higher area ratios must be used. This increase of performance is actually the result of the entrainment ratio being affected by the area ratio, which was observed in the Figure 31, entrainment ratio increasing as the area ratio increases.

It should also be noted that the area ratio parameter affects the hypothetical area of the ejector, which increases the water vapor entrained by the primary flow from the boiler.

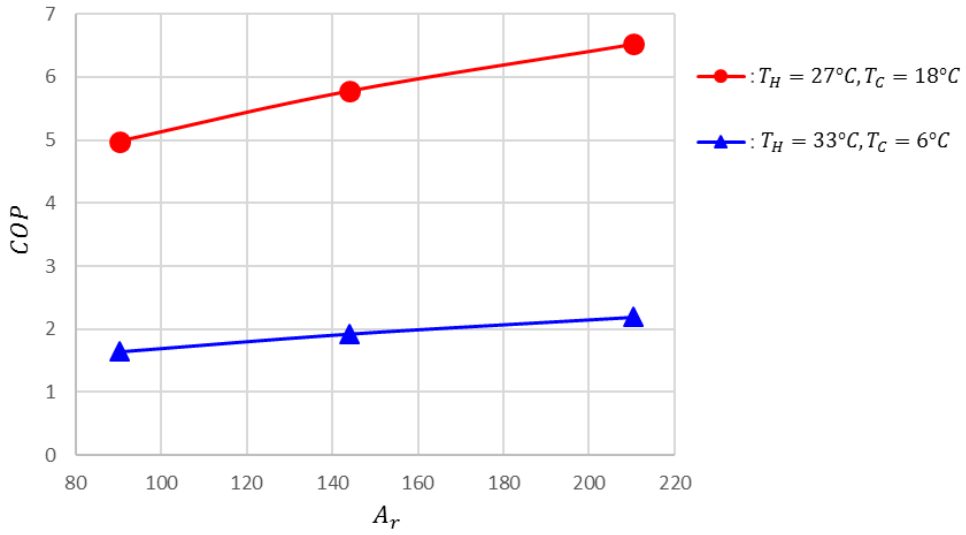

Figure 30. Performance of steam-ejector refrigeration system in different area ratio of the ejector.

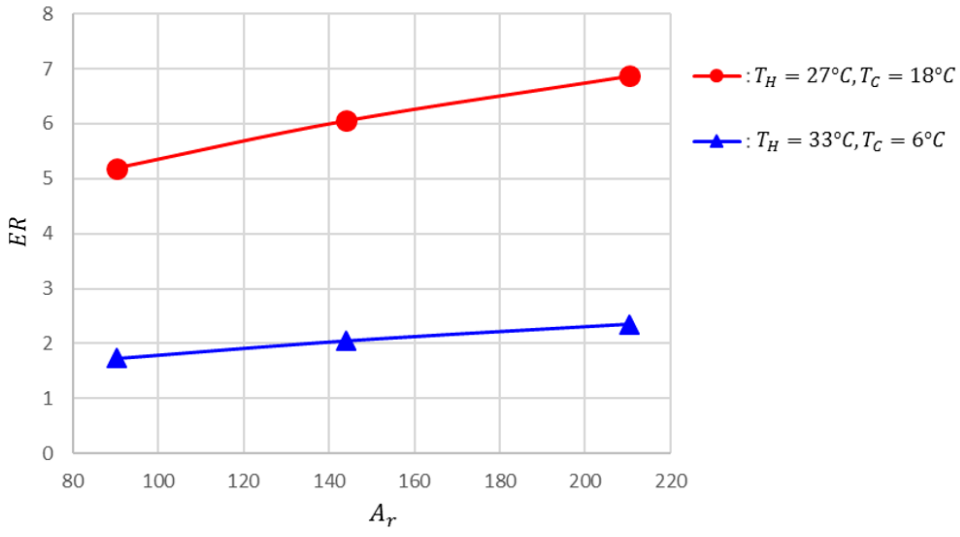

Figure 31. Entrainment ratio of the ejector in steam-ejector refrigeration system in different area ratio.

Additional understanding can be gained by observing the system behaviors shown in Figure 31 . Specifically, the entrainment ratio of the steam-ejector refrigeration system increase as the temperature difference between the high and low temperature reservoirs decrese, with the two curves representing temperature difference of 27-18°C and 33-6°C, with this 9°C (color in red – top curve) having the better performance.

The effects of area ratio are known from the above result in that all of the curves in Figure 31 and 32 show increase in the dependent variable, ER and COP, as the area ratio increases. The next step in analysis will be to focus on the ejector with the highest area ratio of $A_r = 210.3$, which is shown in both figures. Therefore, for this value of the area ratio, the simulation was used to find COP for the full range of low and high temperature with the results being plotted in Figure 32.0

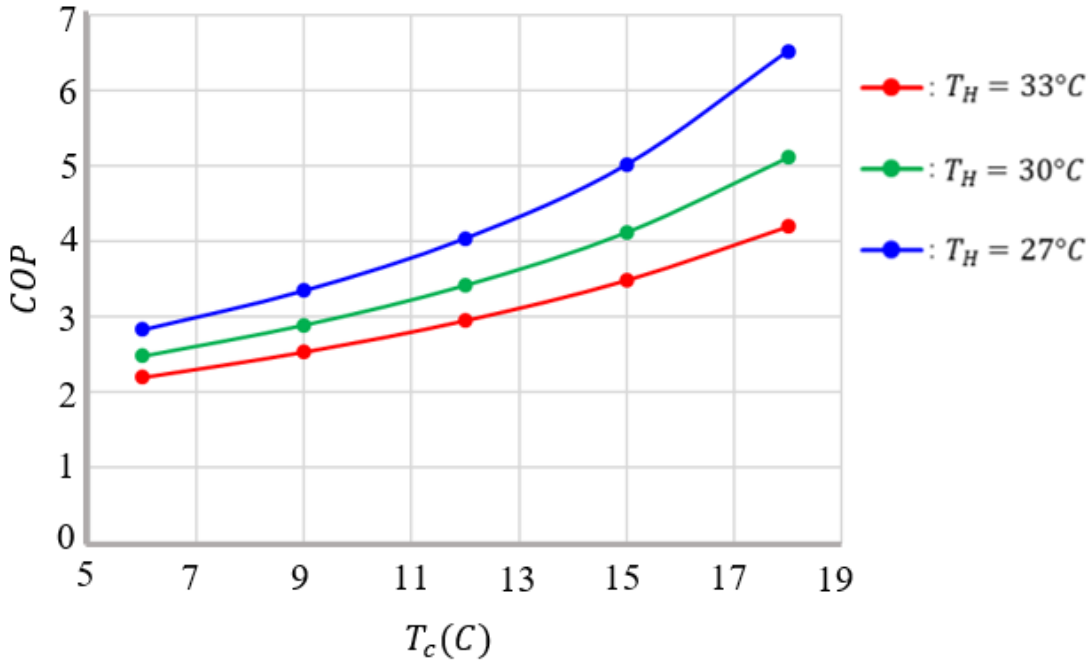

Figure 32. Performance of steam-ejector refrigeration system with different hot and cold region temperature ($A_r = 210.3$).

As can be seen in Figure 32, the performance (COP) of the steam-ejector refrigeration system increases with cold region temperature. In addition, the performance decreases, with increases in the hot region temperature. Furthermore, these Figures 32 curves confirm the fact that the refrigeration system performance increases with decreases in temperature differences (ΔT) between the hot and cold region temperatures. As was shown earlier, entrainment ratio is proportional to refrigeration system performance. Therefore, combining the results of Figures 31 and 32, it can be stated that the entrainment ratio increases with cold region temperature increases and decreases with hot region temperature increases.

To better understand the behavior of the steam-ejector refrigeration system, the performance of major components are investigated, starting with the boiler since it drives the primary flow to the ejector. As can be seen in Figure 33, the required boiler temperature reaches a maximum point for certain specific cold region temperatures. Therefore, higher refrigeration system performances can be obtained by increasing the cold region temperature because less energy is required to entrain more steam from the evaporator. Furthermore, the performance of the evaporator can be predicted by using polynomial increases that are proportional to the performance curves based on the performance equation. In addition, Figure 32 shows that increasing the hot region temperature will increase the required temperature of the boiler.

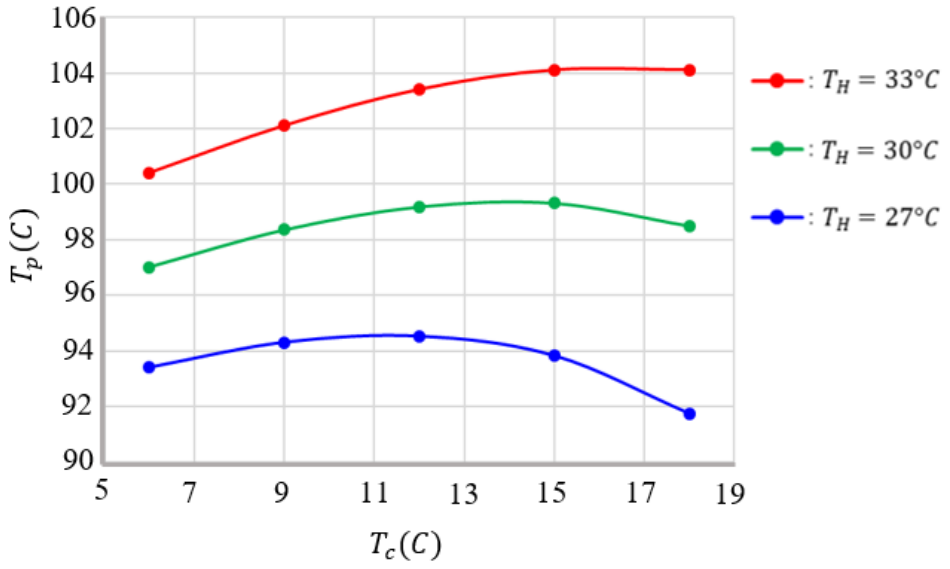

Figure 33. Required boiler temperature in optimum operation for steam-ejector refrigeration system.

In Summary, the coefficient of performance (COP) of the steam-ejector refrigeration system for area ratio of 210.3, which produces the best performance is around 2.2 to 6.5 depending on the input temperature conditions.

Membrane-Ejector Dehumidifier

As explained earlier in Chapter 3, the membrane-ejector dehumidifier is modelled similar to the steam-ejector refrigeration system in that the ejector system has the same function of creating a vacuum, which in this case facilitates water vapor being transferred through a membrane. A major difference in the other with two ejectors. As explained during the development of the ejector simplification method, the ejector operating system depends on the operating conditions and geometry of each ejector. In order to obtain the optimum result, a pre-analysis is

carried out to find the geometry and operating conditions that results in the optimum working conditions for the ejectors.

The procedure to identify an optimum point is performed by simulating different geometries and working conditions, by simulating 2880 cases based the input parameters discussed in Chapter 3.

As can be seen in Figures 34, 35, and 36, the smaller the nozzle diameter of the ejector No. 1, then the better the ejector performance as measured by ER results regardless the effect of ambient temperature (T_{amb}) or membrane performance as indicated by humidity ratio (ω). It should be noted that the performance of the membrane-ejector dehumidifier in Figures 34, 36, and 36 can be described in terms on overall entrainment ratio for two ejectors, which is the ratio of the entrained mass vapor to the total mass flow rate of steam from boiler No. 1 and boiler No. 2 as follows

$$ER_{overall} = \frac{m_{s1}}{m_{p1} + m_{p2}} \tag{67}$$

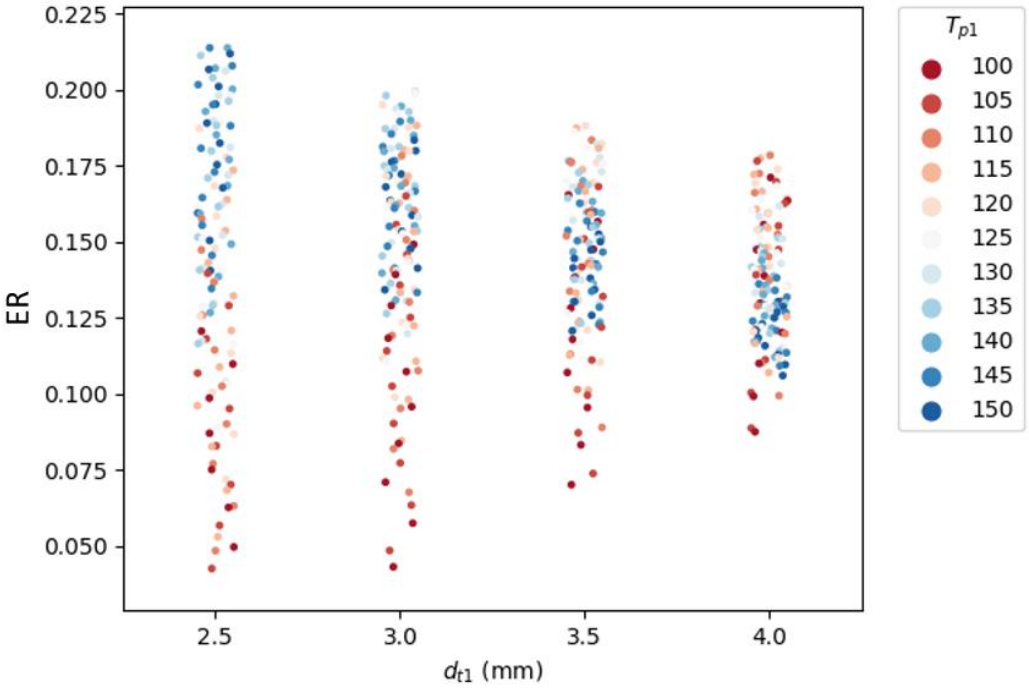

Figure 34. Overall entrainment ratio at humidity ratio $\omega = 13$ and $T_{amb} = 27°C$

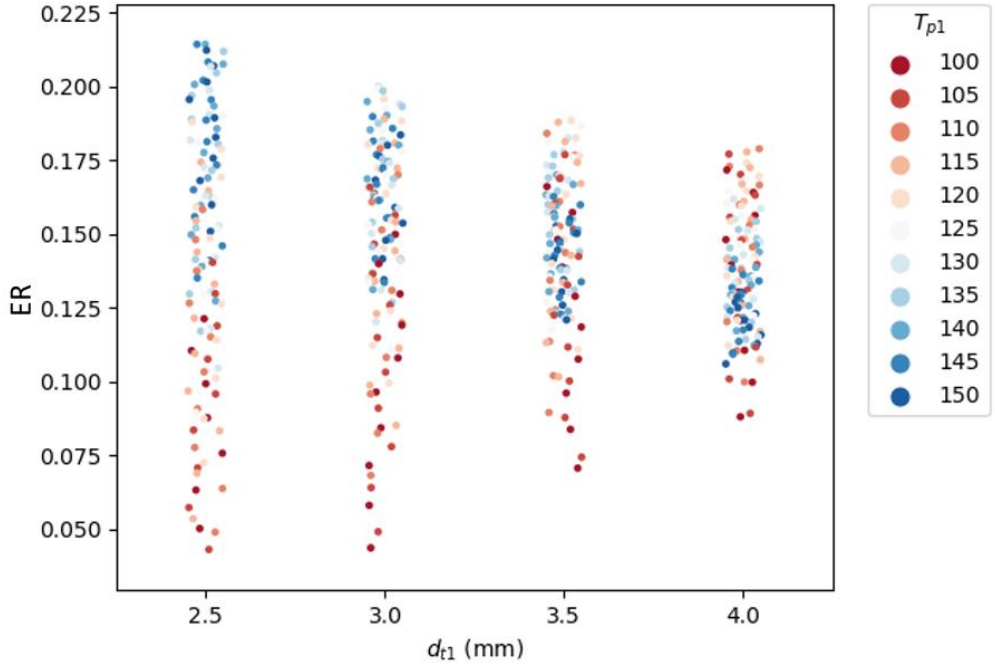

Figure 35. Overall entrainment ratio at humidity ratio $\omega = 13$ and $T_{amb} = 30°C$

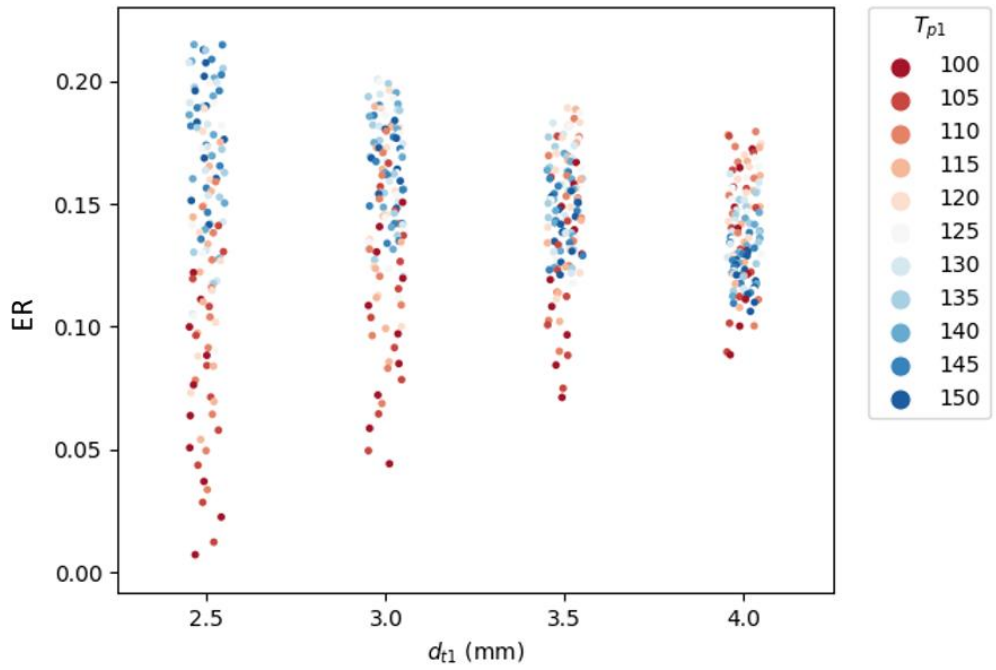

Figure 36. Overall entrainment ratio at humidity ratio $\omega = 10$ and $T_{amb} = 30°C$

In addition to the increasing of nozzle diameter for ejector no. 1 causing the entrainment ratio to decrease, it can also be seen for the $d_{t1} = 2.5\,mm$ group that the entrainment ratio increases with increases in boiler No. 1 temperature. This behavior is because ejector No. 1 is the first ejector, and it thus creates a vacuum condition. Therefore, the temperature of boiler 1 has a significant effect on the overall performance of membrane-ejector dehumidifier.

Geometry specifications for the ejector and the temperature of the two boilers that provides the best performance for given conditions are tabulated in Table 6. These values will henceforth be used in the system simulation. Because the parameters in Table 6 apply for all conditions, the simulation is carried out to find the membrane-ejector dehumidifier COP by changing the ambient temperature and membrane performance, ω.

Table 6. Optimum geometry and condition for given condition.

Description	Condition
Throat diameter of nozzle (d_{t1})	2.5 mm
Boiler 1 Temperature (T_{p1})	140°C
Boiler 2 Temperature (T_{p2})	150°C

Using geometry and conditions from Table 6, the performance of the membrane-ejector dehumidifier was simulated and plotted in Figure 37, which shows COP increasing with humidity ratio and being unaffected by the hot region temperature. Specifically, the performance significantly increases from humidity ratio of 1 to 7; and then the curve increases linearly beyond the humidity ratio value 7. Of special importance, varying ambient temperature has no significant effect on the performance.

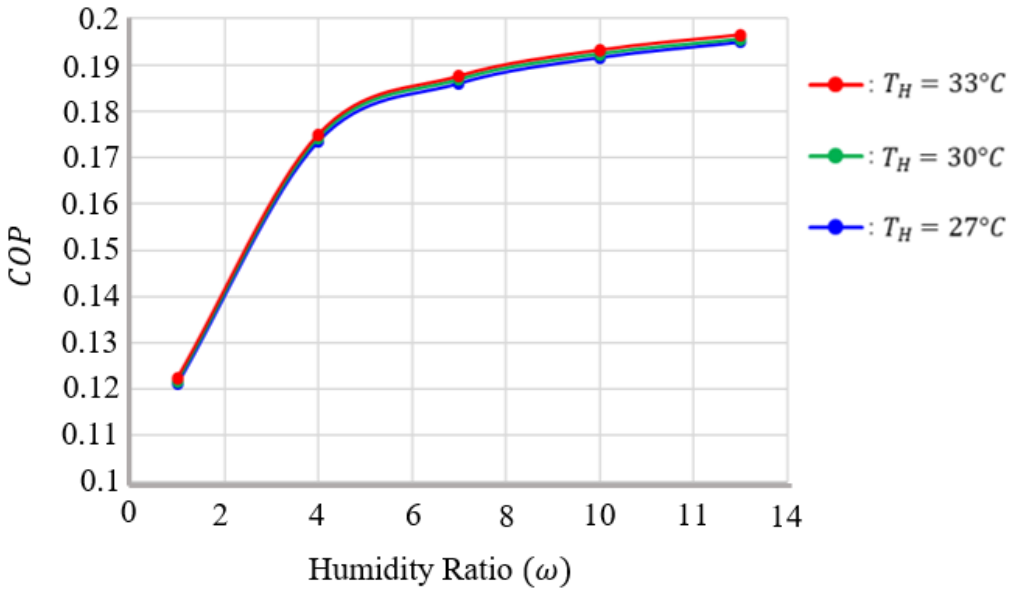

Figure 37. Performance curve of membrane-ejector dehumidifier.

As discussed earlier the ejector performance in this system can also be measured by the value of the overall entrainment ratio, and therefore the overall entrainment ratio was plotted as a function of humidity ratio and ambient temperature in Figure 38. As can be seen in Figure 38, the overall entrainment ratio of the membrane-ejector dehumidifier decreases with increases in membrane performance. Because higher membrane performances transfer more water vapor from the air to the vacuum chamber, then the ejectors use more energy to entrain the increased water vapor going to the ejector. Therefore, more primary steam is needed as a result of the lower entrainment ratio obtain. In addition, the overall entrainment ratio decreases with increases in ambient temperature. Because the higher ambient temperature means the water vapor carries more energy, which makes ejectors work harder.

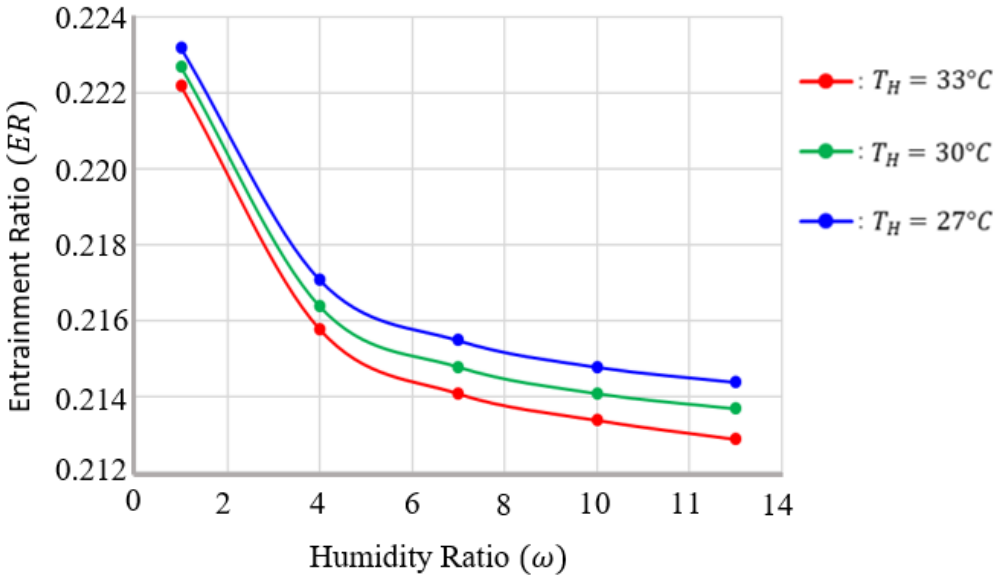

Figure 38. Overall entrainment ratio of membrane-ejector dehumidifier

Another important parameter that characterizes the membrane-ejector dehumidifier is energy consumption with two boilers. The system simulation results reveal that lower energy is consumed by the system at higher overall entrainment ratios. As can be seen in Figure 39, the

boiler consumes more energy when the performance of the ejectors increases, which is the result of the higher membrane performance transfering more water vapor so that more boiler steam is needed to induce the increased water vapor in the vacuum chamber. Additionally, higher ambient temperatures slightly decrease boiler consumption since the water vapor in the case of higher ambient temperatures has a higher energy.

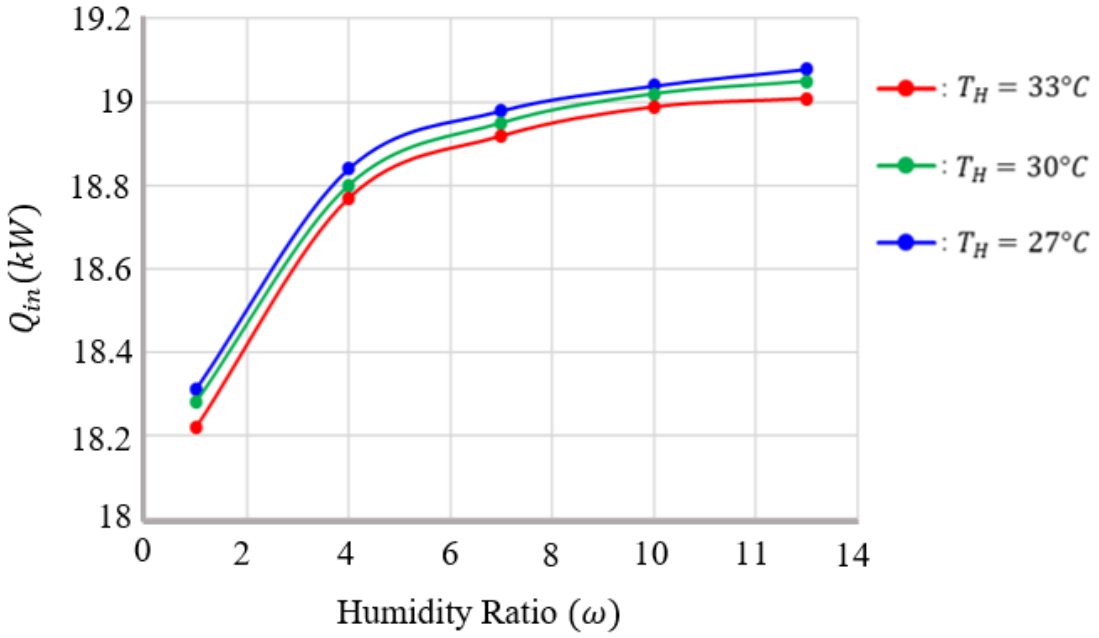

Figure 39. Energy consumption for membrane-ejector dehumidifier

The membrane-ejector dehumidifier has a COP around 0.12 to 0.19 for the given operating conditions. Based on the simulations in this study, this number is below the other systems, however, based on simulation results, the system can be improved by installing an additional condenser between the ejectors. This modification will reduce the water vapor load on ejector 2 since some amount of water vapor will be condensed in this intermediate condenser. This modified system is presented and analyzed with next section.

Improved Membrane-Ejector Dehumidifier

Due to the low performance of the membrane-ejector system at the given conditions that was analyzed previously, improvement were made to reduce energy consumption at ejector 2 by adding another condenser between the two ejectors. A schematic of the improved membrane-ejector dehumidifier is shown in Figure 40.

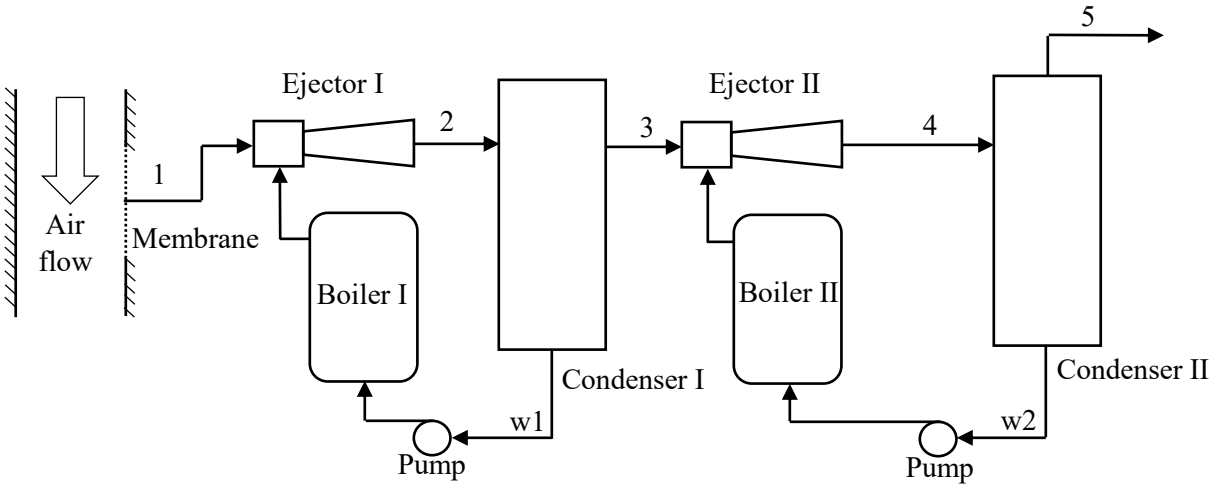

Figure 40. Schematic of improved membrane-ejector dehumidifier

As can be seen in the Figure 41 schematic, this system requires two condensers to condense water and two pumps to supply the boilers with the condensate from each condenser. As before, both condenser are cooled by ambient air, otherwise refered to the hot region. Of special importance, condenser I located is between the two ejectors needs a minimum condition in order for condensation to occur in the condenser. All of the inputs used in the previous analysis remain the same with the highest hot-region sink temperature being 33°C which gives the minimum partial pressure for the water vapor to condense. From the steam tables, the saturation pressure at the highest ambient temperature is 5 kPa. From this information, along with input data for the ejector dimensions and conditions, the simulation of the membrane-ejector dehumidifier can be used to

classify the minimum nozzle throat diameter and boiler condition that satisfies the minimum partial pressure of the vapor between the two ejectors.

Overall entrainment ratios as a function of throat diameter and boiler temperature for various humidity ratios and ambient temperature are plotted in Figures 41, 42, and 43, and it can be observed that the optimum throat diameter of ejector I remains the same for different ambient temperatures and membrane performances. Furthermore, the plots show that at optimum nozzle geometry of ejector I, the highest performance occurs at the high temperature of boiler I. To summarize, it can be seen that $d_{t1} = 2.5\,mm$ and $T_{p1} = 150°C$ results in the highest overall entrainment ratio for the improved membrane-ejector dehumidifier with two condensers.

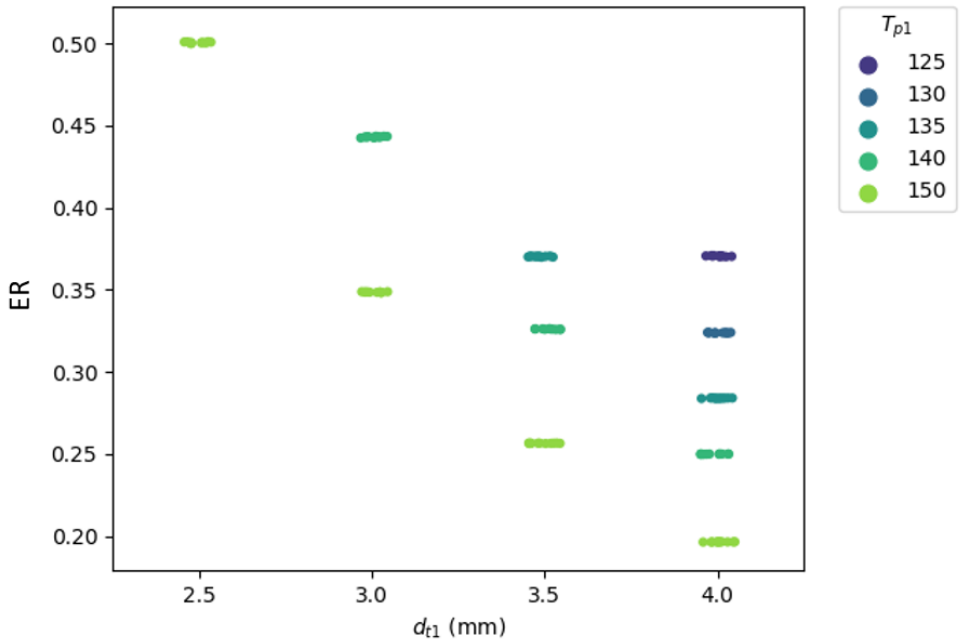

Figure 41. Overall entrainment ratio at humidity ratio $\omega = 13$ and $T_{amb} = 27°C$

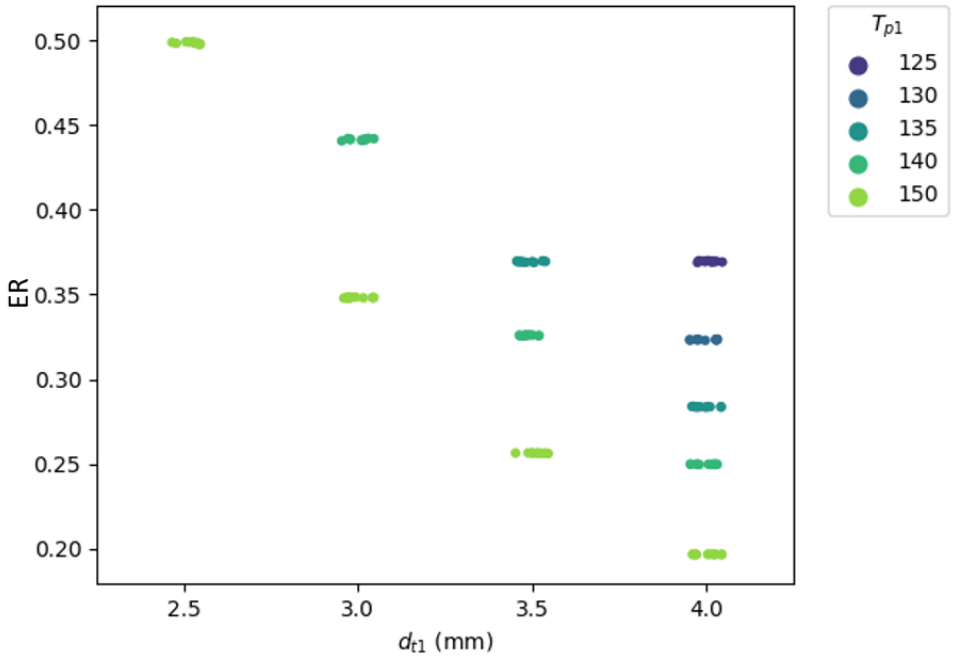

Figure 42. Overall entrainment ratio at humidity ratio $\omega = 13$ and $T_{amb} = 30°C$

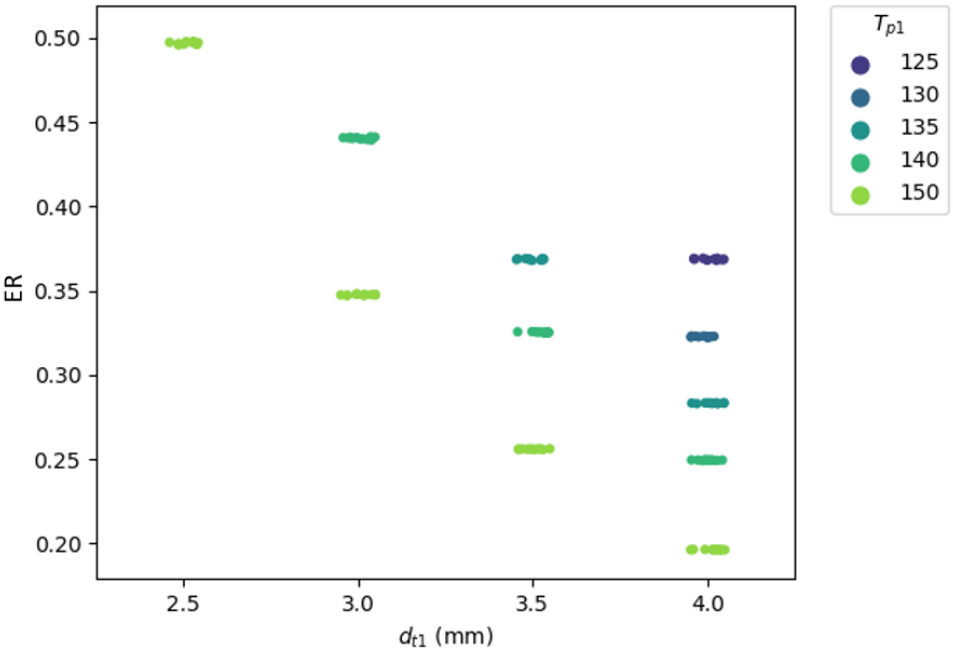

Figure 43. Overall entrainment ratio at humidity ratio $\omega = 10$ and $T_{amb} = 30°C$

Further analysis to find the performance characteristics of the improved membrane-ejector dehumidifier with two condensers can be carried out by simulating the geometry and conditions obtained above for different membrane performances and ambient temperatures. As was done before for the single-condenser membrane ejector dehumidifier. The coefficient of performance (COP) as a function of ambient temperature and humidity ratio is calculated and plotted for the two condensers system. As can be seen in Figure 44, the characteristic performance trends of the improved membrane-ejector system are similar to that of the membrane-ejector system in that the system performance increases with increases in membrane performance. Also shown in Figure 45 is the fact that the COP performance slightly decreases with the increase of ambient temperature. As a comparison, the improved system has a higher performance than the original ejector dehumidification system.

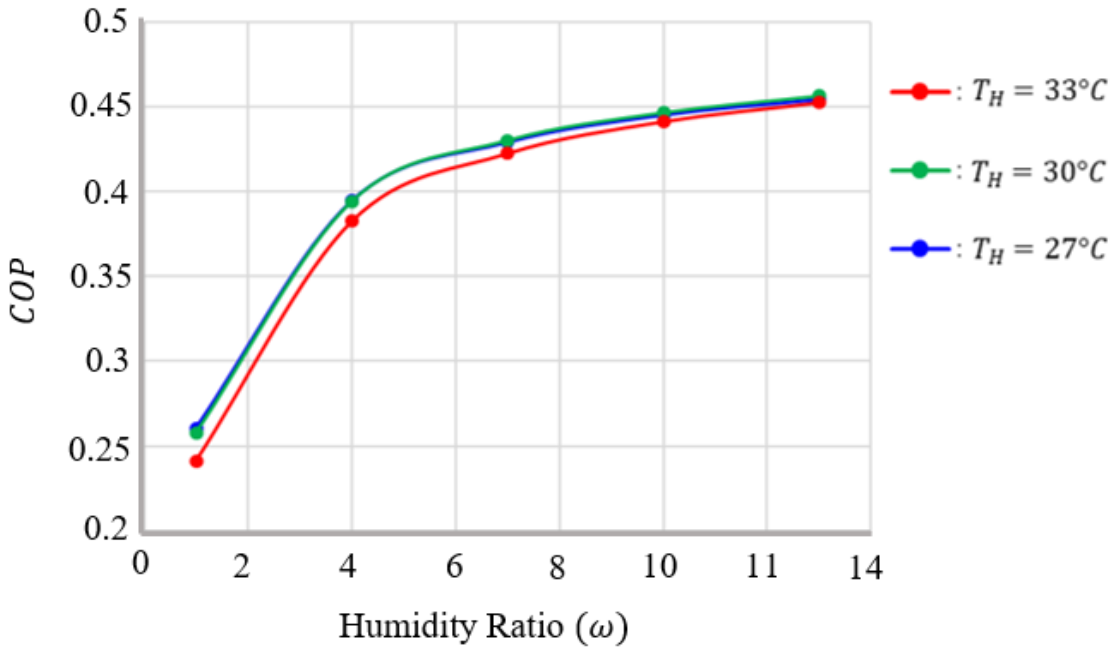

Figure 44. Performance curve of improved membrane-ejector dehumidifier

As can be seen in Figure 45, this new system has a different characteristic from the original membrane-ejector dehumidifier. Specifically, the improved membrane-ejector dehumidifier consumes less energy, with the reason being that the water vapor is condensed in the condenser between the ejectors, which means that the second ejector needs less energy to operate. Also, it can be seen that an increase in ambient temperature will increase the energy consumption, because less energy is rejected by condenser I before the fluid enters ejector 2.

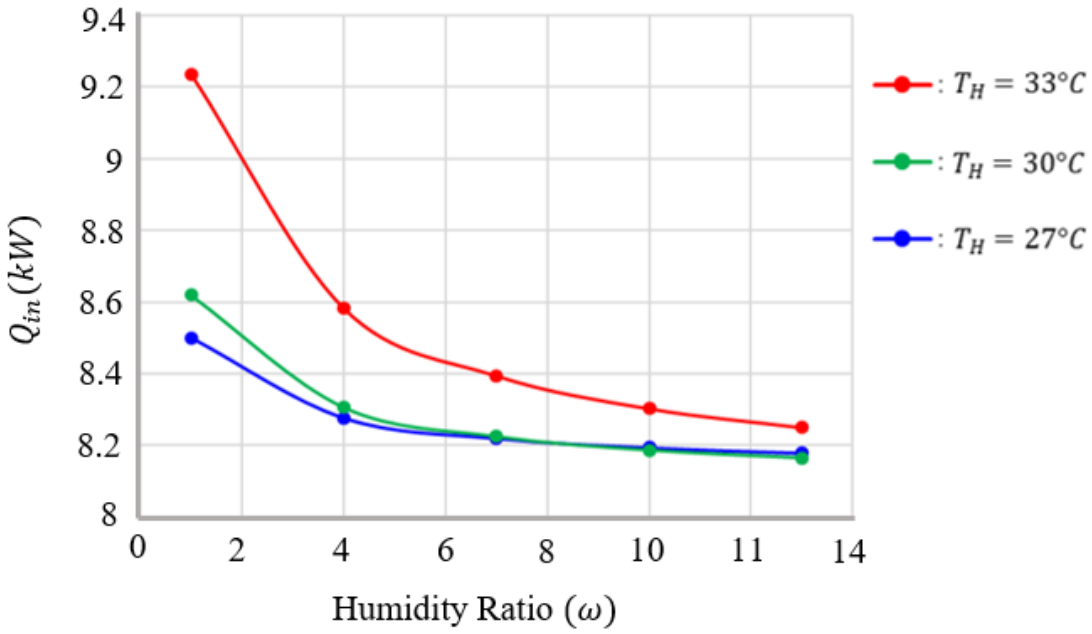

Figure 45. Energy consumption of improved membrane-ejector dehumidifier

As can be seen in Figure 46, lower ambient temperatures increase the overall entrainment ratio. The overall entrainment is different from the regular membrane-ejector dehumidifier because the water vapor entrained by the steam in the second ejector is reduced by the first

condenser. Also of special importance, the condenser is affected by the ambient temperature because it controls the amount of energy rejected to the environment.

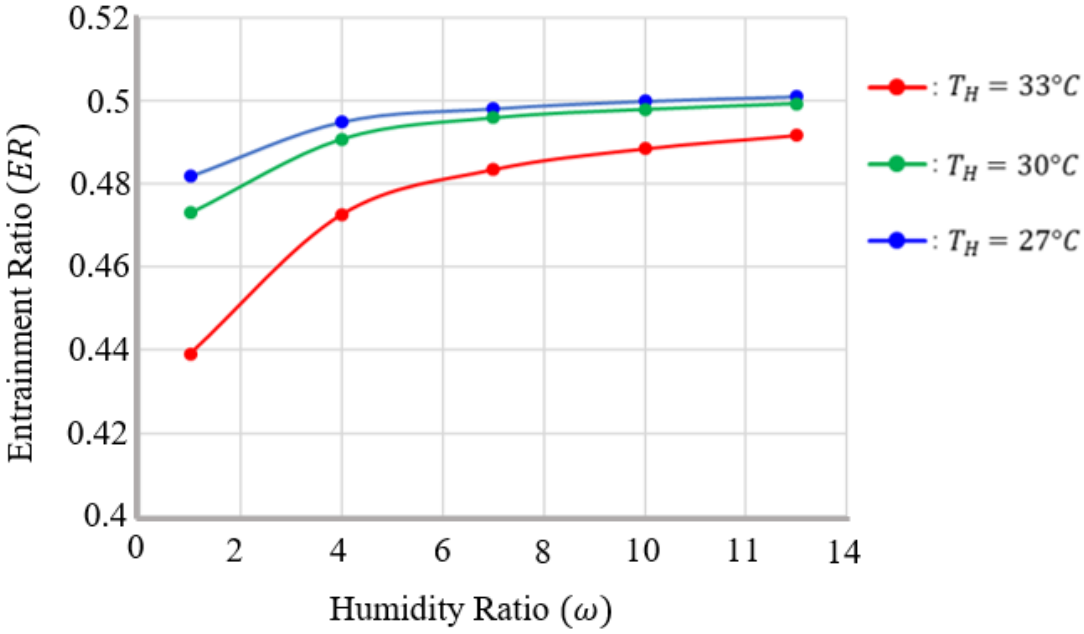

Figure 46. Overall entrainment ratio of improved membrane-ejector refrigeration

In Summary, the improved membrane-ejector refrigeration system can increase the performance of the original system since the additional condenser reduces the heat load on ejector 2. However, the COP systems is still small compared to other type of systems but this can be increased which means that there are lots of opportunities for improvement and optimization. It should also be noted that the energy to operate the system is based on thermal energy rather than electrical energy, which indicates a direct COOP comparison

CHAPTER VI

SYSTEMS COMPARISONS

In this study, four air conditioning systems, which either cool or dehumidify air, are modelled and simulated with the results is being used to identify characteristics and behaviors of each system. Although refrigeration system and dehumidifier systems are different, both systems use energy to dehumidify air. With the refrigeration system dehumidifying air with a heat exchanger (evaporator) while the dehumidifier removes water vapor directly from the air by using a membrane vacuum. Even though, the COP performance and behavior of each system for given conditions is tabulated in Table 7 for general information, the COP value should not be compared among different technologies especially between cooling and dehumidification COP. The reason that this comparison should not be made is that idealized assumption can have very different effects among technologies plus the degree of optimization for possible system configuration and design have widely different emphasize in that a new technology the membrane ejectors systems have not been studied for improvement. Of special importance, the leakage of air through the non-ideal membrane lowers the COP considerably. Also input conditions are different for the different systems. Other reasons that COP comparison should be made with caution is that the energy input are different, either thermal or electrical of the systems were compared on the same units of energy from a cost basic, then the membrane COP's would increases considerably.

Table 7. Comparison of all systems

System	Abbreviation	COP	Influential parameter
Vapor-Compression Refrigeration System (R22)	VCRS-R22	8.95-30.12 (cooling)	Temperature difference between Hot region and cold region
Vapor-Compression Refrigeration System (R410A)	VCRS-R410A	8.45-28.75 (cooling)	Temperature difference between Hot region and cold region
Steam-Ejector Refrigeration System	SERS	2.2-6.5 (cooling)	Temperature difference between Hot region and cold region
Membrane-Ejector Dehumidifier System	MEDS	0.12-0.19 (dehumidifier)	Membrane performance (humidity ratio) and ambient temperature
Improved Membrane-Ejector Dehumidifier System	IMEDS	0.44-0.5 (dehumidifier)	Membrane performance (humidity ratio) and ambient temperature

CHAPTER VII

CONCLUSIONS

All of the refrigeration and dehumidification system were simulated by using Engineering Equation Solver (EES) Software with processes, which were all idealized except for the membrane and conditions being assumed. As a first step, a conventional vapor-compression refrigeration system was simulated for varying low and high side temperature conditions of $T_C = 6°C - 18°C$ and $T_H = 27°C - 33°C$ with refrigerant R22 and R410A. The results of the simulation showed that R22 has a higher COP compared to R410A. Specially, R22 had a maximum COP of 30 and for R410A had a maximum COP around 28. Of special note though, actual system in the real world with non-idealized processes would expect to see maximums that are less than half of these maximum COPs, typically ranging from 3 to 10. The optimum performance and energy input for steam-ejector refrigeration system was obtained by optimization equations that resulted in an area ratio of 210 for the best performance which in turn achieved a maximum COP 6.5 at the smallest temperature difference between hot region and cold region. Furthermore, the energy consumption increases occurred with the increases of high-side temperature. It should be noted that it is not possible to do a direct COP comparison of the conventional vapor-compression system, which uses electrical work to operate, and the ejector system, which uses thermal energy, because of the two different forms of energy input used and because idealized models are being simulated in both cases.

In addition to the simulations of two different refrigeration systems, along with their resulting performances, two dehumidification systems based on membrane technology were also simulated and analyzed, with both of these systems using membranes to remove water vapor from

the air. These two systems differ in how the low-pressure side of the membrane is maintained, with two steam ejectors with and without a condenser installed between them.

For the membrane-ejector dehumidifier, the highest performance is obtained for an optimum nozzle throat geometry is $d_{t1} = 2.5\ mm$ and a boiler 1 condition of $T_{p1} = 140°C$ and $T_{p2} = 150°C$. This condition produces maximum COP of around 0.20 with the ambient temperature not affecting the performance significantly. The overall entrainment ratio decreases as the performance of the membrane increases. To increase the COP, an additional condenser was placed between the two ejectors with the additional condenser improving the membrane-ejector dehumidifier performance more than 100%, resulting in a COP values of 0.2 to 0.5.

Of special importance, one cannot directly compare COPs for the two refrigeration cycles with COPs for the two dehumidification process as COP's are defined differently for cooling and dehumidification. Another reason that the comparison cannot be made is because the compressor is operated with an electrical motor while the ejector operated with thermal energy either in the form of natural gas, solar, geothermal, and waste heat. The value of focusing on COPs as a performance indicator in this study is not to make COP comparisons among systems, but rather as an indicator of how the system performance for each individual system is a function of various variables so that design improvement can be made in the future for any given technology. Furthermore, the resulting system models and simulations performed in this study can be used in future follow up studies to optimize parameters and to investigate system modifications and their effect on performance.

REFERENCES

Abdel-Salam, A. H., Ge, G., Simonson, C. J., 2014. Thermo-economic performance of a solar membrane liquid desiccant air conditioning system, Sol. Energy 102 (4). 56–73.

Al-Khalidy, N., Zayonia, A., 1995. Design and experimental investigation of an ejector in an air-conditioning and refrigeration system. ASHRAE Trans. 101 (2). 383–91.

Aly, N. H., Karameldin, A., Shamloul, M. M., 1999. Modeling and simulation of steam jet ejectors. Desalination 123. 1–8.

Aphornratana, S., 1996. Theoretical study of a steam-ejector refrigerator. RERIC Int. Energy J. 18 (1). 61–74.

Aphornratana, S., Eames, I.W., 1997. A small capacity steam ejector refrigerator: experimental investigation of a system using ejector with movable primary nozzle. Int. J. Refrigeration 20 (5), 352-358.

Bartosiewicz, Y., Aidoun, Z., Desevaux, P, Mercadier, Y., 2005. Numerical and experimental investigations on supersonic ejectors. International Journal of Heat and Fluid Flow 26.56–70.

Bartosiewicz, Y., Aidoun, Z., Desevaux, P., Mercadier, Y., 2005. Numerical and experimental investigation on supersonic ejectors. Int. J. Heat Fluid Flow 26 (1), 56-70.

Bue, G. C., Makinen, J., 2011. Hollow Fiber Flight Prototype Spacesuit Water Membrane Evaporator Design and Testing. International Conference of Environmental System. 2011-5259

Chen, W. X., Liu, M., Chong, D. T., Yan, J. J., Little, A. B., Bartosiewicz, Y., 2013. A 1D model to predict ejector performance at critical and sub-critical operational regimes. Int. J. Refrigeration 36 (5), 1750-1761.

Chen, X., Omer, S., Worall, M., Riffat, S., 2013. Recent developments in ejector refrigeration technologies. Renewable and Sustainable Energy Reviews 19. 629–651.

Chen, Y. M., Sun, C. Y., 1997. Experimental study of the performance characteristics of a steam-ejector refrigeration system. Exp. Fluid Sci. 15, 384–94.

Chen, Z., Zhu, J., Bai, H., Yan, Y., Zhang, L., 2017. Experimental study of a membrane-based dehumidification cooling system. Applied Thermal Engineering 115. 1315-1321.

Chunnanond, K., Aphornratana, S., 2000. A study of steam ejector refrigeration cycle, effect of ejector geometries on ejector performance. In: The Second Regional Conference on Energy Technology towards a Clean Environment. pp. 390–7.

Chunnanond, K., Aphornratana, S., 2003. An experimental investigation of steam-ejector refrigerator, the analysis of pressure profile along ejector. The Asia-Pacific Conference on Sustainable Energy and Environment Technologies,184–8.

Chunnanond, K., Aphornratana, S., 2004. Ejectors: applications in refrigeration technology. Renewable and Sustainable Energy Reviews 8 (4), 129-155.

Cizungu, K., Groll, M., Ling, Z. G., 2005. Modelling and optimization of two-phase ejectors for cooling systems. Applied Thermal Engineering 25. 1979-1994.

Desevaux, P., Marynowski, T., Khan, M., 2006. CFD prediction of supersonic ejector performance. International Journal of Turbo and Jet Engines 23. 173-81.

Domanski, P.A., 1999. Evolution of Refrigerant Application. Proc. International Congress on Refrigeration, Milan, Italy.

El-Dessouky, H., Ettouney, H., Alatiqi, I., Al-Nuwaibit, G. 2002. Evaluation of steam jet ejectors. Chemical Engineering and Processing 41. 551-561.

Grazzini, G., Rocchetti, A., 2002. Numerical optimization of a two-stage ejector refrigeration plant, Int. J. Refrig. 25. 621.

Hemidi, A., Henry, F., Leclaire, S., Seynhaeve, J. M., Bartosiewicz, Y., 2009. CFD Analysis of a Supersonic Air Ejector. Part I: Experimental Validation of Single-Phase and Two-Phase Operation. Applied Thermal Engineering 2008. Applied Thermal Engineering 29 (8-9):1523–1531.

Huang, B. J., Jiang, C. B., Hu, F. L., 1985. Ejector performance characteristics and design analysis of jet refrigeration system. Trans. ASME 107. 792–802.

Huang, B.J., Chang, J.M., Petrenko, V.A., Zhuk, K.B., 1998. A solar ejector cooling system using refrigeration R141b. Sol. Energy 64 (4-6), 223-226.

Huang, B.J.,Chang, J.M., Wang, C.P., Petrenko, V.A., 1999. A 1-D analysis of ejector performance. Int. J. Refrigeration 22 (5),354-364.

Huang, S. M., Zhang, L.Z., 2013. Researches and trends in membrane-based liquid desiccant air dehumidification. Renew. Sustain. Energy Rev. 28. 425–440.

Ito, A., 2000. Dehumidification of air by a hygroscopic liquid membrane supported on surface of a hydrophobic microporous membrane. J. Membr Sci. 175 (1). 35–42.

Jensen, J. B., Skogestad, S., 2007. Control and optimal operation of simple heat pump cycles. Computer Aided Chemical Engineering 20. 1429-1434.

Keenan, J.H., Neumann, E.P., 1942. A simple air ejector. J. Appl. Mech. Trans. ASME 64, A75-A81.

Keenan, J.H., Neumann, E.P., Lustwerk, F., 1950. An investigation of ejector design by analysis and experiment. J. Appl. Mech. Trans. ASME 17, 299-309.

Klein, S.A., 2009. Engineering Equation Solver, Academic Professional, Version 8. Madison, WI. www.fchart.com.

Li, C., Li, Y., Wang, L., Configuration dependence and optimization of the entrainment performance for gas-gas and gas-liquid ejectors. ATE In press.

Liao, C., 2008. Gas ejector modelling for design and analysis. Dissertation of Nuclear Engineering. Texas A&M University

Ma, X., Zhang, W., Omer, S. A., Riffat, S. B., 2010. Experimental investigation of a novel steam ejector refrigerator suitable for solar energy applications. Appl. Therm. Eng. 30, 1320–1325.

McGovern, R. K., Bulusu, K. V., Antar, M., A., Lienhard, J. H., One-dimensional Model of an Optimal Ejector and Parametric Study of Ejector Efficiency. International Conference on Efficiency, Cost, Optimization and Simulation of Energy Conversion Systems and Processes 25.

McLinden, M., 1987. Thermodynamic evaluation of Refrigerants in the Vapor-Compression Cycle Using Reduced Properties. International Journal of Refrigeration, Vol. 11, pp. 134-143.

Moran, M. J., Shapiro, H. N., 2006. Fundamentals of Engineering Thermodynamics: Fifth Edition SI Units. John Wiley and Sons, Inc.

Nahdi, E., Champoussin, J. C., Hostache, G., Cheron, J., 1993. Optimal geometric parameters of a cooling ejector-compressor. Revue International du Froid 16 (1).67-72.

Payne, W. V., Domanski, P. A., 2002. A Comparison of an R22 and an R410A Air Conditioner Operating at High Ambient Temperatures. National Institute of Standards and Technology.

Sriveerakul, T., Aphornratana, S., Chunnanond, K., 2007. Performance prediction of steam ejector using computational fluid dynamics: part 1. Validation of the CFD results. Int. J. Therm. Sci. 46 (8), 812-822.

Sun, D. W., 1996. Variable geometry ejectors and their applications in ejector refrigeration systems. Energy 21(10). 919–29.

Sun, D.W., 1999. Comparative study of the performance of an ejector refrigeration cycle operating with various refrigerants. Energy Convers. Manag. 40. 873–884.

Sun, D.W., Eames, I.W., 1995. Recent developments in the design theories and applications of ejectors. Review. J. Inst. Energy 68, 65-79.

Varga, S., Oleviera, A. C., Diaconu, B., 2009. Numerical Assessment of Steam Ejector Efficiencies using CFD, International Journal of Refrigeration 32:1203-11.

Wang, J., Chen, G., Jiang, H., 1998. Study on a solar-driven ejection absorption refrigeration cycle. Int. J. Energy Res. 22. 733–9.

Wu, S., Eames, I. W., 1998. A novel absorption-recompression refrigeration cycle. Appl. Therm. Eng. 19. 1149–57.

Yang, Bo., Yuan, W., Gao, F., Guo, B. 2013. A review of membrane-based air dehumidification. Indoor and Built Environment 24 (1). 11-26.

Yuan, W. X., Li, Y. X., Wang, C. J., 2012. Comparison study of membrane dehumidification aircraft environmental control system. J. Aircraft 49 (3). 815–821.

Zhang, X. J., Wang, R. Z., 2002. A new combined adsorption-ejector refrigeration and heating hybrid system powered by solar energy. Appl. Therm. Eng. 22. 1245–58.

Zhu, Y., Cai, W., Wen, C., Li, Y., 2008. Simplified ejector model for control and optimization. Energy Conversion and Management 49. 1424-32.

APPENDIX A

SAMPLE MANUAL CALCULATION

Membrane-Ejector Dehumidifier

Two-stage ejector design calculation with condenser schematic arrangement as described in Figure 22.

Input :

- Boiler

Boiler 1 temperature (T_{p1}) = 120°C

Boiler 2 temperature (T_{p2}) = 120°C

Boiler 1 pressure (p_{p1}) = 200 Kpa (saturated gas from input T_{p1})

Boiler 2 pressure (p_{p2}) = 200 Kpa (saturated gas from input T_{p2})

- Dimension of ejector 1 (best dimension from iteration in program)

Throat diameter (d_{t1}) = 3.5 mm

- Vacuum condition (from membrane)

Mass flowrate of air ($\dot{m}_{s1a}$) = 0.4 kg/hr

Mass flowrate of vapor ($\dot{m}_{s1v}$) = 5.198 kg/hr

Pressure of vacuum (p_{s1}) = 1.6 kPa

Temperature of vacuum (T_{s1}) = 32°C

- Initial guess parameter and constraint

Area ratio for ejector 1 (A_{r1}) = 30

Area ratio upper limit (A_{lu}) = 500

Area ratio lower limit (A_{ll}) = 0

Throat diameter (d_{t2}) = 3.5 mm

Throat diameter (d_{tlu}) = 50 mm

Throat diameter (d_{tll}) = 0 mm

- Efficiency

Efficiency for primary flow (η_p) = 100%

Efficiency for secondary flow (η_s) = 100%

Efficiency for primary flow at cross section y-y (η_{py}) = 100%

Mixing coefficient (ϕ_m) = 88%

- Additional

Output of ejector 2 (p_p) = 11.3 kPa

Output condenser temperature (T_{s4}) = 42°C

Calculation of vapor-air mixture properties of vacuum s1

-Humidity ratio.

$$\omega_{s1} = \frac{\dot{m}_{s1v}}{\dot{m}_{s1a}} = \frac{5.198\ \text{kg/hr}}{0.4\ \text{kg/hr}} = 13$$

-Vapor pressure of vacuum.

$$p_{s1v} = \omega_{s1}\left(\frac{p_{s1}}{0.622 + \omega_{s1}}\right) = 13.\left(\frac{1.6\ kPa}{0.622 + 13}\right) = 1.527\ kPa$$

-Enthalpy calculation.

$$h_{s1v} = h(T_{s1}, p_{s1v}) = 2560\ kJ/kg$$

$$h_{s1a} = h(T_{s1}) = 305.6\ kJ/kg$$

$$h_{s1} = \frac{\dot{m}_{s1v}.h_{s1v} + \dot{m}_{s1a}.h_{s1a}}{\dot{m}_{s1v} + \dot{m}_{s1a}} = \frac{5.198\frac{\text{kg}}{\text{hr}}.2560\frac{kJ}{kg} + 0.4\frac{\text{kg}}{\text{hr}}.305.6\frac{kJ}{kg}}{5.198\frac{\text{kg}}{\text{hr}} + 0.4\frac{\text{kg}}{\text{hr}}} = 2399\ kJ/kg$$

-Specific heat capacity calculation.

$cp_{s1v} = cp(T_{s1}, p_{s1v}) = 1.875\ kJ/kg.K$

$cp_{s1a} = cp(T_{s1}) = 1.005\ kJ/kg.K$

$$cp_{s1} = \frac{\dot{m}_{s1v}.cp_{s1v} + \dot{m}_{s1a}.cp_{s1a}}{\dot{m}_{s1v} + \dot{m}_{s1a}} = \frac{5.198\frac{\text{kg}}{\text{hr}}.1.875\ kJ/kg.K + 0.4\frac{\text{kg}}{\text{hr}}.1.005\ kJ/kg.K}{5.198\frac{\text{kg}}{\text{hr}} + 0.4\frac{\text{kg}}{\text{hr}}}$$

$$= 1.813\ kJ/kg.K$$

$cv_{s1v} = cv(T_{s1}, p_{s1v}) = 1.411\ kJ/kg.K$

$cv_{s1a} = cv(T_{s1}) = 0.718\ kJ/kg.K$

$$cv_{s1} = \frac{\dot{m}_{s1v}.cv_{s1v} + \dot{m}_{s1a}.cv_{s1a}}{\dot{m}_{s1v} + \dot{m}_{s1a}} = \frac{5.198\frac{\text{kg}}{\text{hr}}.1.411\ kJ/kg.K + 0.4\frac{\text{kg}}{\text{hr}}.0.718\ kJ/kg.K}{5.198\frac{\text{kg}}{\text{hr}} + 0.4\frac{\text{kg}}{\text{hr}}}$$

$$= 1.361\ kJ/kg.K$$

-Specific heat ratio.

$$\kappa_{s1} = \frac{cp_{s1}}{cv_{s1}} = \frac{1.813\ kJ/kg.K}{1.361\ kJ/kg.K} = 1.33$$

-Specific gas constant.

$R_{s1} = cp_{s1} - cv_{s1} = 1.813\ kJ/kg.K - 1.361\ kJ/kg.K\ = 0.452\ kJ/kg.C$

Calculation of steam properties from boiler

-Specific heat capacity calculation

$$cp_{p1} = cp(T_{p1}, p_{p1}) = 2.126\ kJ/kg.K$$

$$cv_{p1} = cv(T_{p1}, p_{p1}) = 1.575\ kJ/kg.K$$

-Specific heat ratio

$$\kappa_{p1} = \frac{cp_{p1}}{cv_{p1}} = \frac{2.126\ kJ/kg.K}{1.575\ kJ/kg.K} = 1.35$$

-Specific gas constant

$$R_{p1} = cp_{p1} - cv_{p1} = 2.126\ kJ/kg.K - 1.575\ kJ/kg.K\ = 0.5518\ kJ/kg.K$$

-Enthalpy calculation

$$h_{p1} = h_g(\ p_{p1}) = 2707\ kJ/kg$$

Dimension calculation of ejector 1

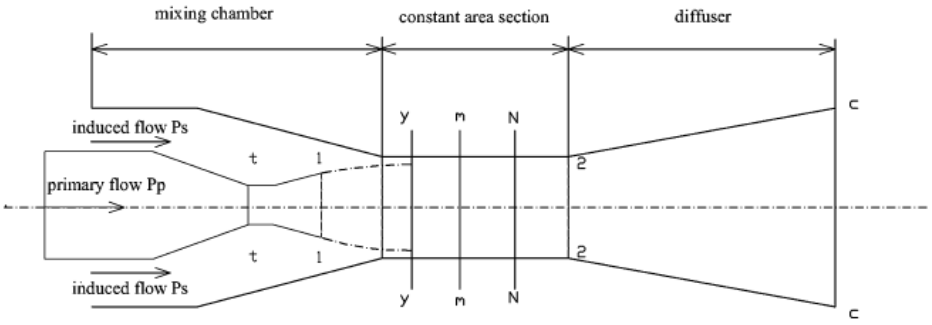

-Area calculation at cross section t-t

$$A_{t1} = 0.25\ .\ d_{t1}^2.\pi = 0.25\ .\ (3.5\ mm)^2.\pi.\frac{10^{-6}m^2}{mm^2} = 0.000009621\ m^2$$

-Area calculation at cross section 1-1

$$d_{11} = 1.5d_{t1} = 1.5\ .\ 3.5\ mm = 5.25\ mm$$

$$A_{11} = 0.25\ .\ d_{11}^2.\pi = 0.25\ .\ (5.25\ mm)^2.\pi.\frac{10^{-6}m^2}{mm^2} = 0.000021648\ m^2$$

-Guessing Area at cross section 2-2

$$A_{21} = A_{r1}.A_t = 30\,.0.000009621\,m^2 = 0.00028863\,m^2$$

Ejector 1 Calculation

-Calculation of mass flow rate from boiler ($\dot{m}_p$)

$$\dot{m}_{p1} = p_{p1}A_{t1}\sqrt{\kappa_p\eta_p\left[\frac{\left(\frac{2}{\kappa_p+1}\right)^{\left(\frac{\kappa_p+1}{\kappa_p-1}\right)}}{T_{p1}R_{p1}}\right]}$$

$$= 200\,kPa.0.000009621\,m^2.\sqrt{1.35\,.1\left[\frac{\left(\frac{2}{1.35+1}\right)^{\left(\frac{1.35+1}{1.35-1}\right)}}{120.2\,C.0.5518\,kJ/kg.C}\right]}$$

$$= 0.002722\frac{kg}{s} \simeq 9.7992\,kg/hr$$

-Calculation of Mach number of primary flow at cross section 1-1

$$\left[\frac{A_{11}}{A_{t1}}\right] = \frac{1}{M_{p11}^2}\left[\left(\frac{2}{\kappa_p+1}\right).\left(1+\frac{(\kappa_p-1).M_{p11}^2}{2}\right)\right]^{\left(\frac{\kappa_p+1}{\kappa_p-1}\right)}$$

$$\left[\frac{0.000021648\,m^2}{0.000009621\,m^2}\right] = \frac{1}{M_{11}^2}\left[\left(\frac{2}{1.35+1}\right).\left(1+\frac{(1.35-1).M_{p11}^2}{2}\right)\right]^{\left(\frac{1.35+1}{1.35-1}\right)}$$

$$M_{p11} = 3.55$$

-Calculation of pressure of primary flow at cross section 1-1

$$p_{p11} = \frac{p_{p1}}{\left[1+(\kappa_p-1).\frac{M_{p11}^2}{2}\right]^{\left(\frac{\kappa_p}{\kappa_p-1}\right)}} = \frac{200\,kPa}{\left[1+(1.35-1).\frac{3.55^2}{2}\right]^{\left(\frac{1.35}{1.35-1}\right)}} = 2.243\,kPa$$

-Assumption at arbitrary location of y-y

$$M_{s1y} = 1$$

y-y is the location where the secondary flow reaches sonic condition

-Calculation of pressure of secondary flow at cross section y-y

$$p_{s1y}^{*} = p_{s1}\left[1 + (\kappa_{s1} - 1).\frac{M_{s1y}^{2}}{2}\right]^{\frac{-\kappa_{s1}}{\kappa_{s1}-1}} = 1.6\ kPa.\left[1 + (1.33 - 1).\frac{1^{2}}{2}\right]^{\frac{-1.33}{1.33-1}} = 0.8645\ kPa$$

-Assumption condition at cross section y-y

$$p_{s1y}^{*} = p_{s1y}$$

$$p_{s1y}^{*} = p_{p1y}$$

$$p_{s1y}^{*} = p_{m1}$$

-Calculation of Mach number at primary flow at cross section y-y

$$\frac{p_{p1y}}{p_{p11}} = \frac{\left[1 + \left[\frac{\kappa_{s1} - 1}{2}\right].M_{p11}^{2}\right]^{\left(\frac{\kappa_{s1}}{\kappa_{s1}-1}\right)}}{\left[1 + \left[\frac{\kappa_{s1} - 1}{2}\right].M_{p1y}^{2}\right]^{\left(\frac{\kappa_{s1}}{\kappa_{s1}-1}\right)}}$$

$$\frac{0.8632\ kPa}{2.243\ kPa} = \frac{\left[1 + \left[\frac{1.33 - 1}{2}\right].3.55^{2}\right]^{\left(\frac{1.33}{1.33-1}\right)}}{\left[1 + \left[\frac{1.33 - 1}{2}\right].M_{p1y}^{2}\right]^{\left(\frac{1.33}{1.33-1}\right)}}$$

$$M_{p1y} = 4.212$$

-Calculation of cross section area of primary flow of cross section y-y

$$\frac{A_{p1y}}{A_{11}} = \frac{\frac{\eta_{py}}{M_{p1y}}\left[\left(\frac{2}{\kappa_p + 1}\right)\left(1 + \left(\frac{\kappa_p - 1}{2}\right).M_{p1y}^{2}\right)\right]^{\left(\frac{\kappa_p + 1}{2.(\kappa_p - 1)}\right)}}{\frac{1}{M_{p11}}\left[\left(\frac{2}{\kappa_p + 1}\right)\left(1 + \left(\frac{\kappa_p - 1}{2}\right).M_{p11}^{2}\right)\right]^{\left(\frac{\kappa_p + 1}{2.(\kappa_p - 1)}\right)}}$$

$$\frac{A_{p1y}}{0.000021648\ m^{2}} = \frac{\frac{0.88}{4.212}\left[\left(\frac{2}{1.35 + 1}\right)\left(1 + \left(\frac{1.35 - 1}{2}\right).4.215^{2}\right)\right]^{\left(\frac{1.35+1}{2.(1.35-1)}\right)}}{\frac{1}{3.55}\left[\left(\frac{2}{1.35 + 1}\right)\left(1 + \left(\frac{1.35 - 1}{2}\right).3.55^{2}\right)\right]^{\left(\frac{1.35+1}{2.(1.35-1)}\right)}}$$

$$A_{p1y} = 0.0001337\ m^2$$

-Calculation of cross section of secondary flow at cross section y-y

$$A_{s1y} = A_{21} - A_{p1y} = 0.00028863\ m^2 - 0.0001337\ m^2 = 0.0001549\ m^2$$

-Calculation of temperature of secondary flow at cross section y-y

$$T_{s1y} = T_{s1}.\left(\frac{p_{s1y}}{p_{s1}}\right)^{\left(\frac{\kappa_{s1}-1}{\kappa_{s1}}\right)} = (32+273)K.\left(\frac{0.8645\ kPa}{1.6\ kPa}\right)^{\left(\frac{1.33-1}{1.33}\right)} = 261\ K$$

-Calculation of temperature of primary flow at cross section y-y

$$\frac{T_{p1}}{T_{p1y}} = 1 + \left(\frac{\kappa_p - 1}{2}\right).M_{p1y}^2$$

$$\frac{(120.2+273)K}{T_{p1y}} = 1 + \left(\frac{1.35-1}{2}\right).4.212^2$$

$$T_{p1y} = 95.8\ K$$

-Calculation of velocity of secondary flow at cross section y-y

$$V_{s1y} = M_{s1y}.\sqrt{\kappa_{s1}R_{s1}T_{s1y}} = 1.\sqrt{1.33.0.452\ kJ/kg.K.261\ K} = 396.109\ m/s$$

-Calculation of velocity of primary flow at cross section y-y

$$V_{p1y} = M_{p1y}.\sqrt{\kappa_p R_p T_{p1y}} = 4.212\sqrt{1.35.0.5518\ kJ/kg.K.95.8\ K} = 1125.2\ m/s$$

-Calculation the mass flow rate of secondary flow from guessing value– Critical

$$\dot{M}_{s1} = p_{s1}A_{s1y}\sqrt{\kappa_{s1}\eta_s\left[\frac{\left(\frac{2}{\kappa_{s1}+1}\right)^{\left(\frac{\kappa_{s1}+1}{\kappa_{s1}-1}\right)}}{T_{s1}R_{s1}}\right]}$$

$$\dot{M}_{s1} = 1.6\ kPa.0.0001549\ m^2 \sqrt{1.33.1\left[\frac{\left(\frac{2}{1.33+1}\right)^{\left(\frac{1.33+1}{1.33-1}\right)}}{(32+273)K.0.452\ kJ/kg.K}\right]} = 0.000013089\frac{kg}{s}$$

$$\simeq 0.04712\ kg/hr$$

-Vacuum flow calculation

$\dot{m}_{s1} = \dot{m}_{s1a} + \dot{m}_{s1v} = 0.4\ kg/hr\ + 5.198\ kg/hr\ = 5.598\ kg/hr$

From calculation above, guess value of mass flow rate of vacuum is significantly smaller than actual mass flow of vacuum. Iteration is needed to obtain correct dimension of ejector which has value mass flow rate the same as actual mass flow of vacuum. Fast iteration algorithm is used by using bisection method. This method makes program possible to run many cases faster. Upper limit and lower limit are the constraint which the real value is in between these parameters.

-Bisection method to find Area ratio (A_{r1})

$$\dot{m}_{s1-margin} = \dot{m}_{s1} - \dot{M}_{s1} = 5.598\frac{kg}{hr} - 0.04712\frac{kg}{hr} = 5.55088\frac{kg}{hr}$$

If $\dot{m}_{s1-margin} > 0$ then,

$A_{r1} = A_{ll} = 30$ (current condition)

$A_{lu} = A_{lu} = 1000$ (as is)

If $\dot{m}_{s1-margin} < 0$ then,

$A_{ll} = A_{ll}$ (as is)

$A_{r1} = A_{lu}$ (change)

Next area ratio A_{r1}

$$A_{r1} = \frac{A_{ll} + A_{lu}}{2} = \frac{30 + 1000}{2} = 515$$

The iteration goes on until $\dot{m}_{s1-margin} = 0.0001 \simeq 0.1$ % error

The new area ratio is inputted back to the equation above until reach the criteria.

From the calculation it takes 50 iterations with the result as below:

$A_{r1} = 74.65$

-Calculation of velocity mixture

$$\phi_m\left(\dot{m}_{p1}.V_{p1y} + \dot{m}_{s1}.V_{s1y}\right) = \left(\dot{m}_{p1} + \dot{m}_{s1}\right).V_{m1}$$

$$0.88.\left(0.002722\frac{kg}{s}.1125.2\frac{m}{s} + 0.001555\frac{kg}{s}.396.109\frac{m}{s}\right)$$

$$= \left(0.002722\frac{kg}{s} + 0.001555\frac{kg}{s}\right).V_m$$

$V_{m1} = 756.9\ m/s$

-Calculation of enthalpy of mixture

$$\dot{m}_{p1}\left(cp_p T_{p1y} + \frac{V_{p1y}^2}{2}\right) + \dot{m}_{s1}\left(cp_{s1} T_{s1y} + \frac{V_{s1y}^2}{2}\right) = \left(\dot{m}_{p1} + \dot{m}_{s1}\right).\left(h_{m1} + \frac{V_{m1}^2}{2}\right)$$

$$0.002722\frac{kg}{s}\left(2.126\ kJ/kg.K.95.8\ K + \frac{(1125.2\frac{m}{s})^2}{2}\right)$$

$$+ 0.001555\frac{kg}{s}\left(1.813\ kJ/kg.K.261\ K + \frac{(396.109\frac{m}{s})^2}{2}\right)$$

$$= \left(0.002722\frac{kg}{s} + 0.001555\frac{kg}{s}\right).\left(h_{m1} + \frac{(756.9\frac{m}{s})^2}{2}\right)$$

$h_{m1} = 446.61\ kJ/kg$

-Calculation of flow composition of mixture

$$\dot{m}_{m1} = \dot{m}_{p1} + \dot{m}_{s1} = 0.002722\frac{kg}{s} + 0.001555\frac{kg}{s} = 0.04277\frac{kg}{s} \simeq 15.39\ kg/hr$$

$$\dot{m}_{m1v} = \dot{m}_{p1} + \left[\frac{\omega_{s1}}{\omega_{s1}+1}\right]\dot{m}_{s1} = 0.002722\frac{kg}{s} + \left[\frac{13}{13+1}\right]0.001555\frac{kg}{s} = 0.0041659\frac{kg}{s}$$

$$\simeq 14.99\ kg/hr$$

$$\dot{m}_{m1a} = \dot{m}_{m1} - \dot{m}_{m1v} = 15.39\frac{kg}{hr} - 14.99\frac{kg}{hr} = 0.4\frac{kg}{hr} \simeq 0.0001111\frac{kg}{s}$$

$$\omega_{m1} = \frac{\dot{m}_{m1v}}{\dot{m}_{m1a}} = \frac{14.99\ kg/hr}{0.4\ kg/hr} = 37.51$$

-Calculation of temperature of mixing flow at constant cross section area

$$h_{m1}\frac{= (\dot{m}_{m1v}cp_g(Vapor, T_m) + \ \dot{m}_{m1a}cp(Air, T_m))T_{m1}}{\dot{m}_{m1}}$$

$$446.61\ kJ/kg\ \frac{= (0.0041659.\frac{kg}{s}cp_g(Vapor, T_{m1}) + \ 0.0001111\frac{kg}{s}.cp(Air, T_{m1}))T_{m1}}{0.04277\frac{kg}{s}}$$

$$T_{m1} = 245\ K$$

-Calculation of properties of mixture flow

-Specific heat capacity calculation

$$cp_{m1v} = cp_g(T_{m1}, p_{m1v}) = cp_g(245\ K) = 1.856\ kJ/kg.K$$

$$cp_{m1a} = cp(T_{m1}) = cp(245\ K) = 1.003\ kJ/kg.K$$

$$cp_{m1} = \frac{\dot{m}_{m1v}.cp_{m1v} + \ \dot{m}_{m1a}.cp_{m1a}}{\dot{m}_{m1v} + \dot{m}_{m1a}}$$

$$= \frac{0.0041659\frac{kg}{s}.1.856\ kJ/kg.K + 0.0001111\frac{kg}{s}.1.003\ kJ/kg.K}{0.0041659\frac{kg}{s} + 0.0001111\frac{kg}{s}}$$

$$= 1.833\ kJ/kg.K$$

$$cv_{m1v} = cv_g(T_{m1}) = cv_g(245\ K) = 1.395\ kJ/kg.K$$

$$cv_{m1a} = cv(T_{s1}) = cv(245\ K) = 0.716\ kJ/kg.K$$

$$cv_{m1} = \frac{\dot{m}_{m1v}.cv_{m1v} + \dot{m}_{m1a}.cv_{m1a}}{\dot{m}_{m1v} + \dot{m}_{m1a}}$$

$$= \frac{0.0041659\frac{kg}{s}.1.395\ kJ/kg.K + 0.0001111\frac{kg}{s}.0.716\ kJ/kg.K}{0.0041659\frac{kg}{s} + 0.0001111\frac{kg}{s}}$$

$$= 1.377\ kJ/kg.K$$

-Specific heat ratio

$$\kappa_{m1} = \frac{cp_{m1}}{cv_{m1}} = \frac{1.833\ kJ/kg.K}{1.377\ kJ/kg.K} = 1.33$$

-Specific gas constant

$$R_{m1} = cp_{m1} - cv_{m1} = 1.833\ kJ/kg.K - 1.377\ kJ/kg.K\ = 0.456\ kJ/kg.K$$

-Calculation of Mach number of mixture flow

$$M_{m1} = \frac{V_{m1}}{\sqrt{\kappa_{m1}R_{m1}T_{m1}}} = \frac{756.9\ m/s}{\sqrt{1.33.0.456\frac{kJ}{kg}.K.245\ K}} = 1.96$$

-Calculation of pressure at cross section 2-2

$$\frac{p_{21}}{p_{m1}} = 1 + 2\left[\frac{\kappa_{m1}}{\kappa_{m1}+1}\right].(M_{m1}^2 - 1)$$

$$\frac{p_{21}}{0.8645\ kPa} = 1 + 2\left[\frac{1.33}{1.33+1}\right].(1.96^2 - 1)$$

$$p_{21} = 3.669\ kPa$$

-Calculation of Mach number at cross section 2-2

$$M_{21}^2 = \frac{1 + \left[\frac{\kappa_{m1}-1}{2}\right].M_{m1}^2}{\kappa_{m1}.M_{m1}^2 - \left[\frac{\kappa_{m1}-1}{2}\right]} = \frac{1 + \left[\frac{1.33-1}{2}\right].1.96^2}{1.33.1.96^2 - \left[\frac{1.33-1}{2}\right]} = 0.33$$

-Calculation of stagnation pressure at arbitrary cross section c-c

$$\frac{p_{c1}}{p_{21}} = \left[1 + \left[\frac{\kappa_{m1}-1}{2}\right].M_{21}^2\right]^{\left[\frac{\kappa_{m1}}{\kappa_{m1}-1}\right]}$$

$$\frac{p_{c1}}{3.669\ kPa} = \left[1 + \left[\frac{1.33-1}{2}\right].0.33^2\right]^{\left[\frac{1.33}{1.33-1}\right]}$$

$$p_{c1} = 4.561\ kPa$$

-Calculation of entrainment ratio

$$\omega_1 = \frac{\dot{m}_{s1}}{\dot{m}_{p1}} = \frac{5.598\ kg/hr}{9.7992\ kg/hr} = 0.5713$$

-Calculation of enthalpy at the output of ejector

$$h_{c1} = \frac{\omega_1 h_{s1} + h_p}{\omega_1 + 1} = \frac{0.5713.2399\ kJ/kg + 2707\ kJ/kg}{0.5713 + 1} = 2569\ kJ/kg$$

-Calculation of partial pressure of vapor at the output of ejector

$$p_{c1v} = \omega_{m1}\frac{p_{c1}}{0.622 + \omega_{m1}} = 37.51\frac{4.561\ kPa}{0.622 + 37.51} = 4.486\ kPa$$

-Calculation of temperature at output of ejector

$$h_{c1} = \frac{h(Air, T_{c1}) + \omega_{m1}.h(Steam, T_{c1}, p_{c1v})}{1 + \omega_{m1}}$$

$$2569\ kJ/kg = \frac{h(Air, T_{c1}) + 37.51.h(Steam, T_{c1}, p_{c1v})}{1 + 37.51}$$

$$T_{c1} = 68.57°C$$

Calculation of vapor-air mixture properties of vacuum s2

-Humidity ratio

$$\omega_{s2} = \omega_{m1} = 37.51$$

-Pressure and temperature for vacuum s2

$$p_{s2} = p_{c2} = 4.561\ kPa$$

$$T_{s2} = T_{c1} = 68.57°C$$

-Mass flow rate for vacuum s2

$$\dot{m}_{s2} = \dot{m}_{m1} = 0.004277 \frac{kg}{s} \simeq 15.39\ kg/hr$$

$$\dot{m}_{s2v} = \dot{m}_{m1v} = 0.0041659 \frac{kg}{s} \simeq 14.99\ kg/hr$$

$$\dot{m}_{s2a} = \dot{m}_{m1a} = 0.0001111 \frac{kg}{s} \simeq 0.4 kg/hr$$

-Vapor pressure of vacuum

$$p_{s2v} = p_{c2v} = 4.486\ kPa$$

-Enthalpy calculation

$$h_{s2} = h_{c1} = 2569\ kJ/kg$$

-Specific heat capacity calculation

$$cp_{s2v} = cp(T_{s2}, p_{s2v}) = cp(68.57°C, 4.486\ kPa) = 1.889\ kJ/kg.K$$

$$cp_{s2a} = cp(T_{s2}) = cp(68.57°C) = 1.007\ kJ/kg.K$$

$$cp_{s2} = \frac{\dot{m}_{s2v}.cp_{s2v} + \dot{m}_{s2a}.cp_{s2a}}{\dot{m}_{s2v} + \dot{m}_{s2a}}$$

$$= \frac{14.99\ kg/hr.1.875\ kJ/kg.K + 0.4\ kg/hr.1.005\ kJ/kg.K}{14.99\ kg/hr + 0.4\ kg/hr}$$

$$= 1.853\ kJ/kg.K$$

$$cv_{s2v} = cv(T_{s2}, p_{s2v}) = 1.424\ kJ/kg.K$$

$$cv_{s2a} = cv(T_{s2}) = 0.7204\ kJ/kg.K$$

$$cv_{s2} = \frac{\dot{m}_{s2v}.cv_{s2v} + \dot{m}_{s2a}.cv_{s2a}}{\dot{m}_{s2v} + \dot{m}_{s2a}}$$

$$= \frac{14.99\ kg/hr.1.411\ kJ/kg.K + 0.4\ kg/hr.0.718\ kJ/kg.K}{14.99\ kg/hr + 0.4\ kg/hr}$$

$$= 1.393\ kJ/kg.K$$

-Specific heat ratio

$$\kappa_{s2} = \frac{cp_{s2}}{cv_{s2}} = \frac{1.853\ kJ/kg.K}{1.393\ kJ/kg.K} = 1.33$$

-Specific gas constant

$$R_{s2} = cp_{s2} - cv_{s2} = 1.853\ kJ/kg.K - 1.393\ kJ/kg.K\ = 0.46\ kJ/kg.K$$

Ejector 2 Calculation

-Calculation of cross section area of secondary flow at cross section y-y

$$\dot{m}_{s2} = p_{s2} A_{s2y} \sqrt{\kappa_{s1} \eta_s \left[\frac{\left(\frac{2}{\kappa_{s2}+1}\right)^{\left(\frac{\kappa_{s2}+1}{\kappa_{s2}-1}\right)}}{T_{s2} R_{s2}} \right]}$$

$$0.04277 \frac{kg}{s} = 4.561\ kPa.A_{s2y} \sqrt{1.33.1 \left[\frac{\left(\frac{2}{1.33+1}\right)^{\left(\frac{1.33+1}{1.33-1}\right)}}{(68.57+273)\ K.0.46\ kJ/kg.K} \right]}$$

$$A_{s2y} = 0.0006135\ m^2$$

-Area calculation at cross section t-t

$$A_{t2} = 0.25\ .\ d_{t2}^2.\pi = 0.25\ .\ (3.5\ mm)^2.\pi.\frac{10^{-6} m^2}{mm^2} = 0.000009621\ m^2$$

-Area calculation at cross section 1-1

$$d_{12} = 1.5 d_{t2} = 1.5\ .\ 3.5\ mm = 5.25\ mm$$

$$A_{12} = 0.25\ .\ d_{12}^2.\pi = 0.25\ .\ (5.25\ mm)^2.\pi.\frac{10^{-6} m^2}{mm^2} = 0.000021648\ m^2$$

-Calculation of mass flow rate from boiler ($\dot{m}_p$)

$$\dot{m}_{p1} = p_{p2} A_{t1} \sqrt{\kappa_p \eta_p \left[\frac{\left(\frac{2}{\kappa_p + 1}\right)^{\left(\frac{\kappa_p + 1}{\kappa_p - 1}\right)}}{T_{p2} R_p} \right]}$$

$$= 200\ kPa . 0.000009621\ m^2 . \sqrt{1.35\ .1 \left[\frac{\left(\frac{2}{1.35 + 1}\right)^{\left(\frac{1.35 + 1}{1.35 - 1}\right)}}{(120.2 + 273)\ K . 0.5518\ kJ/kg.C} \right]}$$

$$= 0.002722 \frac{kg}{s} \simeq 9.7992\ kg/hr$$

-Calculation of Mach number of primary flow at cross section 1-1

$$\left[\frac{A_{12}}{A_{t2}}\right] = \frac{1}{M_{p21}^2} \left[\left(\frac{2}{\kappa_p + 1}\right) . \left(1 + \frac{(\kappa_p - 1) . M_{p21}^2}{2}\right) \right]^{\left(\frac{\kappa_p + 1}{\kappa_p - 1}\right)}$$

$$\left[\frac{0.000021648\ m^2}{0.000009621\ m^2}\right] = \frac{1}{M_{p21}^2} \left[\left(\frac{2}{1.35 + 1}\right) . \left(1 + \frac{(1.35 - 1) . M_{p21}^2}{2}\right) \right]^{\left(\frac{1.35 + 1}{1.35 - 1}\right)}$$

$M_{p21} = 3.55$

-Calculation of pressure of primary flow at cross section 1-1

$$p_{p21} = \frac{p_p}{\left[1 + (\kappa_p - 1) . \frac{M_{p21}^2}{2}\right]^{\left(\frac{\kappa_p}{\kappa_p - 1}\right)}} = \frac{200\ kPa}{\left[1 + (1.35 - 1) . \frac{3.55^2}{2}\right]^{\left(\frac{1.35}{1.35 - 1}\right)}} = 2.243\ kPa$$

-Assumption at arbitrary location of y-y

$M_{s1y} = 1$

y-y is the location where the secondary flow reaches sonic condition

-Calculation of pressure of secondary flow at cross section y-y

$$p_{s2y}^{*} = p_{s2}\left[1 + (\kappa_{s2} - 1).\frac{M_{s2y}^{2}}{2}\right]^{\frac{-\kappa_{s2}}{\kappa_{s2}-1}} = 4.561\ kPa.\left[1 + (1.33 - 1).\frac{1^{2}}{2}\right]^{\frac{-1.33}{1.33-1}} = 2.464\ kPa$$

-Assumption condition at cross section y-y

$$p_{s2y}^{*} = p_{s2y}$$

$$p_{s2y}^{*} = p_{p2y}$$

$$p_{s2y}^{*} = p_{m2}$$

-Calculation of Mach number at primary flow at cross section y-y

$$\frac{p_{p2y}}{p_{p21}} = \frac{\left[1 + \left[\frac{\kappa_{s2} - 1}{2}\right].M_{p21}^{2}\right]^{\left(\frac{\kappa_{s2}}{\kappa_{s2}-1}\right)}}{\left[1 + \left[\frac{\kappa_{s2} - 1}{2}\right].M_{p2y}^{2}\right]^{\left(\frac{\kappa_{s2}}{\kappa_{s2}-1}\right)}}$$

$$\frac{2.464\ kPa}{2.243\ kPa} = \frac{\left[1 + \left[\frac{1.33 - 1}{2}\right].3.55^{2}\right]^{\left(\frac{1.33}{1.33-1}\right)}}{\left[1 + \left[\frac{1.33 - 1}{2}\right].M_{p1y}^{2}\right]^{\left(\frac{1.33}{1.33-1}\right)}}$$

$$M_{p2y} = 3.489$$

-Calculation of cross section area of primary flow of cross section y-y

$$\frac{A_{p2y}}{A_{21}} = \frac{\frac{\eta_{py}}{M_{p2y}}\left[\left(\frac{2}{\kappa_p + 1}\right)\left(1 + \left(\frac{\kappa_p - 1}{2}\right).M_{p2y}^{2}\right)\right]^{\left(\frac{\kappa_p + 1}{2.(\kappa_p - 1)}\right)}}{\frac{1}{M_{p21}}\left[\left(\frac{2}{\kappa_p + 1}\right)\left(1 + \left(\frac{\kappa_p - 1}{2}\right).M_{p21}^{2}\right)\right]^{\left(\frac{\kappa_p + 1}{2.(\kappa_p - 1)}\right)}}$$

$$\frac{A_{p2y}}{0.000021648\ m^{2}} = \frac{\frac{0.88}{3.489}\left[\left(\frac{2}{1.35 + 1}\right)\left(1 + \left(\frac{1.35 - 1}{2}\right).3.489^{2}\right)\right]^{\left(\frac{1.35+1}{2.(1.35-1)}\right)}}{\frac{1}{3.55}\left[\left(\frac{2}{1.35 + 1}\right)\left(1 + \left(\frac{1.35 - 1}{2}\right).3.55^{2}\right)\right]^{\left(\frac{1.35+1}{2.(1.35-1)}\right)}}$$

$$A_{p2y} = 0.0000179\ \ m^{2}$$

-Calculation of cross section of secondary flow at cross section y-y

$$A_{22} = \ A_{s2y} + A_{p2y} = 0.0006135\ m^{2} + 0.0000179\ \ m^{2} = 0.0006314\ m^{2}$$

-Calculation of temperature of secondary flow at cross section y-y

$$T_{s2y} = T_{s2}.\left(\frac{p_{s2y}}{p_{s2}}\right)^{\left(\frac{\kappa_{s2}-1}{\kappa_{s2}}\right)} = (68.57 + 273)K.\left(\frac{2.464\ kPa}{4.561\ kPa}\right)^{\left(\frac{1.33-1}{1.33}\right)} = 293\ K$$

-Calculation of temperature of primary flow at cross section y-y

$$\frac{T_p}{T_{p2y}} = 1 + \left(\frac{\kappa_p - 1}{2}\right).M_{p2y}^2$$

$$\frac{(120.2 + 273)K}{T_{p2y}} = 1 + \left(\frac{1.35 - 1}{2}\right).3.489^2$$

$$T_{p2y} = 125.6\ K$$

-Calculation of velocity of secondary flow at cross section y-y

$$V_{s2y} = M_{s2y}.\sqrt{\kappa_{s2}R_{s2}T_{s2y}} = 1.\sqrt{1.33.0.46\ kJ/kg.K.293\ K} = 423.388\ m/s$$

-Calculation of velocity of primary flow at cross section y-y

$$V_{p2y} = M_{p2y}.\sqrt{\kappa_p R_p T_{p2y}} = 3.489\sqrt{1.35.0.5518\ kJ/kg.K.125.6\ K} = 1067.21\ m/s$$

-Calculation of velocity mixture

$$\phi_m\left(\dot{m}_{p2}.V_{p2y} + \dot{m}_{s2}.V_{s2y}\right) = \left(\dot{m}_{p2} + \dot{m}_{s2}\right).V_{m2}$$

$$0.88.\left(0.002722\frac{kg}{s}.1067.21\frac{m}{s} + 0.004277\frac{kg}{s}.423.388\frac{m}{s}\right)$$

$$= \left(0.002722\frac{kg}{s} + 0.004277\frac{kg}{s}\right).V_m$$

$$V_{m2} = 592.925\ m/s$$

-Calculation of enthalpy of mixture

$$\dot{m}_{p2}\left(cp_p T_{p2y} + \frac{V_{p2y}^2}{2}\right) + \dot{m}_{s2}\left(cp_{s2}T_{s2y} + \frac{V_{s2y}^2}{2}\right) = \left(\dot{m}_{p2} + \dot{m}_{s2}\right).\left(h_{m2} + \frac{V_{m2}^2}{2}\right)$$

$$0.002722\frac{kg}{s}\left(2.126\ kJ/kg.K.125.6\ K+\frac{(1067.21\frac{m}{s})^2}{2}\right)$$

$$+0.004277\frac{kg}{s}\left(1.853\ kJ/kg.K.293\ K+\frac{(423.388\ m/s)^2}{2}\right)$$

$$=\left(0.002722\frac{kg}{s}+0.004277\frac{kg}{s}\right).\left(h_{m2}+\frac{(592.925\ m/s)^2}{2}\right)$$

$h_{m2}=536.08\ kJ/kg$

-Calculation of flow composition of mixture

$\dot{m}_{m2}=\dot{m}_{p2}+\dot{m}_{s2}=0.002722\frac{kg}{s}+0.004277\frac{kg}{s}=0.006999\frac{kg}{s}\simeq 25.196\ kg/hr$

$\dot{m}_{m2v}=\dot{m}_{p2}+\left[\frac{HR_{s2}}{HR_{s2}+1}\right]\dot{m}_{s2}=0.002722\frac{kg}{s}+\left[\frac{37.51}{37.51+1}\right]0.004277\frac{kg}{s}=0.006888\frac{kg}{s}$

$\simeq 24.79\ kg/hr$

$\dot{m}_{m2a}=\dot{m}_{m2}-\dot{m}_{m2v}=25.196\ kg/hr-24.79\ kg/hr=0.4\frac{kg}{hr}\simeq 0.0001111\frac{kg}{s}$

$\omega_{m1}=\frac{\dot{m}_{m2v}}{\dot{m}_{m2a}}=\frac{24.79\ kg/hr}{0.4\ kg/hr}=61.975$

-Calculation of temperature of mixing flow at constant cross section area

$$h_{m2}=\frac{(\dot{m}_{m2v}cp_g(Vapor,T_{m2})+\ \dot{m}_{m2a}cp(Air,T_{m2}))T_{m2}}{\dot{m}_{m2}}$$

$$536.08\ kJ/kg=\frac{(0.006888\frac{kg}{s}cp_g(Vapor,T_{m2})+\ 0.0001111\frac{kg}{s}.cp(Air,T_{m2}))T_{m2}}{0.006999\frac{kg}{s}}$$

$T_{m2}=287.5\ K$

-Calculation of properties of mixture flow

-Specific heat capacity calculation

$cp_{m2v}=cp_g(T_{m2},p_{m2v})=cp_g(287.5\ K)=1.877\ kJ/kg.K$

$$cp_{m2a} = cp(T_{m2}) = cp(287.5\ K) = 1.004\ kJ/kg.K$$

$$cp_{m2} = \frac{\dot{m}_{m2v}.cp_{m2v} + \dot{m}_{m2a}.cp_{m2a}}{\dot{m}_{m2v} + \dot{m}_{m2a}}$$

$$= \frac{0.006888\frac{kg}{s}.1.877\ kJ/kg.K + 0.0001111\frac{kg}{s}.1.004\ kJ/kg.K}{0.006888\frac{kg}{s} + 0.0001111\frac{kg}{s}}$$

$$= 1.863\ kJ/kg.K$$

$$cv_{m2v} = cv_g(T_{m2}) = cv_g(287.5\ K) = 1.411\ kJ/kg.K$$

$$cv_{m2a} = cv(T_{s2}) = cv(287.5\ K) = 0.7172\ kJ/kg.K$$

$$cv_{m2} = \frac{\dot{m}_{m2v}.cv_{m2v} + \dot{m}_{m2a}.cv_{m2a}}{\dot{m}_{m2v} + \dot{m}_{m2a}}$$

$$= \frac{0.006888\frac{kg}{s}.1.411\ \ kJ/kg.K + 0.0001111\frac{kg}{s}.0.7172\ kJ/kg.K}{0.006888\frac{kg}{s} + 0.0001111\frac{kg}{s}}$$

$$= 1.399\ kJ/kg.K$$

-Specific heat ratio

$$\kappa_{m2} = \frac{cp_{m2}}{cv_{m2}} = \frac{1.863\ kJ/kg.K}{1.399\ kJ/kg.K} = 1.33$$

-Specific gas constant

$$R_{m2} = cp_{m2} - cv_{m2} = 1.863\ kJ/kg.K - 1.399\ kJ/kg.K\ = 0.464\ kJ/kg.K$$

-Calculation of Mach number of mixture flow

$$M_{m2} = \frac{V_{m2}}{\sqrt{\kappa_{m2}R_{m2}T_{m2}}} = \frac{592.925\ m/s}{\sqrt{1.33.0.464\frac{kJ}{kg}.K.287.5\ K}} = 1.41$$

-Calculation of pressure at cross section 2-2

$$\frac{p_{22}}{p_{m2}} = 1 + 2\left[\frac{\kappa_{m2}}{\kappa_{m2}+1}\right].(M_{m2}^2 - 1)$$

$$\frac{p_{22}}{2.464\ kPa} = 1 + 2\left[\frac{1.33}{1.33+1}\right].(1.41^2 - 1)$$

$p_{22} = 5.244\ kPa$

-Calculation of Mach number at cross section 2-2

$$M_{22}^2 = \frac{1 + \left[\frac{\kappa_{m2} - 1}{2}\right].M_{m2}^2}{\kappa_{m2}.M_{m2}^2 - \left[\frac{\kappa_{m2} - 1}{2}\right]} = \frac{1 + \left[\frac{1.33 - 1}{2}\right].1.41^2}{1.33.1.41^2 - \left[\frac{1.33 - 1}{2}\right]} = 0.535$$

$M_{22} = 0.732$

-Calculation of stagnation pressure at arbitrary cross section c-c for guess value

$$\frac{p_{c2}}{p_{22}} = \left[1 + \left[\frac{\kappa_{m2} - 1}{2}\right].M_{22}^2\right]^{\left[\frac{\kappa_{m2}}{\kappa_{m2} - 1}\right]}$$

$$\frac{p_{c2}}{5.244\ kPa} = \left[1 + \left[\frac{1.33 - 1}{2}\right].0.732^2\right]^{\left[\frac{1.33}{1.33 - 1}\right]}$$

$P_{c2} = 7.378\ kPa$

-Vacuum flow calculation

$\dot{m}_{s1} = \dot{m}_{s1a} + \dot{m}_{s1v} = 0.4\ kg/hr\ + 5.198\ kg/hr\ = 5.598\ kg/hr$

From calculation above, guess value of output pressure from ejector 2 is smaller than actual stagnation pressure. Iteration is needed to obtain correct dimension of ejector which has value output pressure the same as required output pressure.

-Bisection method to find throat diameter (d_{t2})

$p_{c2-margin} = p_{c2} - P_{c2} = 11.3\ kPa - 7.378\ kPa = 3.922\ kPa$

If $p_{c2-margin} > 0$ then,

$d_{t1} = d_{tll} = 3.5\ mm$ (current condition)

$d_{tlu} = d_{tlu} = 50\ mm$ (as is)

If $p_{c2-margin} < 0$ then,

$d_{tll} = d_{tll}$ (as is)

$d_{tlu} = d_{tlu}$ (change)

-Next throat diameter (d_{t2})

$$d_{t2} = \frac{d_{tll} + d_{tlu}}{2} = \frac{3.5\ mm + 50\ mm}{2} = 26.75\ mm$$

The iteration goes on until $\dot{m}_{s1-margin} = 0.0001 \simeq 0.01$ % error

The new area ratio is inputted back to the equation above until reach the criteria.

From the calculation it takes 15 iterations with the result as below:

$d_{t2} = 5.854\ mm$

$A_{r2} = 29.54$

$\dot{m}_{p2} = 27.41\ kg/hr$

$\omega_{m2} = 106.1$

-Calculation of entrainment ratio

$$\omega_2 = \frac{\dot{m}_{s2}}{\dot{m}_{p2}} = \frac{15.39\ kg/hr}{27.41\ kg/hr} = 0.5612$$

-Calculation of enthalpy at the output of ejector

$$h_{c2} = \frac{\omega_2 h_{s2} + h_p}{\omega_2 + 1} = \frac{0.5612.2569\ kJ/kg + 2707\ kJ/kg}{0.5713 + 1} = 2630\ kJ/kg$$

-Calculation of partial pressure of vapor at the output of ejector

$$p_{c2v} = \omega_{m2} \frac{p_{c2}}{0.622 + \omega_{m2}} = 106.1 \frac{7.378\ kPa}{0.622 + 106.1} = 7.335\ kPa$$

-Calculation of temperature at output of ejector

$$h_{c2} = \frac{h(Air, T_{c2}) + \omega_{m2}.h(Steam, T_{c2}, p_{c2v})}{1 + \omega_{m2}}$$

$$2630\ kJ/kg = \frac{h(Air, T_{c2}) + 106.1.h(Steam, T_{c2}, 7.335\ kPa)}{1 + 106.1}$$

$T_{c1} = 81.66°C$

Condenser calculation

-Calculation of pressure at outlet of condenser

$p_{s3} = p_{s4} = 11.3\ kPa$

$p_{s3v} = p_{saturated}(T_{c3}) = p_{saturated}(42°C) = 8.205\ kPa$

-Calculation of humidity ratio at outlet of condenser

$$\omega_{c3} = 0.622\frac{p_{c3v}}{p_{c3} - p_{c3v}} = 0.622\frac{8.205\ kPa}{11.3\ kPa - 8.205\ kPa} = 1.65$$

-Calculation of rejected energy from

$(1 + \omega_{m2}).h_{c2} = Q_{out} + (\omega_{m2} - \omega_{c3}).h_l(T_{c3}) + h(air, T_{c3}) + \omega_{c3}.h_l(T_{c3})$

$$(1 + 106.1).2630\frac{kJ}{kg}$$

$$= q_{out}(1 + 106.1) + (106.1 - 1.65).175.9\frac{kJ}{kg} + 315.7\frac{kJ}{kg} + 1.65.175.9\frac{kJ}{kg}$$

$q_{out} = 2452.8\ kj/kg$

-Enthalpy at the output of condenser

$$h_{c3} = \frac{h(air, T_{c3}) + \omega_{c3}.h_g(T_{c3})}{1 + \omega_{c3}} = \frac{315.7\frac{kJ}{kg} + 1.65.2577\frac{kJ}{kg}}{1 + 1.65} = 1723.68\ \frac{kJ}{kg}$$

$h_w = h_l(T_{c3}) = h_l(42\ C) = 175.9\ kJ/kg$

Overall Calculation

$$ER_{series} = \frac{\dot{m}_{s1}}{\dot{m}_{p1} + \dot{m}_{p2}} = \frac{5.598\ kJ/kg}{9.799\ kJ/kg + 27.41\ kJ/kg} = 0.15$$

-Calculation of energy required

$$Q_{in} = (\dot{m}_{p1} + \dot{m}_{p2}).\left(h_{p1} - h_l\right) = \left(0.002722\frac{kg}{s} + 0.007613\frac{kg}{s}\right).\left(2707\frac{kJ}{kg} - 175.9\frac{kJ}{kg}\right)$$

$$= 26.161\ KW$$

-Calculation of energy rejected

$$Q_{in} = \dot{m}_{m2a}(\omega_{m2} + 1).\, q_{out} = 0.0001111\frac{kg}{s}.\,(106.1 + 1).\,2452.78\; kj/kg = 28.72\; KW$$

APPENDIX B

ENGINEERING EQUATION SOLVER SOURCE CODE

Vapor-Compression Refrigeration System

```
{!!Calculation of refrigeration system using compressor
 The system has specification as follow:
 Refrigerant R-22 operating pressure limit:
p_sl_R22 = 68 [psi]
p_dl_R22 = 250 [psi]

Refrigerant R-410A operating pressure limit:
p_sl_R410A = 118 [psi]
p_dl_R410A = 400 [psi]}

"!Input"
"Ambient condition"
phi_amb = 0.7            "relatif humidity"
omega_amb = 0.0214       "humidity ratio"
p_amb=1*convert('atm','kPa')

"Dehumidified condition"
"omega_deh = 0.0101"     "humidity ratio"
T_dp_deh = 14 [C]        "dew point temperature"
p_v_deh = 1.6 [kPa]      "partial pressure of vapor"
phi_deh=1

REF$ = 'R22'             "Type either 'R22' or 'R410A' uppercase
sensitive"

"Efficiency of the equipment"
eta_com = 1              "isentropic efficiency of compressor"
$ifnot ParametricTable
T_C = 14 [C]             "Refrigerant that will be used"
T_H = 32 [C]             "ambient temperature"
$endif

"!Compressor"
x[1]=1
p[1]=pressure(REF$, T=T[1], x=x[1])
h[1]=enthalpy(REF$, T=T[1], x=x[1])
s[1]=entropy(REF$, T=T[1], x=x[1])
s_is[2]=s[1]
p[2]=p[3]
h_is[2]=enthalpy(REF$, P=p[2],s=s_is[2])
eta_com = (h[2]-h[1])/(h_is[2]-h[1])
T[2]=temperature(REF$, P=p[2],h=h[2])
s[2]=entropy(REF$, T=T[2], h=h[2])
```

```
W_dot=h[1]-h[2]


"!Condenser"
x[3] = 0
T[3]=T_H
h[3]=enthalpy(REF$,T=T[3],x=x[3])
p[3]=pressure(REF$,T=T[3],x=x[3])
s[3]=entropy(REF$, T=T[3],x=x[3])
Q_cond=h[2]-h[3]

"!Expansion Valve"
h[4]=h[3]
p[4]=p[1]
x[4]=quality(REF$,h=h[4],P=p[4])
s[4]=entropy(REF$, T=T[4],x=x[4])
T[4]=T[1]

"!Evaporator"
T[1]=T_C
Q_eva=h[1]-h[4]

"!Performance"
COP=abs(Q_eva/W_dot)

"!Connection"
x[5]=1
p[5]=p[4]
T[5]=temperature(REF$, P=p[5],x=x[5])
h[5]=enthalpy(REF$,T=T[5],x=x[5])

"Humidity Calculation"
omega_deh=humrat(AirH2O,T=T_C,D=T_C,P=p_amb)
```

Ejector Calculation

```
"***THE 1-D EJECTOR MODEL ***"

"!SUBROUTINE"
"find mass flow rate of primary flow"
Subprogram sub1(p_p,A_t,gamma,eta_p,T_p,R:m_p)
m_p=p_p*convert(bar,N/m2)*A_t*sqrt(gamma*eta_p*((2/(gamma+1))^
…((gamma+1)/(gamma-1)))/(converttemp('C','K',T_p)*R*conveRt(kJ,N-m)))
End

Subprogram sub2(A_p1,A_t,gamma,eta_p,T_p,R,p_p:M_p1,p_p1)
"find Mach number of primary flow at cross section 1-1"
(A_p1/A_t)^2=(1/M)*((2/(gamma+1))*(1+(((gamma-1)*M)/2)))^
```

```
…((gamma+1)/(gamma-1))
M_p1=sqrt(M)
"find pressure of primary flow at cross section 1-1"
p_p1=p_p/(1+((gamma-1)*M_p1^2/2))^(gamma/(gamma-1))
 End

Subprogram sub3(p_s,gamma,M_sy:p_sy,p_py,p_m)
"find pressure of secondary flow at cross section y-y in critical
condition"
p|star_sy=p_s*(1+((gamma-1)*(M_sy^2)/2))^(-gamma/(gamma-1))
"condition at cross section y-y"
p|star_sy=p_sy
p|star_sy=p_py
p|star_sy=p_m
End

Subprogram sub4(p_py,p_p1,gamma,M_p1,A_p1,eta_py:M_py,A_py)
"find Mach number of primary flow at cross section y-y"
(p_py/p_p1)=(((1+((gamma-1)/2)*M_p1^2))^(gamma/(gamma-1)))/
…((1+((gamma-1)/2)*M_py^2))^(gamma/(gamma-1))
"find cross section area of primary flow at cross section y-y"
(A_py/A_p1)=((eta_py/M_py)*((2/(gamma+1))*(1+((gamma-1)/2)*M_py^2))^
…((gamma+1)/(2*(gamma-1))))/((1/M_p1)*((2/(gamma+1))*(1+((gamma-1)/2)*
…M_p1^2))^((gamma+1)/(2*(gamma-1))))
End

Subprogram sub5(A_py,A_2,T_s,T_p,p_sy,p_s,gamma,c_p,M_py,M_sy,R:
…A_sy,T_sy,T_py,V_sy,V_py)
"find cross section area of secondary flow at cross section y-y"
A_py+A_sy=A_2
"find temperature of secondary flow at cros section y-y"
T_sk=converttemp('C','K',T_s)
(T_syk/T_sk)=(p_sy/p_s)^((gamma-1)/gamma)
T_sy=converttemp('K','C',T_syk)
"find temperature of primary flow at cros section y-y"
T_pk=converttemp('C','K',T_p)
(T_pk/T_pyk)=(1+((gamma-1)/2)*M_py^2)
T_py=converttemp('K','C',T_pyk)
"find velocity of secondary flow at cross section y-y "
V_sy=M_sy*sqrt(gamma*R*convert(kJ,kg-
m^2/s^2)*converttemp('C','K',T_sy))
"find velocity of primary flow at cross section y-y "
V_py=M_py*sqrt(gamma*R*convert(kJ,kg-
m^2/s^2)*converttemp('C','K',T_py))
 End

"find the mass flow rate of secondary flow-Critical"
Function m_sc(p_s,A_sy,gamma,eta_s,T_s,R)
m_sc=p_s*convert(bar,N/m2)*A_sy*sqrt(gamma*eta_s*((2/(gamma+1))^
…((gamma+1)/(gamma-1)))/(converttemp('C','K',T_s)*R*conveRt(kJ,N-m)))
End

"find the mass flow rate of secondary flow-Subcritical"
Function m_ss(p_s,A_sy,gamma,eta_s,T_s,R,M_sy)
```

```
"find the mass flow rate of secondary flow"
m_ss=p_s*convert(bar,N/m2)*A_sy*M_sy*sqrt(gamma*eta_s*
…((2/(2+((gamma-1)*M_sy^2)))^((gamma+1)/(gamma-1)))/
…(converttemp('C','K',T_s)*R*conveRt(kJ,N-m))
End

Subprogram sub6(psi_m,m_p,V_py,m_s,V_sy,c_p,T_py,T_sy,gamma,R,p_m:
…V_m,T_m,M_m,p_2,M_2,p|star_c)
"find velocity of mixture"
psi_m*((m_p*V_py)+(m_s*V_sy))=(m_p+m_s)*V_m
"find temperature of mixture"
m_p*((c_p*convert(kJ,kg-m^2/s^2)*converttemp('C','K',T_py))+
…(V_py^2/2))+m_s*((c_p*convert(kJ,kg-m^2/s^2)*
…converttemp('C','K',T_sy))+(V_sy^2/2))=(m_p+m_s)*
…((c_p*convert(kJ,kg-m^2/s^2)*converttemp('C','K',T_m))+(V_m^2/2))
"find the mach number of mixture"
M_m=V_m/sqrt(gamma*R*convert(kJ,kg-
m^2/s^2)*abs(converttemp('C','K',T_m)))
"find pressure at cross section 2-2"
(p_2/p_m)=1+((2*gamma/(gamma+1))*(M_m^2-1))
"find the mach number at cross section 2-2"
M_2^2=(1+(((gamma-1)/2)*M_m^2))/((gamma*M_m^2)-((gamma-1)/2))
"find the pressure at cross section at c-c"
(p|star_c/p_2)=(1+((gamma-1)/2)*M_2^2)^(gamma/(gamma-1))
End

"!PROCEDURE"
Procedure solve(T_p,p_p,T_s,p_s,T_c,p_c,c_p,c_v,gamma,R,eta_p,
…eta_s,eta_py,psi_m,A_t,A_p1,A_2:m_s,omega,m_p,M_sy,p|staR_c,
…A_py, A_sy, T_sy, T_py, T_m, p_m)
Call sub1(p_p,A_t,gamma,eta_p,T_p,R:m_p)
Call sub2(A_p1,A_t,gamma,eta_p,T_p,R,p_p:M_p1,p_p1)
"Critical condition"
M_sy=1
Call sub3(p_s,gamma,M_sy:p_sy,p_py,p_m)
Call sub4(p_py,p_p1,gamma,M_p1,A_p1,eta_py:M_py,A_py)
Call sub5(A_py,A_2,T_s,T_p,p_sy,p_s,gamma,c_p,M_py,M_sy,R:A_sy,T_sy,
…T_py,V_sy,V_py)
m_s=m_sc(p_s,A_sy,gamma,eta_s,T_s,R)
Call sub6(psi_m,m_p,V_py,m_s,V_sy,c_p,T_py,T_sy,gamma,R,p_m:
…V_m,T_m,M_m,p_2,M_2,p|staR_c)

IF(p_c<=p|star_c) Then
omega=m_s/m_p
Else
"Subcritical condition"
Repeat
M_sy=M_sy-0.01
Call sub3(p_s,gamma,M_sy:p_sy,p_py,p_m)
Call sub4(p_py,p_p1,gamma,M_p1,A_p1,eta_py:M_py,A_py)
Call sub5(A_py,A_2,T_s,T_p,p_sy,p_s,gamma,c_p,M_py,M_sy,R:
…A_sy,T_sy,T_py,V_sy,V_py)
m_s=m_ss(p_s,A_sy,gamma,eta_s,T_s,R,M_sy)
Call sub6(psi_m,m_p,V_py,m_s,V_sy,c_p,T_py,T_sy,gamma,R,p_m:
```

```
…V_m,T_m,M_m,p_2,M_2,p|staR_c)
Until(abs(p|staR_c-p_c)/p_c<=0.01)
omega=m_s/m_p
Endif
End

"!INPUT"
"Varying input condition"
$ifnot ParametricTable
"condition"
T_p=120 [C]
T_s=10 [C]
T_c=33 [C]
"geometry"
d_t=2 [mm]
d_1=8 [mm]
d_2=19[mm]
$endif

"Condition input"
p_p=p_sat(Steam,T=T_p)
p_s=p_sat(Steam,T=T_s)
p_c=p_sat(Steam,T=T_c)


"Properties"
c_p=cp(Steam,T=T_p,x=1)
c_v=cv(Steam,T=T_p,x=1)
gamma=c_p/c_v
R=c_p-c_v

"Geometry of ejector"
A_t=0.25*(d_t^2)*pi*convert(mm^2,m^2)
A_p1=0.25*(d_1^2)*pi*convert(mm^2,m^2)
A_2=0.25*(d_2^2)*pi*convert(mm^2,m^2)
A_r=A_2/A_t

"Idealized condition"
psi_m=1
eta_p=1
eta_s=1
eta_py=1

 "!PROGRAM EXECUTION"
 Call solve(T_p,p_p,T_s,p_s,T_c,p_c,c_p,c_v,gamma,R,eta_p,eta_s,
…eta_py,psi_m,A_t,A_p1,A_2:m_s,omega,m_p,M_sy,p|staR_c,
…A_py, A_sy, T_sy, T_py, T_m, p_m)
```

Steam-Ejector Refrigeration System

```
"EJECTOR REFRIGERATION SYSTEM"

"!Input"
$ifnot ParametricTable
T_H = 33 [C]
T_C = 15 [C]
A_r = 90.25
$endif

p_amb = 100 [kPa]


"!Condition Calculation"
"Condition 1"
x[1] = 1
T[1] = T_H
p[1] = pressure(Water, T=T[1], x=x[1])
h[1] = enthalpy(Water, T=T[1], x=x[1])

"Condition 2"
x[2] = 0
T[2] = T_H
p[2] = pressure(Water, T=T[2], x=x[2])
h[2] = enthalpy(Water, T=T[2], x=x[2])
s[2] = entropy(Water, T=T[2], x=x[2])

"Condition 3"
T[3] = T_C
p[3] = pressure(Water, T=T[3], h=h[3])
x[3] = quality(Water, T=T[3], h=h[3])

"Condition 4"
x[4] = 1
T[4] = T[3]
p[4] = pressure(Water, T=T[4], x=x[4])
h[4] =  enthalpy(Water, T=T[4], x=x[4])

"Condition 5"
p[5] = p[6]
s[5] = s[2]
h[5] = enthalpy(Water, P=p[5], s=s[5])
T[5] = temperature(Water, P=p[5], h=h[5])

"Condition 6"
x[6] = 1
T[6] = temperature(Water, P=p[6], x = x[6])
h[6] =enthalpy(Water, T=T[6], x = x[6])
```

```
"!Component Calculation"
"Ejector"
p_r = p[6]/p[4]
a = 0.9509*A_r +13.033
b = -1E-6*A_r^2 + 0.0007*A_r - 1.0563
c = -3E-7*A_r^2 + 5E-5*A_r - 0.0673
omega = a*p_r^b+c
h[1]=(omega*h[4]+h[6])/(1+omega)

"Condenser"
q_out = h[1] - h[2]

"Expansion Valve"
h[3] = h[2]

"Evaporator"
q_eva = omega*(h[4] - h[3])

"Pump"
w_pump = h[5] - h[2]

"Boiler"
q_in = h[6] - h[5]

"!Performance Calculation"
COP = q_eva/(q_in + w_pump)
```

Membrane-Ejector Dehumidifier

```
"!======= EJECTOR DEHUMIFIER ========"

"!=======  SUBROUTINE ======="

Subprogram vapprop(m_dot_sv,m_dot_sa,p_s,T_s:omega_s,h_s,cp_s,k_s,R_s)
"humidity ratio"
omega_s = m_dot_sv/m_dot_sa
"pressure vapor of water"
p_sv = omega_s*p_s/(0.622+omega_s)
"pressure gas of water"
p_sg = p_sat(Steam,T=T_s)
"relative humidity"
phi_s = p_sv/p_sg
"enthalpy calculation"
h_sv = enthalpy(Water,T=T_s,P=p_sv)
h_sa = enthalpy(Air,T=T_s)
h_s = (m_dot_sv*h_sv + m_dot_sa*h_sa)/(m_dot_sv + m_dot_sa)
"specific heat capacity"
cp_sa = cp(Air,T=T_s)
```

```
cp_sv = cp(Water,T=T_s,x=1)
cv_sa = cv(Air,T=T_s)
cv_sv = cv(Water,T=T_s,x=1)
cp_s = (m_dot_sv*cp_sv + m_dot_sa*cp_sa)/(m_dot_sv+m_dot_sa)
"specific heat ratio"
k_sa = cp_sa/cv_sa
k_sv = cp_sv/cv_sv
k_s = (m_dot_sv*k_sv + m_dot_sa*k_sa)/(m_dot_sv+m_dot_sa)
"specific gas constant"
R_sa = cp_sa - cv_sa
R_sv = cp_sv - cv_sv
R_s = (m_dot_sv*R_sv + m_dot_sa*R_sa)/(m_dot_sv+m_dot_sa)
End

Subprogram boilprop(T_p:k_p,R_p,h_p,cp_p,p_p)
"pressure at saturated condition"
p_p=p_sat(Water,T=T_p)
"specific heat capacity"
cp_p = cp(Water,T=T_p,x=1)
cv_p = cv(Water,T=T_p,x=1)
"specific heat ratio"
k_p = cp_p/cv_p
"specific gas constant"
R_p = cp_p - cv_p
"enthalpy calculation"
h_p = enthalpy(Water,T=T_p,x=1)
End



Subprogram sub1(p_p,A_t,k_v,eta_p,T_p,R_p:m_dot_p)
"find mass flow rate of primary flow"
m_dot_p=p_p*convert(bar, N/m2)*A_t*sqrt(k_v*eta_p*((2/(k_v+1))^
…((k_v+1)/(k_v-1)))/(converttemp('C','K',T_p)*R_p*convert(kJ,N-m)))
End

Subprogram sub2(A_p1,A_t,k_v,p_p:M_p1,p_p1)
"find Mach number of primary flow at cross section 1-1"
(A_p1/A_t)^2=(1/M)*((2/(k_v+1))*(1+(((k_v-1)*M)/2)))^((k_v+1)/(k_v-1))
M_p1=sqrt(M)
"find pressure of primary flow at cross section 1-1"
p_p1=p_p/(1+((k_v-1)*M_p1^2/2))^(k_v/(k_v-1))
End

Subprogram sub3(p_s, k_s :p_sy, p_py, p_m, M_sy)
"Critical condition"
M_sy=1
"find pressure of secondary flow at cross section y-y in critical
condition"
p|star_sy=p_s*(1+((k_s-1)*(M_sy^2)/2))^(-k_s/(k_s-1))
"condition at cross section y-y"
p_sy = p|star_sy
p_py = p|star_sy
```

```
p_m = p|star_sy
End

Subprogram sub4(p_py,p_p1,k_v,M_p1,A_p1,eta_py:M_py,A_py)
"find Mach number of primary flow at cross section y-y"
(p_py/p_p1)=(((1+((k_v-1)/2)*M_p1^2))^(k_v/(k_v-1)))/
…((1+((k_v-1)/2)*M_py^2))^(k_v/(k_v-1))
"find cross section area of primary flow at cross section y-y"
(A_py/A_p1)=((eta_py/M_py)*((2/(k_v+1))*(1+((k_v-1)/2)*M_py^2))^
…((k_v+1)/(2*(k_v-1))))/((1/M_p1)*((2/(k_v+1))*(1+((k_v-1)/2)*M_p1^2))^
…((k_v+1)/(2*(k_v-1))))
End

Subprogram sub5(A_py,A_2,T_s,T_p,p_sy,p_s,k_v,k_s,M_py,M_sy,R_v,R_s:
…A_sy,T_sy,T_py,V_sy,V_py)
"find cross section area of secondary flow at cross section y-y"
A_py+A_sy=A_2
"find temperature of secondary flow at cros section y-y"
T_sk=converttemp('C','K',T_s)
(T_syk/T_sk)=(p_sy/p_s)^((k_s-1)/k_s)
T_sy=converttemp('K','C',T_syk)
"find temperature of primary flow at cros section y-y"
T_pk=converttemp('C','K',T_p)
(T_pk/T_pyk)=(1+((k_v-1)/2)*M_py^2)
T_py=converttemp('K','C',T_pyk)
"find velocity of secondary flow at cross section y-y "
V_sy=M_sy*sqrt(k_s*R_s*convert(kJ,kg-m^2/s^2)*
…converttemp('C','K',T_sy))
"find velocity of primary flow at cross section y-y "
V_py=M_py*sqrt(k_v*R_v*convert(kJ,kg-m^2/s^2)*
…converttemp('C','K',T_py))
End

Subprogram sub6(p_s,A_sy,k_s,eta_s,T_s,R_s:m_dot_s)
"find the mass flow rate of secondary flow-Critical"
m_dot_s=p_s*convert(bar,N/m2)*A_sy*sqrt(k_s*eta_s*((2/(k_s+1))^
…((k_s+1)/(k_s-1)))/(converttemp('C','K',T_s)*R_s*convert(kJ,N-m)))
End

Subprogram sub7(psi_m,m_dot_p,V_py,T_py,p_py,m_dot_s,V_sy,T_sy,
…cp_p, cp_s,omega_s,p_m:V_m,T_m,cp_m,cv_m,k_m,R_m,M_m,p_2,M_2,
…p_c, omega_m,m_dot_mv,m_dot_ma,m_dot_m)
"find velocity of mixture"
psi_m*((m_dot_p*V_py)+(m_dot_s*V_sy))=(m_dot_p+m_dot_s)*V_m
"find enthalpy calculation of primary flow at cross section y-y"
m_dot_p*((cp_p*convert(kJ,kg-m^2/s^2)*converttemp('C','K',T_py))+
…(V_py^2/2))+m_dot_s*((cp_s*convert(kJ,kg-m^2/s^2)*
…converttemp('C','K',T_sy))+(V_sy^2/2))=(m_dot_p+m_dot_s)*
…(h_m*convert(kJ,kg-m^2/s^2)+(V_m^2/2))
"find mass flow composition of mixture"
m_dot_m = m_dot_p+m_dot_s
m_dot_mv =m_dot_p+(omega_s/(1+omega_s))*m_dot_s
m_dot_ma =(1/(1+omega_s))*m_dot_s
omega_m = m_dot_mv/m_dot_ma
```

```
"find temperature calculation of mixing flow at constant cross section
area"
h_m =(m_dot_mv*cp(Water,T=T_m,x=1) +
m_dot_ma*cp(Air,T=T_m))*converttemp('C','K',T_m)/m_dot_m
"find specific heat capacity of mxture"
cp_am = cp(Air,T=T_m)
cp_vm = cp(Water,T=T_m,x=1)
cv_am = cv(Air,T=T_m)
cv_vm = cv(Water,T=T_m,x=1)
cp_m = (m_dot_mv*cp_vm + m_dot_ma*cp_am)/(m_dot_mv+m_dot_ma)
cv_m = (m_dot_mv*cv_vm + m_dot_ma*cv_am)/(m_dot_mv+m_dot_ma)
"specific heat ratio"
k_m = cp_m/cv_m
"specific gas constant"
R_m = cp_m - cv_m
"find the mach number of mixture"
M_m=V_m/sqrt(k_m*R_m*convert(kJ,kg-m^2/s^2)*converttemp('C','K',T_m))
"find pressure at cross section 2-2"
(p_2/p_m)=1+((2*k_m/(k_m+1))*(M_m^2-1))
"find the mach number at cross section 2-2"
M_2^2=(1+(((k_m-1)/2)*M_m^2))/((k_m*M_m^2)-((k_m-1)/2))
"find the pressure at cross section at c-c"
(p_c/p_2)=(1+((k_m-1)/2)*M_2^2)^(k_m/(k_m-1))
End

Subprogram sub8(m_dot_s,m_dot_p, h_s, h_p,omega_m, p_c,eta_e:
…p_cv, omega, h_c, T_c)
" find the entrainment ratio"
omega = m_dot_s/m_dot_p
"find entalphy at the output of ejector"
h_c = eta_e*(omega*h_s + h_p)/(omega + 1)
"find partial pressure at output of ejector"
p_cv = omega_m*p_c/(0.622+omega_m)
"find Temperature at output of ejector"
h_c = ((enthalpy(Air,T=T_c)) +
omega_m*(enthalpy(Water,T=T_c,P=p_cv)))/(1+omega_m)
End

Subprogram sub9(p_s,k_s,eta_s,T_s,R_s,m_dot_s:A_sy)
"find the flow area of secondary flow at critical condition at cross
section y-y"
m_dot_s=p_s*convert(bar,N/m2)*A_sy*sqrt(k_s*eta_s*((2/(k_s+1))^
…((k_s+1)/(k_s-1)))/(converttemp('C','K',T_s)*R_s*convert(kJ,N-m)))
End

Subprogram sub10(A_py,A_sy,T_s,T_p,p_sy,p_s,k_v,k_s,M_py,M_sy,R_v,R_s:
…A_2,T_sy,T_py,V_sy,V_py)
"find cross section area of secondary flow at cross section y-y"
A_py+A_sy=A_2
"find temperature of secondary flow at cros section y-y"
T_sk=converttemp('C','K',T_s)
(T_syk/T_sk)=(p_sy/p_s)^((k_s-1)/k_s)
T_sy=converttemp('K','C',T_syk)
"find temperature of primary flow at cros section y-y"
```

```
T_pk=converttemp('C','K',T_p)
(T_pk/T_pyk)=(1+((k_v-1)/2)*M_py^2)
T_py=converttemp('K','C',T_pyk)
"find velocity of secondary flow at cross section y-y "
V_sy=M_sy*sqrt(k_s*R_s*convert(kJ,kg-
m^2/s^2)*converttemp('C','K',T_sy))
"find velocity of primary flow at cross section y-y "
V_py=M_py*sqrt(k_v*R_v*convert(kJ,kg-
m^2/s^2)*converttemp('C','K',T_py))
End

Subprogram dimension1(d_t, d_1, A_r: A_t, A_p1, A_2)
"find throat area of nozzle"
A_t = 0.25*(d_t^2)*pi*convert(mm^2,m^2)
"find outlet area of nozzle"
A_p1 = 0.25*(d_1^2)*pi*convert(mm^2,m^2)
"find constant area of ejector"
A_2 = A_t*A_r
End

Subprogram dimension2(d_t, d_1: A_t, A_p1)
"find throat area of nozzle"
A_t = 0.25*(d_t^2)*pi*convert(mm^2,m^2)
"find outlet area of nozzle"
A_p1 = 0.25*(d_1^2)*pi*convert(mm^2,m^2)
End

Subprogram finddt(m_dot_s,omega,p_p,k_v,eta_p,T_p,R_s:m_dot_p,d_t)
"find mass flow of primary flow"
m_dot_p = m_dot_s/omega
"find area of nozzle throat"
m_dot_p=p_p*convert(bar,
N/m2)*A_t*sqrt(k_v*eta_p*((2/(k_v+1))^((k_v+1)/(k_v-1)))/
…(converttemp('C','K',T_p)*R_s*convert(kJ,N-m)))
"find throat diameter of nozzle"
A_t = 0.25*(d_t^2)*pi*convert(mm^2,m^2)
End

Subprogram condenser(m_dot_mv, m_dot_ma, p_c1, omega_in, h_c1, T_c2,
…p_c2:p_cv2,omega_out,q_c,h_cout,h_cw, m_dot_cvout,
…m_dot_caout, m_dot_cout, m_dot_cwout, p_cout)
"find saturated partial pressure of vapour"
p_cv2=p_sat(Water,T=T_c2)
"find partial pressure of vapor for mixture at inlet of condenser"
omega_out = 0.622*p_cv2/(p_c1-p_cv2)
"find omega_m2 og mixture at oulet of condenser"
(1+omega_in)*h_c1 = q_c*(omega_in+1) + (omega_in - omega_out)*
…enthalpy(Water,T=T_c2,x=0) + enthalpy(Air,T=T_c2) +
…omega_out*enthalpy(Water,T=T_c2,x=1)
"find enthalpy at output of condenser"
h_cout = ((enthalpy(Air,T=T_c2)) +
omega_out*(enthalpy(Water,T=T_c2,x=1)))/(1+omega_out)
"find enthalpy of water out from condenser"
h_cw = enthalpy(Water,T=T_c2,x = 0)
```

```
"find mass flowrate at outlet of condenser"
m_dot_cvout = omega_out*m_dot_ma
m_dot_caout = m_dot_ma
m_dot_cout = m_dot_cvout+m_dot_caout
m_dot_cwout = m_dot_mv-m_dot_cvout
"find pressure at outlet of condenser"
p_cout = p_c2
End

Procedure findmdots(m_dot_sv,
m_dot_sa,p_s,k_s,eta_s,T_s,R_s,A_py,T_p,p_sy,k_p,M_py,M_sy,R_p,A_rl,
…A_rh,A_t:m_dot_s,A_sy,T_sy,T_py,V_sy,V_py,A_rt)
A_r = (A_rl + A_rh)/2
A_2 = A_t*A_r
Call
sub5(A_py,A_2,T_s,T_p,p_sy,p_s,k_p,k_s,M_py,M_sy,R_p,R_s:A_sy,T_sy,
…T_py,V_sy,V_py)
Call sub6(p_s,A_sy,k_s,eta_s,T_s,R_s:m_dot_s)
m_dot_st = m_dot_sv + m_dot_sa
m_dot_smar = m_dot_st - m_dot_s
i = 0

Repeat
If (m_dot_smar > 0) Then
A_rl = A_r
Else
A_rh = A_r
Endif

A_r = (A_rl + A_rh)/2
A_2 = A_t*A_r
Call
sub5(A_py,A_2,T_s,T_p,p_sy,p_s,k_p,k_s,M_py,M_sy,R_p,R_s:A_sy,T_sy,
…T_py,V_sy,V_py)
Call sub6(p_s,A_sy,k_s,eta_s,T_s,R_s:m_dot_s)
m_dot_smar = m_dot_st - m_dot_s
i = i + 1
Until (abs(m_dot_smar) <= 0.000001)
A_rt = A_r
End

Procedure findpc(d_tl, d_th, p_p, k_v, eta_p, T_p, R_v, p_s, k_s,
…eta_py, A_sy, T_s, R_s, psi_m, m_dot_s, cp_p, cp_s, omega_s, p_ct:
…A_t,m_dot_p,M_p1,p_p1,M_sy,M_py,A_py,A_2,T_sy,T_py,T_m,R_m,M_m,p_2,
…M_2,p_c, omega_m,m_dot_mv,m_dot_ma,m_dot_m, d_tt, A_r)
d_t = (d_tl + d_th)/2
d_1 = 1.5*d_t
Call dimension2(d_t, d_1: A_t, A_p1)
Call sub1(p_p,A_t,k_v,eta_p,T_p,R_v:m_dot_p)
Call sub2(A_p1,A_t,k_v,p_p:M_p1,p_p1)
Call sub3(p_s, k_s :p_sy, p_py, p_m, M_sy)
Call sub4(p_py,p_p1,k_v,M_p1,A_p1,eta_py:M_py,A_py)
Call sub10(A_py,A_sy,T_s,T_p,p_sy,p_s,k_v,k_s,M_py,M_sy,R_v,R_s:
…A_2,T_sy,T_py,V_sy,V_py)
```

```
Call sub7(psi_m,m_dot_p,V_py,T_py,p_py,m_dot_s,V_sy,T_sy,
…cp_p, cp_s,omega_s,p_m:V_m,T_m,cp_m,cv_m,k_m,R_m,M_m,p_2,M_2,
…p_c, omega_m,m_dot_mv,m_dot_ma,m_dot_m)
p_cmar = p_ct - p_c
i = 0

Repeat
If (p_cmar > 0) Then
d_tl = d_t
Else
d_th = d_t
Endif

d_t = (d_tl + d_th)/2
d_1 = 1.5*d_t
Call dimension2(d_t, d_1: A_t, A_p1)
Call sub1(p_p,A_t,k_v,eta_p,T_p,R_v:m_dot_p)
Call sub2(A_p1,A_t,k_v,p_p:M_p1,p_p1)
Call sub3(p_s, k_s :p_sy, p_py, p_m, M_sy)
Call sub4(p_py,p_p1,k_v,M_p1,A_p1,eta_py:M_py,A_py)
Call sub10(A_py,A_sy,T_s,T_p,p_sy,p_s,k_v,k_s,M_py,M_sy,R_v,R_s:
…A_2,T_sy,T_py,V_sy,V_py)
Call sub7(psi_m,m_dot_p,V_py,T_py,p_py,m_dot_s,V_sy,T_sy, cp_p,
…cp_s,omega_s,p_m:V_m,T_m,cp_m,cv_m,k_m,R_m,M_m,p_2,M_2,p_c,
…omega_m,m_dot_mv,m_dot_ma,m_dot_m)
p_cmar = p_ct - p_c
i = i + 1
Until (abs(p_cmar) <= 0.000001)
d_tt = d_t
A_r = A_2/A_t
End

"!======= INPUT ========"

$ifnot in parametric table
T_p[1] =  120 [C]
T_p[2] = 120 [C]
d_t1 = 3.5 [mm]
T_amb = 33 [C]
ome = 13
$endif

"=======  EJECTOR CONDITION INPUT ======="
"Input for ejector I condition"
p_s[1] = 0.016 [bar]
T_s[1] = T_amb
m = 5.6*convert(kg/hr,kg/s)
m_dot_sv[1] = m-m_dot_sa[1]
m_dot_sa[1] = m/(ome+1)
p_s[3]= 0.113 [bar]

" Ejector IA"
d_11 = 10 [mm]
" Initial value"
```

```
A_r1i = 30
"Limit"
A_r1l = 0
A_r1h = 500

"coefficient"
eta_p1 = 1
eta_s1 = 1
eta_py1 = 1
eta_e1 = 1
phi_m1 = 0.88

" Ejector IB"
"Limit"
d_t2l = 0
d_t2h = 1000

"coefficient"
eta_p2 = 1
eta_s2 = 1
eta_py2 = 1
eta_e2 = 1
phi_m2 = 0.88

"=======  CONDENSER PARAMETER INPUT======="

T_s[4] = T_amb

"!======= CALCULATION ========"

"=======  EJECTOR CALCULATION IA ======="

Call dimension1(d_t1, d_11, A_r1i: A_t1, A_p11, A_21)
Call boilprop(T_p[1]:k_p[1],R_p[1],h_p[1],c_pp[1], p_p[1])
Call vapprop(m_dot_sv[1],m_dot_sa[1],p_s[1],T_s[1]:
…omega_s[1],h_s[1],c_ps[1],k_s[1],R_s[1])
Call sub1(p_p[1],A_t1,k_p[1],eta_p1,T_p[1],R_p[1]:m_dot_p[1])
Call sub2(A_p11,A_t1,k_p[1],p_p[1]:M_p11,p_p11)
Call sub3(p_s[1], k_s[1] :p_sy1, p_py1, p_m1, M_sy1)
Call sub4(p_py1,p_p11,k_p[1],M_p11,A_p11,eta_py1:M_py1,A_py1)
Call findmdots(m_dot_sv[1], m_dot_sa[1],p_s[1],k_s[1],eta_s1,T_s[1],
…R_s[1],A_py1,T_p[1],p_sy1,k_p[1],M_py1,M_sy1,R_p[1],A_r1l,A_r1h,A_t1:
…m_dot_s[1],A_sy1,T_sy1,T_py1,V_sy1,V_py1,A_r1)
Call sub7(phi_m1,m_dot_p[1],V_py1,T_py1,p_py1,m_dot_s[1],
…V_sy1,T_sy1,c_pp[1], c_ps[1],omega_s[1],p_m1:V_m1,T_m1,c_pm1,c_vm1,
…k_m1,R_m1,M_m1,p_21,M_21,p_s[2], omega_m1,m_dot_mv1,m_dot_ma1,
…m_dot_m1)
Call sub8(m_dot_s[1],m_dot_p[1], h_s[1], h_p[1],omega_m1, p_s[2],
…eta_e1:p_sv[2], omega_1, h_c1, T_s[2])

"transfer parameters for next ejector"

m_dot_sa[2] = m_dot_ma1
m_dot_sv[2] = m_dot_mv1
```

```
m_dot_s[2] = m_dot_sa[2] + m_dot_sv[2]

"=======  EJECTOR CALCULATION IB ======="

Call vapprop(m_dot_sv[2],m_dot_sa[2],p_s[2],T_s[2]:omega_s[2],h_s[2],
…c_ps[2],k_s[2],R_s[2])
Call boilprop(T_p[2]:k_p[2],R_p[2],h_p[2],c_pp[2], p_p[2])
Call sub9(p_s[2],k_s[2],eta_s2,T_s[2],R_s[2],m_dot_s[2]:A_sy2)
Call findpc(d_t2l, d_t2h, p_p[2], k_p[2], eta_p2, T_p[2], R_p[2],
…p_s[2], k_s[2], eta_py2, A_sy2, T_s[2], R_s[2], phi_m2, m_dot_s[2],
…c_pp[2], c_ps[2], omega_s[2],p_s[3]:A_t2,m_dot_p[2],M_p12,p_p12,M_sy2,
…M_py2,A_py2,A_22,T_sy2,T_py2,T_m2,R_m2,M_m2,p_22,M_22,p_c2,
…omega_s[3],m_dot_sv[3],m_dot_sa[3],m_dot_s[3], d_t2, A_r2)
Call sub8(m_dot_s[2],m_dot_p[2], h_s[2], h_p[2],omega_s[3], p_s[3],
…eta_e2:p_sv[3], omega_2, h_s[3], T_s[3])

"=======  CONDENSER CALCULATION ======="

Call condenser(m_dot_sv[3],m_dot_sa[3], p_s[3], omega_s[3], h_s[3],
…T_s[4], p_s[3]:p_sv[4],omega_s[4],q_c,h_s[4],h_cw, m_dot_sv[4],
…m_dot_sa[4], m_dot_s[4], m_dot_cw, p_s[4])

"======= ENERGY ========"

Q_in_1 = m_dot_p[1]*(h_p[1]-h_cw)
Q_in_2 = m_dot_p[2]*(h_p[2]-h_cw)
omega_overall=m_dot_s[1]/(m_dot_p[1]+m_dot_p[2])
```